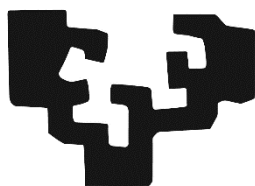eman ta zabal zazu

Universidad
del País Vasco
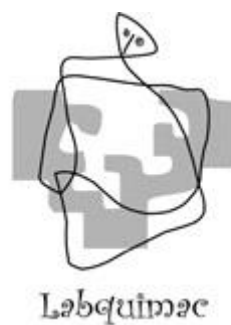
Euskal Herriko
Unibertsitatea

Design and development of high-performance thermoplastic vulcanizates with vibration damping properties

Memoria para optar al Grado de Doctor por la Universidad del País Vasco (UPV/EHU) presentada por

Aizeti Burgoa Beitia

Leioa, agosto 2020

Acknowledgements

Abstract

Lightweight components of electric vehicles will face new challenges related with their noise and vibration performance because, in the absence of the internal combustion engine, the noise generated by their vibration will become more apparent. To overcome these new challenges, traditional design and material selection must be reconsidered. In this context, thermoplastic vulcanizates (TPVs) are interesting materials due to their light weight, recyclability, ease processing and design flexibility. This Thesis aims to advance on the design and development of high-performance TPVs for structural vibration damping applications. For that, novel TPVs based on polyamide 6 (PA6) and hydrogenated acrylonitrile butadiene rubber (HNBR) have been developed and their microstructure-property relationship thoroughly investigated. First, the reactive compatibilization of PA6/HNBR blends by means of carboxylic HNBR (XHNBR) addition was studied. Secondly, peroxide cured PA6/XHNBR blends containing metal oxides and phenolic antioxidants were formulated as a new concept to design high-performance vibration damping TPVs. Lastly, the relationship between microstructure of TPVs and their nonlinear quasi-static and dynamic mechanical behaviour was explored. Overall, the results obtained pointed out the potential of carboxylic TPVs as high-performance vibration damping materials. On one hand, the explored approach based on the reactive compatibilization of PA6/HNBR blends by adding XHNBR revealed new approaches to develop thermoplastic elastomer blends with superior thermal and mechanical properties by controlling interfacial interactions and morphology. Furthermore, the achieved results highlighted that the generation of ionic crosslinks, via the addition of metal oxides, represents a very promising way to develop high-performance TPVs with a broad vibration damping temperature range. Besides, the investigation of the material's microstructure and their nonlinear mechanical performance allowed to link the identified micromechanical deformation processes to the corresponding underlying microstructural features. Finally, physical interpretations for the observed deformation mechanisms have been introduced in order to build a knowledge-base for the micromechanical modelling of TPVs. In conclusion, this Thesis opens new possibilities to obtain high-performance TPVs with customized thermal, mechanical and vibration damping properties as well as to foresee their performance by means of micromechanical modelling tools.

Resumen

Los componentes ligeros de vehículos eléctricos se enfrentarán a nuevos requerimientos relacionados con su generación de ruido y vibración debido a que, en ausencia de un motor de combustión interna, el ruido que se genere por su vibración se hará más evidente. Para afrontar estos nuevos desafíos, los conceptos de diseño y selección de materiales tradicionales deberán reconsiderarse. En este contexto, los termoplásticos elastómeros vulcanizados (TPVs, por sus siglas en inglés) son materiales interesantes debido a su baja densidad, reciclabilidad, facilidad de procesamiento y flexibilidad de diseño. Esta Tesis se enfoca en el diseño y desarrollo de TPVs de alto rendimiento para aplicaciones de amortiguación de vibraciones estructurales. Para ello, se han desarrollado nuevas formulaciones de TPVs basadas en poliamida 6 (PA6) y caucho de acrilonitrilo butadieno hidrogenado (HNBR) y se ha investigado a fondo la relación existente entre su microestructura y sus propiedades. En primer lugar, se estudió la compatibilización reactiva de las mezclas de PA6/HNBR mediante la adición de HNBR carboxílico (XHNBR). En segundo lugar, se formularon mezclas de PA6/XHNBR vulcanizadas con peróxido que contienen óxidos metálicos y antioxidantes fenólicos como un nuevo concepto para diseñar TPVs de amortiguación de vibraciones de alto rendimiento. Finalmente, se investigó la relación entre la microestructura de los materiales desarrollados y su comportamiento cuasi-estático y dinámico mecánico no lineal. En general, los resultados obtenidos han señalado el potencial de los TPVs carboxílicos como materiales de amortiguación de vibraciones de alto rendimiento. Por un lado, el enfoque explorado, basado en la compatibilización reactiva de las mezclas de PA6/HNBR añadiendo XHNBR, reveló nuevas estrategias para desarrollar mezclas de elastómeros termoplásticos con propiedades térmicas y mecánicas superiores mediante el control de las interacciones interfaciales y la morfología. Además, los resultados obtenidos resaltaron que la generación de reticulaciones iónicas mediante la adición de óxidos metálicos, representa una estrategia muy prometedora para desarrollar TPVs de alto rendimiento con propiedades de amortiguación de vibraciones en un amplio rango de temperaturas. Además, la investigación de la microestructura y el comportamiento mecánico no lineal de los materiales permitió identificar y vincular los procesos de deformación micromecánica con sus correspondientes características microestructurales. Finalmente, se han presentado interpretaciones físicas de los mecanismos de deformación observados con el fin de construir una base de conocimiento para el modelado micromecánico de TPVs. En conclusión, esta Tesis abre nuevas posibilidades para obtener TPVs de alto rendimiento con propiedades térmicas, mecánicas y de amortiguación de vibraciones personalizadas, así como para prever su comportamiento mediante herramientas de modelado micromecánico.

Laburpena

Ibilgailu elektrikoen osagai arinek zaratari eta bibrazioari lotutako eskakizun berriei egin beharko diete aurre; izan ere, barne-errekuntzako motorrik ezean, osagaien bibrazioek sortutako zarata nabarmenagoa izango baita. Testuinguru honetan, termoplastiko elastomero bulkanizatuak (TPV-ak, ingeleseko siglak direla eta) material interesgarriak dira, beraien dentsitate bajua, birziklagarritasuna, prozesatzeko erraztasuna eta diseinu-malgutasuna direla eta. Tesi honen helburua errendimendu handiko TPV-en diseinua eta garapena sustatzea da, auto osagaien egiturazko bibrazioak moteltzeko. Horretarako, poliamida 6-an (PA6) eta akrilonitrilo butadieno hidrogenatuko kautxuan (HNBR) oinarritutako TPV berriak garatu dira, eta hauen mikroegituraren eta propietateen arteko erlazioa sakonki ikertu da. Lehenik eta behin, PA6/HNBR nahasketen bateragarritasun erreaktiboa aztertu zen, HNBR karboxilikoa gehituta (XHNBR). Bigarrenik, bibrazioak moteltzeko errendimendu handiko TPVak diseinatzeko kontzeptu berri gisa, peroxido bidez bulkanizatutako eta oxido metalikoak zein antioxidatzaile fenolikoak dituzten PA6/XHNBR nahasteak formulatu ziren. Azkenik, mikroegituraren eta portaera kuasi-estatiko eta dinamiko mekaniko ez-linealaren arteko erlazioa ikertu zen. Oro har, lortutako emaitzek, TPV karboxilikoek bibrazioak moteltzeko errendimendu handiko material gisa duten potentziala adierazi dute. Alde batetik, XHNBR gehitzean oinarritzen zen, PA6/HNBR nahasteen bateragarritasun erreaktiboa burutzeko aztertutako estrategiak, propietate termiko eta mekaniko altuko termoplastiko elastomero nahasketak garatzeko estrategia berriak badaudela demostratu zuen. Estrategia berri horiek, faseen arteko interakzioak eta morfologia kontrolatzean oinarritzen dira. Gainera, lortutako emaitzek nabarmendu zuten, oxido metalikoak gehituz, erretikulazio ionikoak sortzea etorkizun handiko estrategia dela tenperatura-tarte handi batean bibrazioak moteltzeko propietateak dituzten errendimendu handiko TPVak garatzeko. Gainera, mikroegituraren eta portaera mekaniko ez-linealaren arteko erlazioaren ikerketak, deformazio mikromekanikoko prozesuei dagozkien ezaugarri mikroestrukturalak identifikatzea eta lotzea ahalbidetu zuen. Azkenik, behatutako deformazio-mekanismoen interpretazio fisikoak aurkeztu dira, TPVen modelizazio mikromekanikorako ezagutza-oinarri bat eraikitzeko intentzioarekin. Laburbilduz, Tesi honek aukera berriak irekitzen ditu propietate termiko, mekaniko eta bibrazioak moteltzeko propietate pertsonalizatuak dituzten errendimendu handiko TPVak lortzeko, bai eta, modelizazio mikromekanikoko tresnen bidez, horien portaera aurreikusteko ere.

Table of contents

List of figures

List of tables

Chapter 1

Introduction

1.1. Motivation

Automotive and transportation applications have dominated the market of thermoplastic elastomers (TPEs) in 2019. As shown in Figure 1.1 about 44% of all TPE products, consumed worldwide, were used in the automotive industry [1]. The key reasons for adoption of TPEs in automotive applications are their lightweight, ease-of-processing and recyclability.
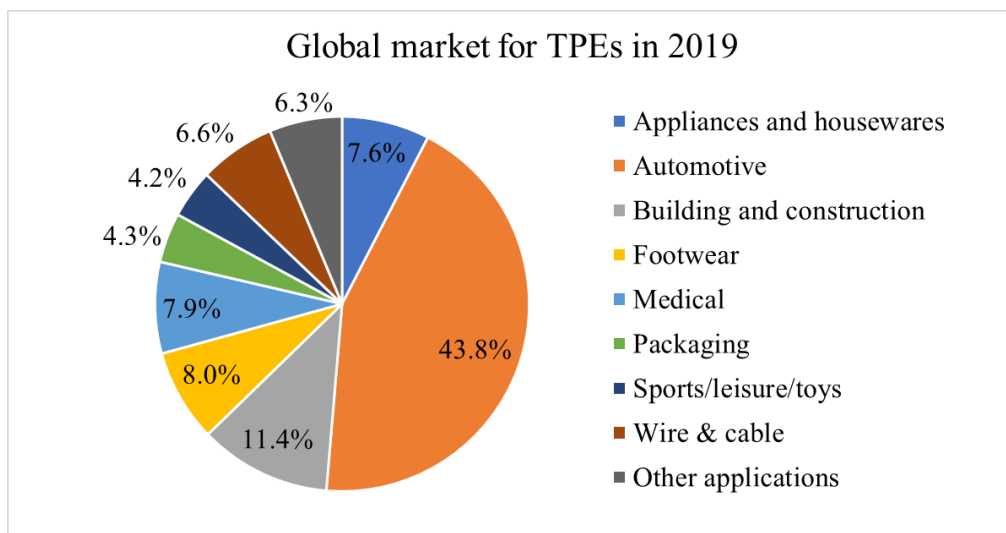
Figure 1.1. Global market for TPEs in 2019.

Table 1.1 summarizes the global TPE market in automotive applications for the years 2014 and 2019 [2]. As can be seen in the table, thermoplastic vulcanizates (TPVs) have become one of the fastest growing TPE types in the automotive industry. The main

reasons for this high growth are ascribed to their outstanding properties and design flexibility. The formulation of TPV materials enables the blending of different rubber, thermoplastic and crosslinking systems to develop elastomeric materials with tailored properties. Currently, classical vulcanized rubbers are starting to be replaced by high-performance TPVs in a wide range of automotive applications. These high-performance TPVs are based on high-performance rubber and thermoplastics, other than those general-purpose TPVs based on PP and EPDM.

Table 1.1. Global automotive market for TPE types in the years 2014 and 2019 (thousand tonnes).

TPE type	2014	2019
TPS	382.8	504.4
TPO	498.7	684.5
TPV	326.0	460.6
TPU	199.9	254.3
TPC	78.4	108.4
TPA	32.0	42.3
Others	20.0	29.8

In recent years, environmental protection and alternative green energies have become one of the main social and political concerns due to the greenhouse gas emissions and the high pollution in modern cities. The road transport is responsible of 75 % of total greenhouse gas emissions of the transport industry [3]. Furthermore, according to the United Nations the world population will experience an increase of 30% from 2017 to 2050, and the number of road vehicles is expected also to grow accordingly [4]. All these factors, together with the introduction of new climate policies, such as the European Union policy to reduce transport greenhouse gas emissions to 60% below 1990 levels by 2050, are accelerating the replacement of conventional internal combustion engine vehicles with electric vehicles (EVs), becoming the electrification of road vehicles one of the leading automotive trends [5]. A great number of original equipment manufacturers (OEMs) have taken a significant step in the field of green transportation by introducing EVs to their product range. This step implies a variety of new technological challenges

that OEMs must face in several engineering fields including new lightweight concepts, new requirements and new materials, among others.

Lightweighting has long been a technological challenge in vehicles powered by combustion engines to aid the climate target of reducing CO_2 emissions. In electric vehicles, lightweighting still will play a critical role in terms of increasing the driving range by means of lowering the energy consumption. However, the main new challenges that lightweight electric vehicle components will face is related with their noise and vibration performance. Noise and vibration performance will be a key aspect in EVs because, in the absence of the internal combustion engine, the noise generated by the vibration of lightweight components will become more apparent [6–8]. Consequently, electric vehicle components will have to meet higher noise and vibration standards than the components of internal combustion engine vehicles. At this point, advanced lightweight materials with vibration damping properties will need to be used to minimize or eliminate the vibration of lightweight EV components in order to increase the acoustic comfort in the vehicle's interior [9]. In the next decades the focus on material research and technology for automotive industry will be driven by these challenges.

To overcome these new demands, traditional design and material choices must be revisited. In this context, thermoplastic vulcanizates are interesting materials due to their light weight, recyclability, easy processing and design flexibility. Moreover, the commercial availability of so many rubbers and thermoplastics with the desired properties for blending, allows the development of advanced TPV materials specifically for EV applications. Thus, a huge number of opportunities arise when looking at the contributions that the mentioned materials can have in the electric vehicles of the future. Nevertheless, still few works exist about the design of high-performance TPV materials for vibration damping applications, which means that there is a great deal of room for research and development in this field. The key for tailoring these new TPV materials will be to understand how their microstructure influences the macroscopic material properties, such as the thermal, mechanical or vibration damping performance, and how to control and modify their properties as desired.

1.2. State of the art

This section summarizes the state of the art concerning to thermoplastic elastomers (TPEs) and the different approaches to obtain high-performance TPEs by blending rubber and thermoplastics, emphasizing on the preparation, structure and properties of TPV materials.

1.2.1. Thermoplastic elastomers (TPEs)

Thermoplastic elastomers (TPEs) are multi-functional polymeric materials that have the processing characteristics of thermoplastics, i.e. they can be processed by traditional melt manufacturing methods such as injection moulding and melt extrusion, while exhibiting the performance properties of conventional vulcanized rubbers [10, 11].

Figure 1.2 highlights the main differences when processing conventional rubbers and TPEs. As it can be seen in the figure, processing of TPE materials is simpler and more economical. Furthermore, TPEs offer the advantage of scrap and waste material recycling since they are not vulcanized during the fabrication into end-use parts [12, 13].
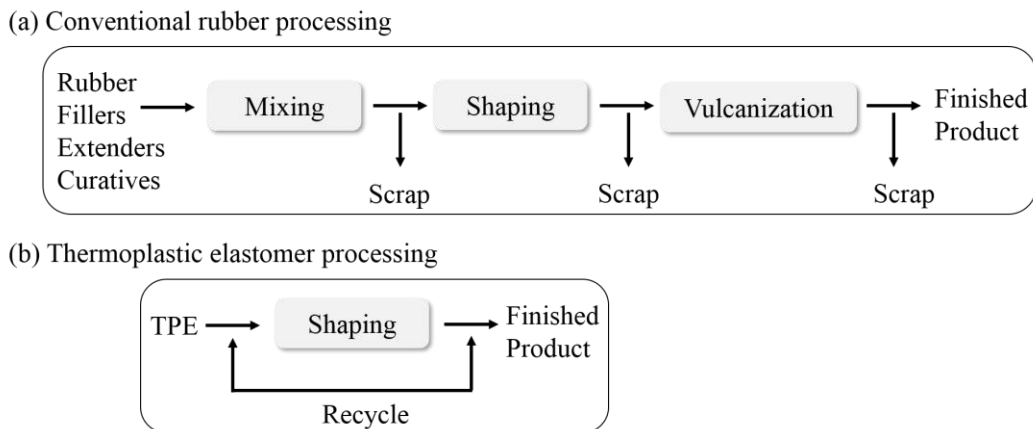
Figure 1.2. Comparison of (a) rubber and (b) TPE processing steps.

In recent years, TPEs are attracting a considerable attention, both in industry and in academia, and are becoming the fastest growing elastomers to replace unrecyclable vulcanized rubbers due to the requirements of environmental protection and resource savings [1].

Phase structure

The unique feature of TPE materials is their biphasic morphology, in which one phase is hard and solid at ambient temperature whereas the other is soft and rubbery in nature. The hard phase provides to the TPEs their strength, while the soft phase provides the elasticity and flexibility to the structure. Without the hard phase, the rubbery phase would be free to flow under stress and the polymeric material would not be functional. So, in some way, the hard phase acts as the crosslinking sites in conventional vulcanized rubbers. However, in comparison with vulcanized rubbers, the hard phase is based on physical interactive forces and gives to TPE materials the melt processability of thermoplastic polymers [14].

Both phases are thermodynamically immiscible and, consequently, act as individual phases. Thus, each phase exhibits its specific glass transition temperature (T_g) or crystalline melting temperature (T_m). As an example of the biphasic nature of TPEs, Figure 1.3 illustrates the change of the modulus with the temperature, where three different regions can be observed.

Below the T_g of the rubbery phase, both phases are hard and, therefore, the TPE material is stiff and brittle. Above its T_g the rubbery phase becomes soft and so the TPE presents an elastic behaviour, which is comparable to the behaviour of conventional vulcanized rubber. Finally, when the T_g or T_m of the hard phase is reached the TPE becomes fluid and so melt processable. Therefore, the service temperature range of TPE materials lies between the T_g of the rubbery phase and the T_g or T_m of the hard phase [15].

Classification

TPEs can be divided in two main categories, namely TPEs based on block copolymers and TPEs based on rubber-plastic blends. A-B-A triblock copolymers and $(A\text{-}B)_n$ multiblock copolymers are the two main types of block copolymer TPEs, whereas TPE blends, which are the focus of this PhD research work, can be divided into thermoplastic polyolefin blends (TPOs) and thermoplastic vulcanizates (TPVs) (Figure 1.4) [16].
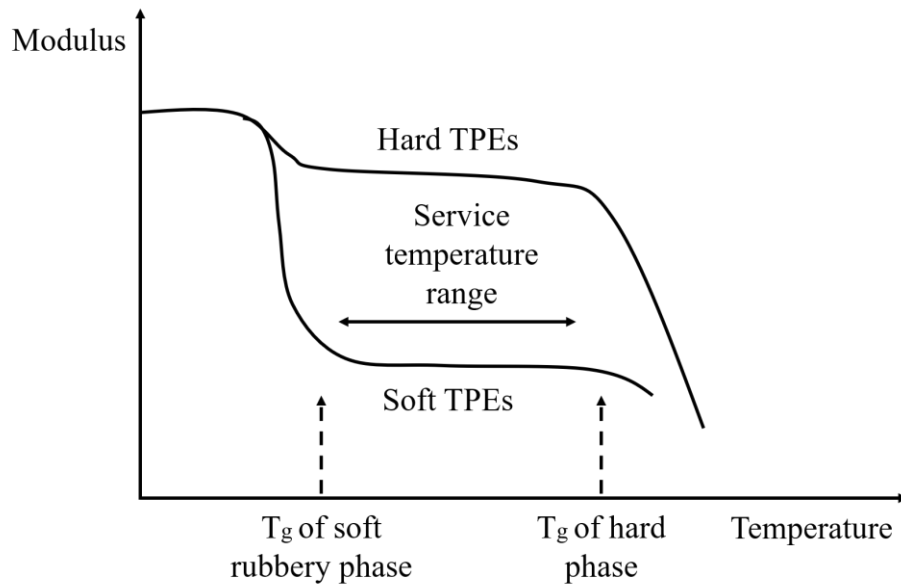
Figure 1.3. Stiffness of typical thermoplastic elastomers at various temperatures. The service temperature range is highlighted.
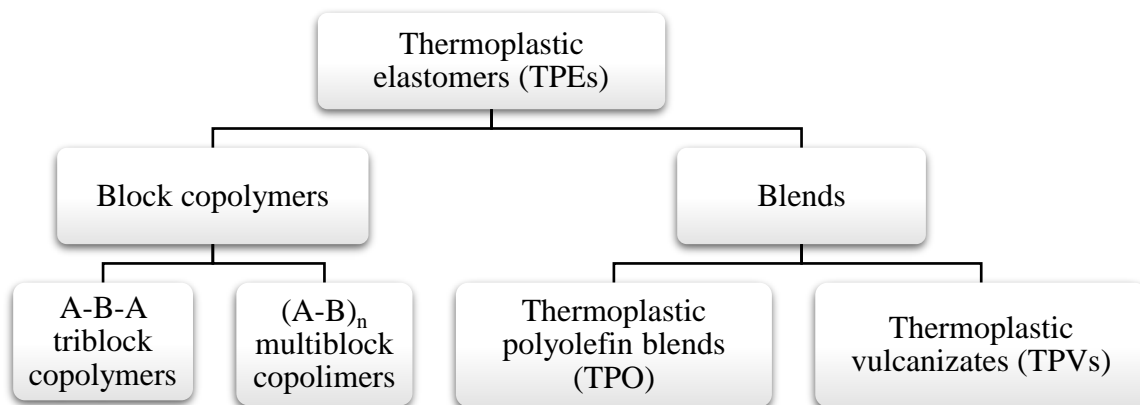
Figure 1.4. Classification of TPE materials.

TPEs based on A-B-A tri-block copolymers have two terminal hard blocks, that usually are polyesters, connected to a soft elastomeric central block. The most common triblock copolymer-type TPE is the polystyrene-block-polybutadiene-block-polystyrene (SBS) [17]. (A-B)$_n$ multiblock copolymers contain repeating hard and soft blocks. The most common multiblock copolymer-type TPEs are copolysters (COPE), copolyamides (COPA) and thermoplastic polyurethanes (TPU). Typically, soft blocks are based on polyethers and hard blocks on polyesters, polyamides or polyurethanes [18]. At service temperature, the hard blocks act as physical crosslinks between the soft blocks creating a three-dimensional network, as is schematically shown for a SBS copolymer in Figure 1.5.

Above the T_g or T_m of the hard blocks, the physical crosslinks disappear, and the copolymer becomes melt-processable [19].

TPE blends are defined as mechanical mixtures of rubbers and semi-crystalline thermoplastics [20]. The main difference between TPOs and TPVs is that the former are co-continuous biphasic systems with neither of the phases crosslinked whereas in the latter the rubber phase is crosslinked and dispersed in a semi-crystalline thermoplastic matrix (Figure 1.6) [21, 22]. The crosslinking of the rubber phase leads to TPEs with superior properties [23–25]. Commercial TPVs possess a high amount of crosslinked rubber particles ($\geq$ 50 wt%) and most of them are based on blends of ethylene-propylene-diene (EPDM) and polypropylene (PP).

The earlier classes of TPEs were based on block copolymers. However, TPE blends are becoming technologically more interesting because, unlike copolymer-type TPEs, both the rubber and thermoplastic phase in TPE blends are usually commercially available, and thus do not require development of new monomers or polymerization routes. Hence, blending represents a smart and economical way to develop new TPE materials.
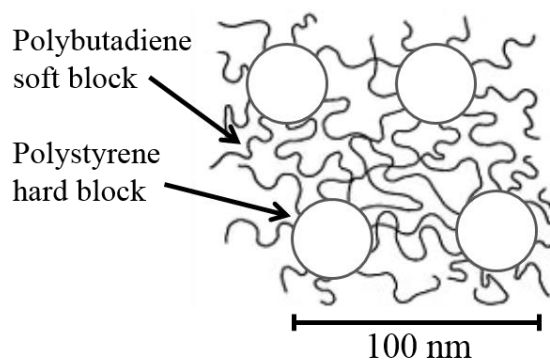
Figure 1.5. Schematic representation of the morphology of a SBS copolymer-type TPE material. The scale bar represents the phase separation length between the hard and soft phases, which usually is around 100 nm.
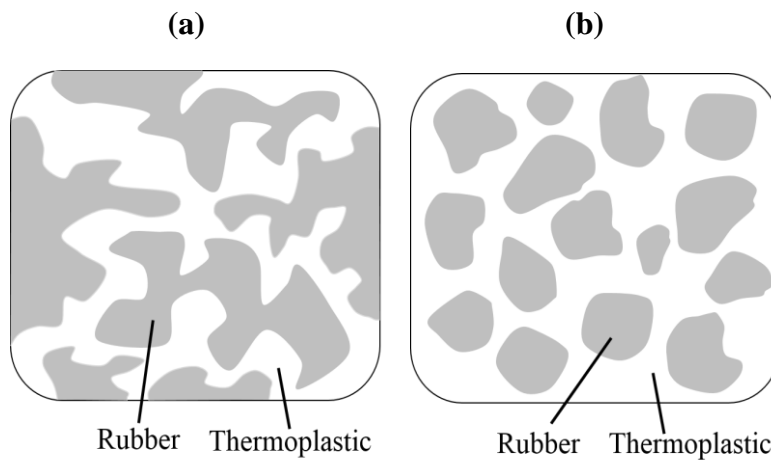
Figure 1.6. Schematic representation of the morphology of (a) TPOs and (b) TPVs.

1.2.2. Preparation of TPEs from rubber-thermoplastic blends

As explained earlier, the elastomeric properties of TPEs are the result of a hard-soft phase-separated structure, i.e., a heterogeneous morphology, which means that in TPE blends the rubber and thermoplastic materials must be thermodynamically not miscible.

Thermodynamics of phase separation

Miscibility is a thermodynamic term that defines the number of phases and the composition that is formed when blending a pair of polymers [26]. The state of miscibility of polymer blends is governed by the free energy of mixing (ΔG_m), which is defined as:

$$\Delta G_m = \Delta H_m - T \cdot \Delta S_m \tag{1.1}$$

where ΔH_m is the enthalpy of mixing, T is the absolute temperature and ΔS_m the entropy of mixing. A polymer blend is miscible if the free energy of mixing is negative, while immiscible if not. ΔS_m approaches to zero as the molecular weights of the components become large. So, when two high-molecular weight polymers are blended, the free energy of mixing will be negative only if the enthalpy of mixing is negative too. That means that, in order to obtain a completely miscible blend, the mixing must be exothermic, i.e., strong interactions are needed between the components [14].

Polymer blends can be classified in three groups in terms of miscibility: completely miscible, partially miscible and fully immiscible. A completely miscible blend presents a homogeneous morphology with a single T_g, whereas partially miscible and immiscible blends exhibit a heterogeneous morphology with at least two T_g values. Partially miscible blends, also known as compatible blends, present a fine phase morphology with part of one component dissolved in the other and T_g values that are dependent on the blend composition. On the other hand, fully immiscible blends exhibit a coarse morphology, sharp interface, poor adhesion between the blend phases, and T_g values that are independent of blend composition, which generally results in performance properties that are inferior to those of the pure components [27].

TPE blends with improved final properties can be obtained only if the rubber and thermoplastic are compatible [28] . But, most of high-molecular weight polymers are fully immiscible due to the low interactions that usually exist between them [29]. Therefore, in order to obtain a technologically useful TPE blend, surface energies of the rubber and thermoplastic phases need to be compatibilized, i.e., the surface energies need to be matched [30–35]. It is therefore necessary to consider the compatibilization of immiscible blends as a key strategy to develop new TPE blends with superior properties. Compatibilized immiscible blends can be prepared by adding interfacial active agents (physical blending) or through interfacial reactions (reactive blending) [36].

Physical blending

In physical blending, pre-made copolymers are synthetized prior to the blending operation, and subsequently added to an immiscible blend. Those copolymers are usually based on block or graft structures. The most widely used are the ones with blocky structures, being one constitutive block miscible with one of the blend components and the other block miscible with the other component. The addition of pre-made copolymers results in an anchoring in the respective homopolymers. Owing to its chemical and molecular characteristics, those copolymers are expected to be located at the interface between the two phases, reducing the interfacial tension and so improving their compatibility (Figure 1.7) [37].
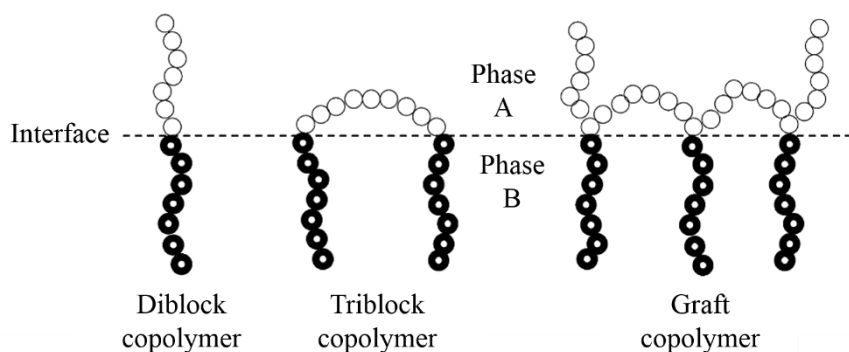
Figure 1.7. Schematic representation of the ideal location of diblock, triblock and graft copolymers at the interface of an immiscible A/B polymer blend.

Many works that analyse the use of copolymers as a strategy to prepare compatible TPE blends can be found in the literature [38–41]. However, this strategy seems not to be suitable in large-scale production due to the commercial unavailability of the materials and the high production cost of specific copolymers by synthesis. Moreover, the obtention of compatible blends by physical blending presents some technical limitations as well. The most important ones are the high viscosities of most block copolymers at the melt-blending temperature, which makes the copolymer diffusion to the interface difficult, and the formation of micelles prior to their location at the interface [42]. Due to these drawbacks, most of the actual efforts are directed to the obtention of TPE blends by reactive blending.

Reactive blending

Reactive blending is a cost-effective technique that is based on the formation of compatible blends by *in situ* chemical reactions that occur at the interface during the melt-mixing. For that, functional groups are incorporated onto the polymeric components of the blend. The chemical reactions between the functional groups generate block or graft copolymers just at the zone where they are needed, i.e., at the interface between the phases [43]. Consequently, the possibility for micelle formation is lower than in the physical blending, which results in a higher compatibilization effectiveness [44].

For most binary polymer blends, the appropriate reactive groups are not presented. In such cases a reactive polymer must be added as a third component of the blend [45]. The reactive polymer must fulfil two main conditions: needs to be miscible with one of the blend components and reactive with the other blend component (Figure 1.8). During melt-blending, the functional groups of the reactive polymer can react with the complementary groups of the other phase. This enables the formation of graft or block copolymers at the interface of the two phases and, consequently, the compatibilization of the immiscible binary blend [46].
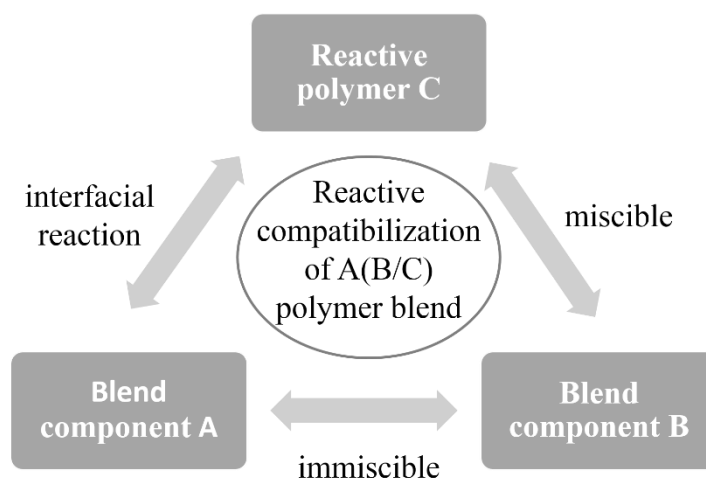
Figure 1.8. Schematic representation of the compatibilization strategy of an immiscible A/B blend using a third polymer (C) as reactive precursor.

Polyamides are one of the most extensively investigated polymers for reactive blending due to the high reactivity of their inherent amine and carboxylic functionalities [47, 48]. Several works have demonstrated that TPE blends obtained from reactive blends based on polyamides generate high levels of block or graft copolymers during the melt blending process [49–55].

The reactive blending of TPE blends can be carried out using either batch or continuous mixing machines. In a batch mixer the blending process is carried out within a single isolated volume. The most common batch mixing machine is the internal mixer, which is composed of two rotors that are enclosed in a mixing chamber [56]. On an industrial scale, TPE blends are typically fabricated using continuous extrusion processes due to the high flexibility that the extrusion process offers. The reactive blending by

extrusion is also known as reactive extrusion [43]. The most widely used continuous processing method for the preparation of TPE blends by reactive blending is the reactive extrusion by using co-rotating twin screw extruder machines [57].

Co-rotating twin screw extruder for reactive blending

The co-rotating twin-screw extruders are the most important commercial machines for the fabrication of TPEs by reactive blending. Besides, they are particularly suitable for the reactive blending between immiscible rubber and thermoplastics because they can cover the whole range of viscosities that each kind of polymer can have in a single reactor. This permits the fabrication of a wide range of TPE blend formulations. Different size twin-screw extruders which can cover production rates from laboratory scale levels up to industrial production levels are available in the market [58].

A co-rotating twin screw extruder is based on two shafts mounted with various screw-elements that are self-wiping in pairs. The self-wiping design cancels the stagnation of the materials and so its subsequent degradation during its flow along the twin-screw extruder. Screw elements can be divided into three categories depending on their mixing function: conveying, kneading and distributive. Conveying screw elements are used to transport the material, both in forward and reverse way. Kneading screw elements are used for melting, dispersing and homogenization. Distributive mixing elements homogenize the spatial distribution of the previously dispersed and homogenized blend components [59]. Figure 1.9 illustrates the effect of dispersive and distributive mixing in an immiscible blend.

The design of twin-screw extruders is based on a modular architecture having modular barrel and screws. This modular architecture provides a high versatility by facilitating the change of the length of different operations that can be done, such as the melting, mixing and homogenization operations, and also the change in screw configurations in order to achieve the optimum design for each kind of compound to be blended. Figure 1.10 shows a photograph of the two shafts mounted with a particular screw configuration.
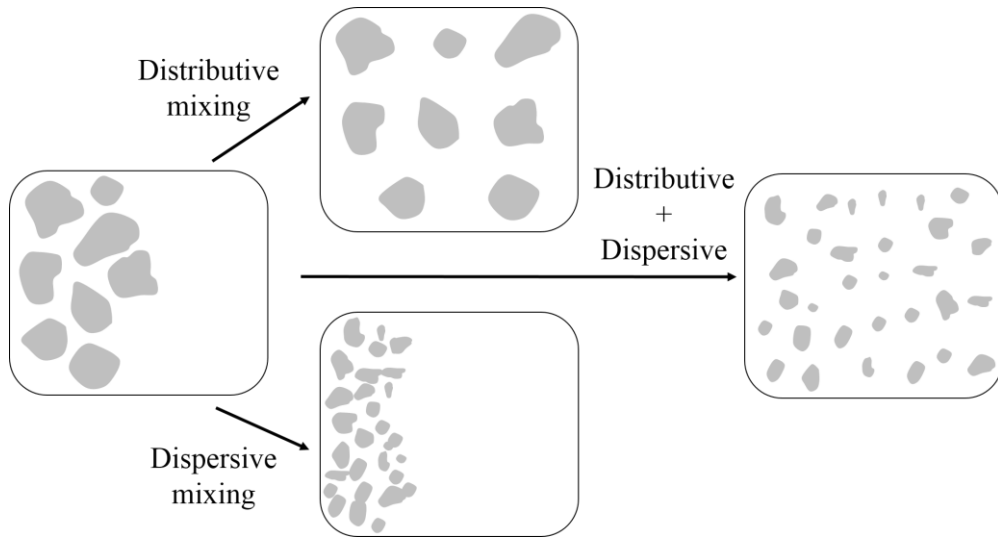
Figure 1.9. Schematic representation of distributive and dispersive mixing effects in immiscible blends.
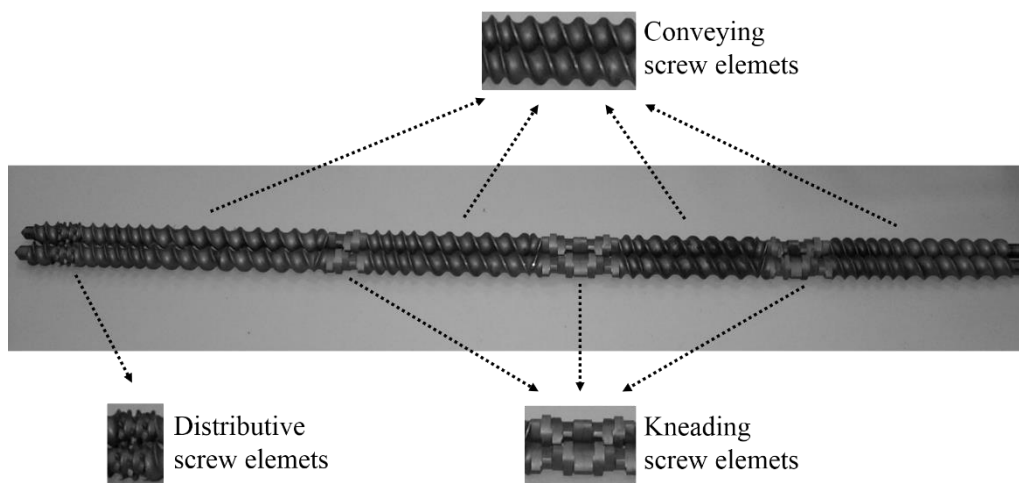
Figure 1.10. Photography of the two shafts mounted with modular screw elements.

1.2.3. Thermoplastic vulcanizates (TPVs)

After reviewing the general state of the art related to the preparation of TPEs from rubber-thermoplastic blends, this section will be entirely dedicated to TPVs, as they represent the central topic of this work.

Preparation of TPVs

TPVs are prepared by a complex reactive blending process characterized by the selective crosslinking of the rubber phase during the melt-blending with the thermoplastic under high shear conditions. This process is known as dynamic vulcanization because contrarily to the crosslinking of rubber materials that takes place under static conditions (applying pressure and temperature in a mould), the crosslinking of TPVs is done under high shear or dynamic conditions. The processing temperature must be high enough not only to melt the thermoplastic material but also to crosslink the rubber phase [60].

The idea of dynamic vulcanization process was claimed by Gessler in 1962 [61]. Ten years later, in 1972, Fisher produced the first TPV that was introduced to the market. This TPV was composed of a partially peroxide crosslinked ethylene propylene diene monomer rubber (EPDM) and polypropylene (PP). The rubber phase was partially crosslinked in order to ensure the melt-processability of the TPV material. In 1978, Coran and Patel were able to obtain TPVs that were melt-processable and acquire superior properties by fully crosslinking the rubber phase under dynamic shear [62]. In 1980 they carried out an extensive research on TPVs based on several thermoplastic-rubber mixtures [63, 64]. This research work was followed by the first commercialization of PP/EPDM TPVs by Monsanto (ExxonMobil) in 1981. This commercial TPV was named as "Santoprene" [65].

The evolution of the TPV material morphology during the dynamic vulcanization process is schematically shown in Figure 1.11. The selective crosslinking of the rubber phase causes the increase of its viscosity and so a change in the biphasic structure of the blend from a co-continuous morphology to a morphology based on crosslinked rubber droplets dispersed in a thermoplastic matrix. This change in the morphology is known as the phase inversion phenomena. Due to the phase inversion phenomena, a droplet matrix morphology can be obtained within a TPV material even if the rubber phase represents more than the 50 wt% of the blend. The applied high shear hinders the coalescence and causes the breakup of the rubber droplets, thus facilitating the obtention of the characteristic morphology of TPVs based on fine dispersion of crosslinked rubber particles in a thermoplastic matrix [66].
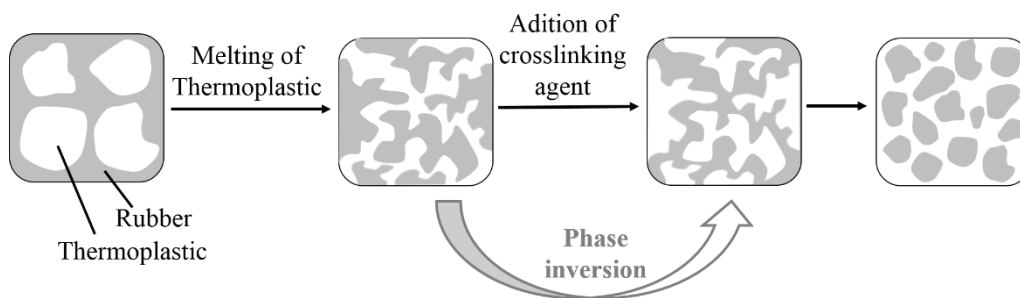
Figure 1.11. Schematic representation of the morphology development during the dynamic vulcanization process.

Figure 1.12 illustrates the two methods that are mostly used to prepare TPVs by means of the dynamic vulcanization process in recent times. The first method consists on the melt-blending of the rubber and thermoplastic materials and the following addition of the crosslinking agents. The melt-blending of the three components is continued under the same temperature and shear rate conditions in order to foment the dynamic vulcanization process and the further mixing of the rubber and thermoplastic phases to obtain a fine dispersion of rubber droplets. The second method comprises the cold-mixing of the rubber and the crosslinking agents and subsequent melt-blending of the premixed rubber compound with the thermoplastic material.
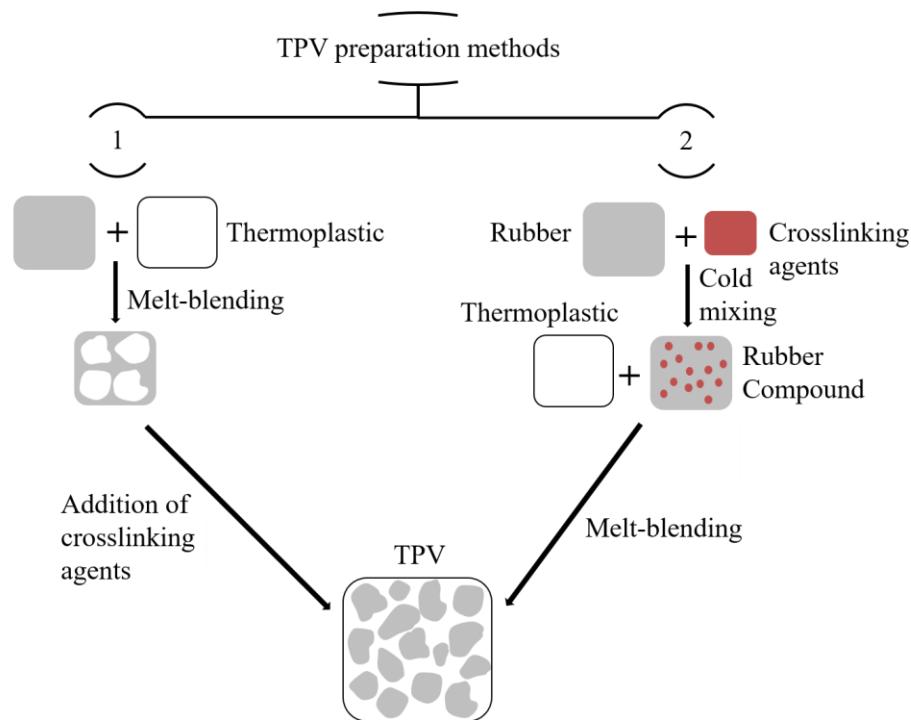
Figure 1.12. Schematic representation of the two major preparation methods of TPV.

Production of high-performance TPVs

Conventional TPVs, such as the ones made from PP and EPDM, exhibit a progressive change of their mechanical properties when exposed to heat and oil, i.e. they are not heat and oil resistant. High-performance TPVs, also known as special TPVs, possess good oil and high temperature resistance properties, consequently, they can operate under aggressive temperature and oil environmental conditions for prolonged time periods without any deterioration of their properties [67].

Over the past decade, many research works explored different strategies to produce high-performance TPVs and highlighted that the main aspects that determine the obtention of high-performance TPVs are the understanding and control of the relationship between the microstructure and the mechanical properties of the TPVs and the selection of high-performance rubber and thermoplastic materials.

Microstructure-mechanical properties relationship

The mechanical performance of TPVs is governed by their microstructural features [68]. Consequently, understanding the relations between microstructure and mechanical properties represents a key strategy to provide a guidance and encourage the field of high-performance TPVs development. The microstructure-mechanical properties of a TPV system depend on the following features:

1) Rubber/thermoplastic composition ratio

Many research works have revealed that a rubber to thermoplastic ratio larger than 1 is necessary to fabricate high-performance TPV systems [66, 69–72]. Usually, the rubber phase comprises more than 50 wt% of the compound in order to obtain TPVs with high elasticity due to the higher intrinsic elasticity of rubber materials [73, 74]. However, several studies revealed that the use of a high amount of rubber could cause an increase of the rubber particle size. For example, Chatterjee *et al.* [66] stated a significant increase of the rubber particle size when increasing the rubber content from 50 wt% to 70 wt% in carboxylated acrylonitrile butadiene rubber (XNBR)/polyamide 12 (PA12) TPV systems. The increase of the rubber particle size with increasing the rubber content is ascribed to the higher probability of coalescence during melt-mixing [75, 76]. On the other hand, several studies described that an increase of the thermoplastic content causes a decrease of the elongation at break of the TPV and an increase in the tensile strength. The stress-strain behaviour shifts to a more thermoplastic-like behaviour [77–79].

2) Size of the rubber particles

Several research works highlighted that a fine dispersion of rubber particles is needed to obtain TPVs with superior properties [80–84]. Usually, a decrease of the rubber particle size produces an improvement in the elastomeric properties by increasing the tensile strength, elongation at break and the elastic recovery capacity [85–88].

3) Crosslinking degree of the rubber phase.

Typically, an increase of the crosslinking degree generates a decrease of the rubber particle size [89–91]. The tensile strength, elongation at break and elasticity increase with the crosslink density of rubber phase. Nevertheless, several studies have found that an additional increase of the crosslinking agent content causes a deterioration of the properties [92–94]. Babu *et al.* studied the effect of peroxide concentration in PP/ethylene octene copolymer (EOC) TPV systems and found that the addition of high amount of peroxide provokes the formation of coarse rubber particles that may act as stress concentrators [93].

4) The rubber network structure

The addition of different types of crosslinking agents generates different rubber network structures [95–97]. For instance, Nakason *et al.* analysed the microstructure-mechanical properties relationship in epoxidized natural rubber (ENR)/PP TPVs containing different mixed crosslink systems. They observed that a rubber network structure comprising carbon-carbon (C-C), carbon-sufur (C-S) and sulfur-sulfur (S-S) crosslinks leads to TPVs with enhanced elongation at break and tensile strength [95].

5) The interfacial interaction between rubber and thermoplastic phases

As discussed in earlier sections, the compatibilization of the rubber and thermoplastic materials represents an essential step in order to obtain TPVs with improved properties. Generally, when interfacial interactions between the rubber and thermoplastic phases are created, a fine dispersion of the rubber particles is obtained, which leads to upgraded elastomeric properties [98–101].

6) Addition of fillers

Characteristically, the addition of fillers has a reinforcing effect on TPV materials and, therefore, causes an increase of tensile strength and modulus [102–105]. Besides, the addition of fillers may decrease the elasticity of TPVs [106].

7) Crystallinity degree of the thermoplastic phase

Generally, an increase of the crystallinity degree of the thermoplastic phase causes a decrease in the elasticity of TPVs [107, 108].

8) The thickness of the plastic ligaments of the thermoplastic phase

Interestingly, TPVs are able to deform elastically and with good elastic recovery capacity, even though their microstructure is based on a thermoplastic matrix (continuous phase) which is supposed to deform through a non-reversible plastic deformation. Several studies have demonstrated that the presence of thin plastic ligaments in the thermoplastic phase determines the deformation and elastic recovery ability of TPV materials [109–112]. Oderkerk *et al.* studied the deformation behaviour of polyamide 6 (PA6)/EPDM TPVs and demonstrated that the thinner the plastic ligaments are, the better the elastic recovery ability of TPVs is [109]. Therefore, the stretching of thin plastic ligaments in the thermoplastic matrix phase represents a key mechanism of the mechanical performance of TPVs [113, 114].

The strong influence of all the above-mentioned microstructural features on the mechanical properties has been proved by many studies, and so they represent crucial aspects to be controlled in order to obtain high-performance TPVs. However, in spite of the numerous research works on the characterization of the microstructure and the corresponding mechanical properties of TPV systems, the effects of the thermoplastic and rubber microstructural constituents in their mechanical behaviour are still not clear [68].

Selection of high-performance rubber and thermoplastics

The melt-blending of high-performance rubbers and thermoplastics represents an effective strategy to produce high-performance TPV compounds. Depending on the selected rubber and thermoplastic, high-performance TPVs can be classified as follows [115]:

1) High-performance TPVs composed of high-performance heat resistant thermoplastic materials such as polyethylene terephthalate and polyamide.

2) High-performance TPVs composed of high-performance heat resistant rubbers such as acrylate rubber, fluorinated rubber and hydrogenated nitrile rubber.

3) High-performance TPVs obtained by blending high-performance thermoplastic and rubbers. In this case they are named super-TPVs.

Table 1.2 presents a summary of the high-performance TPVs that have been studied and developed up to the present time.

Table 1.2. Review of high-performance TPVs.

TPVs	Blend components (thermoplastic/rubber)	Crosslinking agent	Distinctive property	Commercial availability	References
Silicone rubber (SiR) based (SiTPVs)	PA/ SiR; PVDF/ SiR; EOC/PDMS; PU/PDMS	Peroxide	Soft touch; outstanding heat and oil resistance	Commercialized by Dow Corning since 2004 under the trade name TPsiV®.	[116–124]
Acrylic rubber (ACM) based	PA6/ACM; PBT/ACM; PET/ACM; PLA/ACM; PVDF/ACM; PP/ACM	Hexamethylenediamine carbamate (HMDC)	Good heat and oil resistance	PA6/ACM Zeotherm® TPV commercialized by Zeon since 2002	[125–127]
Nitrile-butadiene rubber (NBR) based	PP/NBR	Phenolic resin; peroxide	Outstanding oil resistance, mechanical properties and processability	-	[128–131]
Ethylene-vinyl acetate rubber (EVM) based	EVA/EVM; PVDF/EVM; TPU/EVM	Peroxide	Good heat and oil resistance	-	[132–135]
Isobutylene-isoprene rubber (IIR) based	PA/IIR, PP/IIR	Sulfur; peroxide; N, N'-m-phenylene dismaleimide/zinc oxide(ZnO); zinc diethyldithiocarbamate (ZDEDC)/ZnO	Outstanding gas barrier properties	-	[136–140]
Hydrogenated nitrile rubber (HNBR) based	PA/HNBR; PA/XNBR	Peroxide; phenolic resin	High temperature and oil resistant; outstanding mechanical properties	-	[115, 141, 142]
Fluorinated rubber (FKM) based	PA6/FKM; PP/FKM; PVDF/FKM	Hexamethylenediamine carbamate (HMDC); peroxide	Excellent mechanical properties; good oil and heat resistance	PVDF/FKM Fluoroprene® TPV commercialized by Freudenberg-Nok since 2003	[143–148]

ACM, acrylic rubber; EVA, ethylene-co-vinyl acetate copolymer (VA content<50%); EVM, ethylene-vinyl acetate rubber (the content of vinyl acetate (VA) is 50%); FKM, fluoroelastomer; HNBR, hydrogenated acrylonitrile butadiene rubber; NBR, nitrile butadiene rubber; PA, polyamide; PBT, poly(butylene terephthalate); PDMS, polydimethylsiloxane silicone rubber; PET, polyethylene glycol terephthalate; PLA, poly (Lactic acid); PU, polyurethane; PVDF, poly(vinylidene fluoride); TPU, thermoplastic polyurethanes;.

Among all of the analysed high-performance TPV systems, PA6/HNBR based TPVs represent an interesting choice for the development of high-performance TPVs with vibration damping properties due the outstanding dynamic performance of HNBR rubbers (Figure 1.13) [149]. However, no research work has been found in literature that studies the formulation of PA6/HNBR high-performance TPVs for vibration damping applications.
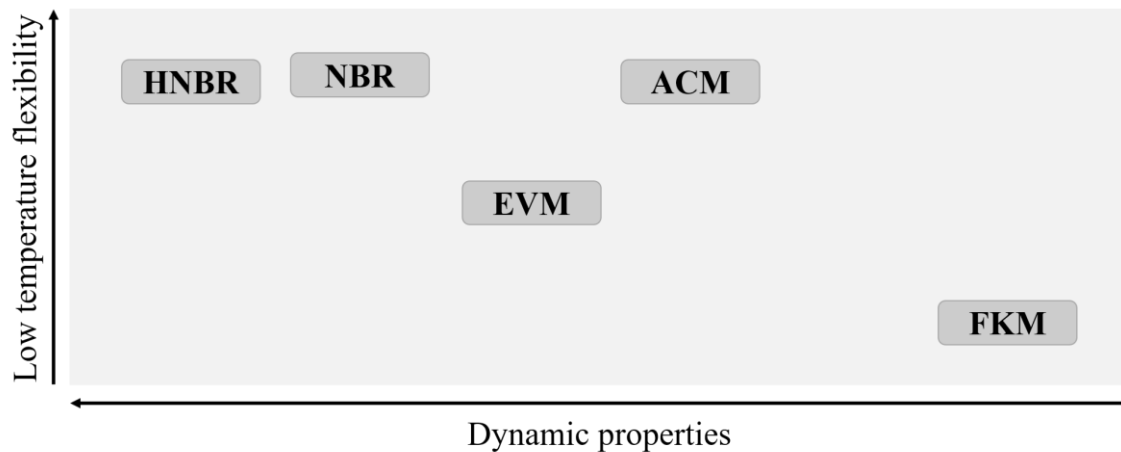
Figure 1.13. Comparison of the dynamic properties of various high-performance rubbers.

HNBR is produced by catalytic hydrogenation of NBR (Figure 1.14). HNBR rubbers with a broad range of final properties can be obtained by changing the amount of acrylonitrile, the hydrogenation level and the molecular weight. Regarding to the crosslinking agents, HNBR is commonly cured by using peroxides because, compared with the sulfur crosslinking, the peroxide crosslinking leads to rubbers with good high temperature resistance and elastic recovery capacity. HNBR rubbers crosslinked with peroxide are able to retain their properties for long term periods of time over the temperature range from -40 to 150 °C [150].

Bayer was the first company in introducing HNBR to the market under the trade name of Therban. Currently, different Therban grades are supplied by Arlanxeo. Figure 1.15 illustrates a comparison of Therban with other high-performance rubbers. Due to its outstanding properties Therban HNBR is mainly used in automotive components such as belts, hoses and dynamic seals [151].
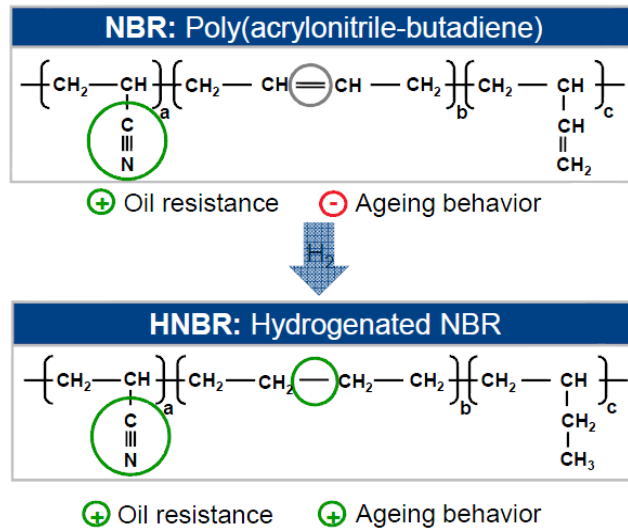
Figure 1.14. Chemical structure of NBR and HNBR.
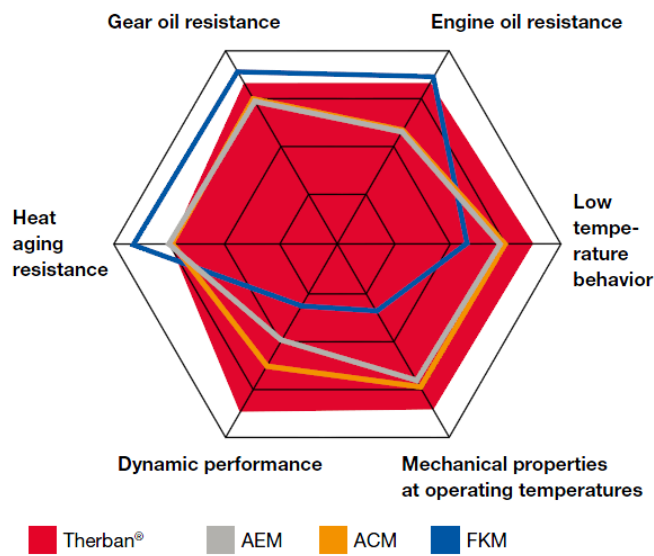
Figure 1.15. Comparison of the properties of Therban HNBR with other high-performance rubbers.

1.3. Objectives of the thesis

The electrification of vehicles is adding new challenges to transport industry related with the noise and vibration of the different vehicle components. As the elimination of the internal combustion engine will eliminate the noise generated by it, the noise generated by many lightweight components that are susceptible to vibrate will become more apparent and so, not comfortable. Consequently, it exists a demand for new solutions based on advanced vibration damping materials that enable multi-material and lightweight designs.

Driven by these demands, the main objective of this thesis is to generate knowledge for the design and development of high-performance thermoplastic vulcanizates (TPVs) with vibration damping properties. For that, TPE blends of HNBR with PA6 have been developed and the relationship between their microstructure and their properties analysed. HNBR and PA6 are two polymeric materials with excellent chemical, wear and heat resistant properties. Therefore, blending HNBR and PA6 would be encouraging in the field of high-performance TPVs that are increasingly replacing traditional vulcanized elastomers. Besides, HNBR rubbers possess remarkable vibration damping properties. Hence, PA6/HNBR blends represent an interesting choice for the development of high-performance TPVs with vibration damping properties.

The main objectives and hypotheses that are covered in the papers published in the thesis are summarized below.

- The objective of the first paper of the thesis entitled "Toward superior applications of thermoplastic elastomer blends: double T_g increase and improved ductility" was to investigate the potential of reactive compatibilization of PA6/HNBR blends by means of carboxylated HNBR (XHNBR) addition. Carboxylic HNBR (XHNRB) has been considered as a potential compatibilizer since is miscible with HNBR and the carboxyl functionalities can react with the amine end groups of PA6, while melt blending. As the glass transition temperature (T_g) is one of the most important properties that governs the service temperature and viscoelastic damping performance range of TPE blends, the main focus was put on the relationship between morphology, phase interactions and glass transition behaviour. A

fundamental understanding of this relationship would let to an effective control of the ultimate performance characteristics of the developed TPE blends.

- The aim of the second paper of the thesis entitled "New ways to improve the damping properties in high-performance thermoplastic vulcanizates" was to explore novel strategies to improve the vibration damping properties of high-performance TPVs. Based on the hypothesis that the addition of metal oxides and hindered phenolic antioxidants can improve the vibration damping properties of carboxylic rubbers, such as XHNBR, via ionic and hydrogen bond generation, the potential of these approaches to enhance the vibration damping performance of peroxide cured TPVs based on PA6 and XHNBR has been explored. The investigated strategy represents a completely new method to develop high-performance vibration damping TPV materials.

- Finally, the main objective of the third paper of the thesis entitled "Experimental investigation of the nonlinear quasi-static and dynamic mechanical behaviour of novel thermoplastic vulcanizates based on PA6 and carboxylated HNBR: linking mechanical nonlinearities to microstructural features" was to obtain a more fundamental understanding of the relationship between the microstructure and the nonlinear quasi-static and dynamic mechanical behaviour of TPV materials. In particular, the impact of different microstructural features of the PA6 matrix and the rubber network on the mechanical behaviour has been investigated with the aim of identifying the underlying microstructural features involved in their micromechanical deformation processes. A detailed knowledge about the correlation between the nonlinear behaviour and the microstructural features is needed to ensure a competitive and confident application of designed TPV materials.

1.4. Results and discussion

A summary of the key experimental results achieved in the thesis, and their discussion, is presented below.

Reactive compatibilization of PA6/HNBR TPE blends

In the first part of the thesis, the reactive blending approach has been explored as an effective technique for improving the compatibility of PA6/HNBR TPE blends. Carboxylic HNBR (XHNRB) has been considered as potential compatibilizer since it is miscible with HNBR and the carboxyl functionalities can react with the amine end groups of PA6, while melt blending. As the final properties of polymer blends are mainly dependent of the morphology and the adhesion between the components, the effect of XHNBR on the phase morphology and interfacial interactions has been investigated.

Four TPEs have been prepared by melt blending of hydrogenated acrylonitrile butadiene rubber (HNBR) with polyamide 6 (PA6) in a co-rotating twin screw extruder, adding different amounts of carboxylated HNBR (XHNBR) as compatibilizer: 40/60/0, 40/42/18, 40/30/30 and 40/18/42 (PA6/HNBR/XHNBR). The resulting blends were investigated using melt rheological measurements, morphological observations (scanning electron microscopy and polarized optical microscopy), dynamic mechanical analysis (DMA), differential scanning calorimetry (DSC) analysis and mechanical tests.

Regarding the phase morphology, dispersed spherical particles of rubber in PA6 matrix were generated in the uncompatibilized sample, i.e. the sample without XHNBR. With the addition of 18% of XHNBR a decrease in the rubber particle size was observed. This has been attributed to the generation of interfacial interactions, via chemical reactions between the carboxyl groups in XHNBR and amide end groups in PA6, that lower the interfacial tension between the rubber and thermoplastic phases. Interestingly, reactively compatibilized TPE blend with co-continuous morphology has been obtained with the addition of 42% of XHNBR.

The investigation of the variation of the complex viscosity and storage modulus of the blends components as a function of the angular frequency at the temperature and shear rate of melt-blending condition, indicated that the addition of XHNBR increases both the

viscosity and elasticity of the rubber phase. Based on this result, models that attempt to predict the phase inversion phenomena in melt-mixed immiscible polymer blends by determining the viscosity and elasticity ratios have been considered and tested. It was observed that by increasing the XHNBR content, the elasticity effects become more important than the viscous ones. Therefore, melt-linear rheological measurements demonstrated that the generation of a co-continuous morphology was mainly caused by the increase of the elasticity of the rubber phase with the addition of XHNBR.

Melt-linear rheology permitted to determine the enhancement of the interfacial interactions. The characterization of the critical stress, estimated as the stress values when the storage modulus is equal to 95% of the plateau, enabled to determine the effect of XHNBR content on the adhesion between the blend components. An increase of the critical stress value with the increase of XHNBR content was observed, which is indicative of the effectiveness of the reactive blending approach.

Mechanical characterization also enabled to establish the enhancement of interfacial interactions and the change of morphology from droplet-matrix to co-continuous revealed by scanning electron microscopy (SEM) and melt-linear rheology measurements. When the reactively compatibilized blend with co-continuous morphology was considered, the obtained elongation at break was 16 times higher than that of the uncompatibilized blend. Thus, a significant brittle to ductile transition was obtained due to the generation of interfacial interactions. The co-continuous morphology was evidenced by the reduction of the hardness with the addition of 42% XHNBR.

The enhancement of the interfacial interactions with the XHNBR addition was also evidenced by the remarkable decrease in crystallinity of PA6 demonstrated by the reactively compatibilized blend with co-continuous morphology. Furthermore, DMA allowed to evaluate the effect of XHNBR content in the glass transition temperature (T_g), which not only determines the service temperature range but also the range of viscoelastic damping performance. A curious double T_g increase phenomenon was noted with the introduction of 42% XHNBR, which has been attributed to a decrease in the mobility of the amorphous domains, of both the PA6 and the rubber phase, caused by the interfacial interactions between the phases.

Novel strategy to design TPVs with improved vibration damping properties

Carboxytated rubbers, such as XHNBR, are interesting materials for vibration damping applications because the addition of different crosslink types allows to customize their vibration damping properties within a wide range of temperature and frequencies. For these reasons, and because hardy any work that analyses the use of carboxylated rubbers to develop viscoelastic damping TPV materials is present in literature, in the second part of the thesis, the dynamic vulcanization of TPEs based on PA6 and HNBR by means of mixed-crosslink systems has been explored.

Several TPVs have been prepared by dynamically vulcanizing the reactively compatibilized TPE blend with co-continuous morphology, i.e. the one with 42% of XHNBR, using mixed crosslink systems of peroxide with metal oxides and hindered phenolic antioxidants. Peroxides provide good properties at high temperatures due to the high bond energy of covalent bonds, whereas metal oxides and hindered phenolic antioxidants improve the damping performance via ionic and hydrogen bonds, respectively. The selected metal oxides were zinc oxide (ZnO) and magnesium oxide (MgO), whereas the selected hindered phenolic antioxidants were Irganox 1010 and Irganox 1098. The developed TPVs were studied by means of SEM, DMA, Fourier Transform Infrared (FTIR) spectroscopy, DSC and tensile test analysis.

The characterization of the phase morphology through SEM analysis showed a droplet-matrix morphology with crosslinked rubber particles in the micron level for all developed TPV compounds. Phase separation was induced by the selectively crosslinking of the rubber phase that results in an abrupt increase of its viscosity.

The vibration damping performance of the designed high-performance TPVs has been investigated through DMA characterization and measuring the loss tangent (*tan δ*). It was observed that the TPV compounds with MgO and ZnO showed an additional relaxation transition peak near room temperature associated with the relaxation transition of ionic bonds. This ionic transition was particularly evident for the TPV system containing the higher amount of MgO. In the case of the TPVs containing Irganox 1010 and Irganox 1098, it was shown that the addition of Irganox 1010 increases the *tan δ* peak height of both rubber and thermoplastic phases, whereas the addition of Irganox 1098 decreases the *tan δ* peak height of the rubber phase dramatically. Interestingly, the peroxide cured

PA6/XHNBR TPV systems containing 5 phr of both Irganox 1010 and MgO showed enhanced vibration damping properties.

FTIR spectroscopy measurements allowed to identify the multiple-network structure based on C-C, ionic and hydrogen bonds that was developed by the dynamic vulcanization via mixed crosslink systems. The investigation of the rubber network structure by means of FTIR analysis revealed the creation of carbon-carbon (C-C) crosslinks in all the TPV samples. Moreover, FTIR studies showed also that Irganox 1098 acts mainly as an inorganic filler, not being coupled with the carboxyl functionalities present in the rubber phase, whereas Irganox 1010 forms hydrogen bonds with XHNBR. Moreover, FTIR measurements confirmed the generation of ionic crosslinks in the PA6/XHNBR TPVs comprising 5 phr of MgO.

In regard to DSC and tensile test results, the TPV systems containing 5 phr of both Irganox 1010 and MgO showed the lowest crystallinity degrees together with greater elastomeric properties, which is further evidence of the strong hydrogen bonding and ionic interactions formed with the carboxylic rubber phase.

Physical mechanisms involved in the mechanical behaviour of TPVs

One of the scientific issues on TPVs that remains open is the understanding of the deformation and recovery mechanisms, and the roles of the plastic and rubber phases in the mechanical behaviour. With the aim of contributing to the further understanding of these questions, the third part of the thesis was focused on the study of the relationship between microstructural features of TPVs and their non-linear quasi-static and dynamic mechanical behaviour.

To carry out this research work, the two peroxide cured TPV compounds that showed the best vibration damping properties, i.e. the ones containing 5 phr of Irganox 1010 and MgO, have been considered. Therefore, one of the analysed TPVs contains a rubber network structure based on C-C and hydrogen bonds, while the other possess a rubber network structure formed by C-C and ionic bonds. The microstructural and mechanical performance properties of the mentioned TPV samples were explored through SEM, DSC, monotonic tensile, cyclic tensile and DMA measurements.

The investigation of the crosslinking densities of the rubber network through DSC measurements revealed a lower peroxide crosslinking degree for the TPV sample containing 5 phr of Irganox 1010. For the TPV sample containing 5 phr of Irganox 1010 only an 85% of the peroxide curing agent was activated, whereas in the TPV containing 5 phr of MgO a 94% of peroxide crosslinking density was obtained. DSC measurements also enabled to determine the crystallinity degree and the thickness of the crystalline lamellae, two key microstructural features of the thermoplastic phase that have impact on the mechanical behaviour of TPVs. It was shown that both TPV samples possess similar crystallinity degree and crystalline lamellae thickness.

Regarding the monotonic tensile behaviour, TPV samples displayed a stress-strain curve that lay in between the curve of pure PA6 and the curve of pure rubber. The stress-strain behaviour of the TPV samples was a combination of the deformation behaviour of the thermoplastic phase at low strain levels and that of the rubber phase at high strain levels. It was found that the stiffness of TPVs was similar due to their similar crystallinity degree. Concerning to the high strain behaviour, it was proved that the formation of a rubber network structure compromising high amount of C-C linkages and ionic crosslinks leads to a TPV with enhanced tensile strength and elongation at break.

Cyclic tensile stress-strain measurements revealed a similar cyclic stress softening (also known as Mullins effect), hysteresis loss and permanent set for both TPV samples below 30% strain level. This has been attributed to the similar PA6 phase crystallinity degree and crystalline lamellae thickness that both TPVs possess, which was demonstrated by means of DSC measurements. Above 30% of strain level the TPV sample containing C-C and ionic bonds exhibited a less significant stress softening.

It was proposed that in order to explain the different cyclic stress softening effects that both TPV compounds show above the 30% strain level, the rubber phase needs to be modelled as a two-network structure formed by covalent and non-covalent bonds. Although both TPV samples contain rubber network structures formed by covalent and non-covalent bonds, their structure differs in the amount of covalent bonds and the strength of the non-covalent bonds (ionic bonds are stronger than hydrogen bonds). Therefore, based on the proposed physical interpretation, the less significant stress softening effect displayed by the peroxide cured TPV sample containing 5phr MgO was

attributed to the better elastic recovery capacity of the rubber network structure formed by a higher amount of covalent C-C linkages and stronger non-covalent bonds.

The differences in the mechanical deformation behaviour, observed by quasi-static mechanical test, were confirmed by SEM analysis. SEM micrographs proved that in the TPV containing C-C and ionic bonds the development of plastic voids and rubber cavitation was suppressed.

Based on the experimental findings, a micromechanical deformation model was proposed. The observed micromechanical processes have been interpreted in terms of the yielding, buckling and bending of thin PA6 ligaments at low strain levels and the rupture of covalent and non-covalent bonds presented in the rubber network at high strain levels. The proposed micromechanical deformation model was able to reflect the full complexity of the nonlinear dynamic mechanical behaviour of both TPV samples.

1.5. References

1. Ellis P (2019) Current and Future Thermoplastic Elastomers Market 2019 to 2025. Presented at the Thermoplastic Elastomers World Summit, Vienna
2. Ellis P (2019) The current and future market for thermoplastic elastomers in automotive applications. TPE Magazine International 11:226–229
3. Transport greenhouse gas emissions. In: European Environment Agency. https://www.eea.europa.eu/airs/2018/resource-efficiency-and-low-carbon-economy/transport-ghg-emissions.
4. Population. In: United Nations. https://www.un.org/en/sections/issues-depth/population/index.html.
5. 2050 long-term strategy. In: Climate Action - European Commission. https://ec.europa.eu/clima/policies/strategies/2050_en.
6. Jung F (2019) 5th International ATZ Conference on Vehicle Acoustics. ATZ Worldw 121:76–77
7. Eisele G, Kauth M, Steffens C, Glusk P (2019) Automotive megatrends and their impact on NVH. In: Bargende M, Reuss H-C, Wagner A, Wiedemann J (eds) 19. Internationales Stuttgarter Symposium. Springer Fachmedien, Wiesbaden, pp 523–539
8. Huang HB, Wu JH, Huang XR, Yang ML, Ding WP (2020) A generalized inverse cascade method to identify and optimize vehicle interior noise sources. Journal of Sound and Vibration 467:115062
9. Bein T, Bös J, Mayer D, Melz T (2012) 10 - Advanced materials and technologies for reducing noise, vibration and harshness (NVH) in automobiles. In: Rowe J (ed) Advanced Materials in Automotive Engineering. Woodhead Publishing, pp 254–298
10. Spontak RJ, Patel NP (2000) Thermoplastic elastomers: fundamentals and applications. Current Opinion in Colloid & Interface Science 5:333–340
11. Bhowmick AK (ed) (2008) Current topics in elastomers research. CRC Press, Boca Raton, Fla.
12. Coran AY, Patel RP (1995) Thermoplastic elastomers by blending and dynamic vulcanization. In: Karger-Kocsis J (ed) Polypropylene Structure, blends and composites: Volume 2 Copolymers and Blends. Springer Netherlands, Dordrecht, pp 162–201
13. McKeen LW (2010) Chapter 10 - Thermoplastic Elastomers. In: McKeen LW (ed) Fatigue and Tribological Properties of Plastics and Elastomers (Second Edition). William Andrew Publishing, Oxford, pp 245–247
14. Drobny JG (2014) Handbook of thermoplastic elastomers, 2. ed. Andrew, Elsevier, Oxford
15. Kutz M (ed) (2017) Applied plastics engineering handbook: processing, materials, and applications, Second edition. Elsevier/William Andrew, Amsterdam Boston Heidelberg
16. Naskar K, Babu RR (2015) Thermoplastic Elastomers (TPEs) and Thermoplastic Vulcanizates (TPVs). In: Kobayashi S, Müllen K (eds) Encyclopedia of Polymeric Nanomaterials. Springer Berlin Heidelberg, Berlin, Heidelberg, pp 2517–2522
17. Holden G (2000) Understanding thermoplastic elastomers. Hanser [u.a.], Munich
18. Holden G, Kricheldorf HR, Quirk RP (eds) (2004) Thermoplastic elastomers, 3. ed. Hanser, Munich

19. Fakirov S (ed) (2005) Handbook of Condensation Thermoplastic Elastomers, 1st ed. https://doi.org/10.1002/3527606610

20. De SK (ed) (1990) Thermoplastic elastomers from rubber plastic blends. Horwood, New York

21. Babu RR, Naskar K (2010) Recent Developments on Thermoplastic Elastomers by Dynamic Vulcanization. In: Heinrich G (ed) Advanced Rubber Composites. Springer Berlin Heidelberg, Berlin, Heidelberg, pp 219–247

22. Paul DR (ed) (2000) Polymer blends. Wiley, New York

23. Banerjee SS, Bhowmick AK (2015) Dynamic vulcanization of novel nanostructured polyamide 6/ fluoroelastomer thermoplastic elastomeric blends with special reference to morphology, physical properties and degree of vulcanization. Polymer 57:105–116

24. Sun Z, Zhang Y, Shao H, He A (2019) In situ reactive compatibilization of polypropylene/trans-1,4-poly(isoprene-co-butadiene) rubber (TBIR) blends with balanced toughness and stiffness via dynamic vulcanization. Reactive and Functional Polymers 142:60–68

25. Chatterjee T, Basu D, Das A, Wiessner S, Naskar K, Heinrich G (2016) Super thermoplastic vulcanizates based on carboxylated acrylonitrile butadiene rubber (XNBR) and polyamide (PA12). European Polymer Journal 78:235–252

26. Ajitha A.R., Thomas S (2020) Introduction. In: Compatibilization of Polymer Blends. Elsevier, pp 1–29

27. Sarath CC, Shanks RA, Thomas S (2014) Polymer Blends. In: Nanostructured Polymer Blends. Elsevier, pp 1–14

28. Adeniyi A, Agboola O, Sadiku ER, Durowoju MO, Olubambi PA, Babul Reddy A, Ibrahim ID, Kupolati WK (2016) Thermoplastic-Thermoset Nanostructured Polymer Blends. In: Design and Applications of Nanostructured Polymer Blends and Nanocomposite Systems. Elsevier, pp 15–38

29. Utracki LA (2002) Compatibilization of Polymer Blends. Can J Chem Eng 80:1008–1016

30. Datta Sarma A, Padmanathan HR, Saha S, Shankar Banerjee S, Bhowmick AK (2017) Design and properties of a series of high-temperature thermoplastic elastomeric blends from polyamides and functionalized rubbers: ARTICLE. J Appl Polym Sci 134:45353

31. Saha S, Bhowmick AK (2017) Computer aided simulation of thermoplastic elastomer from poly (vinylidene fluoride)/hydrogenated nitrile rubber blend and its experimental verification. Polymer 112:402–413

32. Jung HS, Choi MC, Chang Y-W, Kang P-H, Hong SC (2015) Facile preparation of thermoplastic elastomer with high service temperature from dry selective curing of compatibilized EPDM/polyamide-12 blends. European Polymer Journal 66:367–375

33. Hashim F, Ismail H, Rusli A (2017) Comparison of properties of ethylene vinyl acetate/natural rubber/mengkuang leaf fibre (EVA/NR/MLF) and ethylene vinyl acetate/epoxidized natural rubber/mengkuang leaf fibre (EVA/ENR-50/MLF) thermoplastic elastomer composites. Polymer Testing 61:1–7

34. Valerio O, Misra M, Mohanty AK (2018) Statistical design of sustainable thermoplastic blends of poly(glycerol succinate-co-maleate) (PGSMA), poly(lactic acid) (PLA) and poly(butylene succinate) (PBS). Polymer Testing 65:420–428

35. Xu C, Yuan D, Fu L, Chen Y (2014) Physical blend of PLA/NR with co-continuous phase structure: Preparation, rheology property, mechanical properties and morphology. Polymer Testing 37:94–101

36. Shanks RA (2020) Concepts and classification of compatibilization processes. In: Compatibilization of Polymer Blends. Elsevier, pp 31–56

37. Spontak RJ, Ryan JJ (2020) Polymer blend compatibilization by the addition of block copolymers. In: Compatibilization of Polymer Blends. Elsevier, pp 57–102

38. Komalan C, George KE, Varughese KT, Mathew VS, Thomas S (2008) Thermogravimetric and wide angle X-ray diffraction analysis of thermoplastic elastomers from nylon copolymer and EPDM rubber. Polymer Degradation and Stability 93:2104–2112

39. Panigrahi H, Sreenath PR, Bhowmick AK, Dinesh Kumar K (2019) Unique compatibilized thermoplastic elastomer from polypropylene and epichlorohydrin rubber. Polymer 183:121866

40. Liu X, Huang H, Xie Z, Zhang Y, Zhang Y, Sun K, Min L (2003) EPDM/polyamide TPV compatibilized by chlorinated polyethylene. Polymer Testing 22:9–16

41. Papke N, Karger-Kocsis J (2001) Thermoplastic elastomers based on compatibilized poly(ethylene terephthalate) blends: effect of rubber type and dynamic curing. Polymer 42:1109–1120

42. Adedeji A, Lyu S, Macosko CW (2001) Block Copolymers in Homopolymer Blends: Interface vs Micelles. Macromolecules 34:8663–8668

43. Imre B, García L, Puglia D, Vilaplana F (2019) Reactive compatibilization of plant polysaccharides and biobased polymers: Review on current strategies, expectations and reality. Carbohydrate Polymers 209:20–37

44. Koning C (1998) Strategies for compatibilization of polymer blends. Progress in Polymer Science 23:707–757

45. Dedecker K, Groeninckx G (1998) Reactive compatibilisation of A/(B/C) polymer blends. Part 1. Investigation of the phase morphology development and stabilisation. Polymer 39:4985–4992

46. Zeng J-B, Li K-A, Du A-K (2015) Compatibilization strategies in poly(lactic acid)-based blends. RSC Adv 5:32546–32565

47. Macosko CW, Jeon HK, Hoye TR (2005) Reactions at polymer–polymer interfaces for blend compatibilization. Progress in Polymer Science 30:939–947

48. Harrats C, Groeninckx G (2004) Reactive Processing Of Polymer Blend Using Reactive Compatibilization And Dynamic Crosslinking: Phase Morphology Control And Microstructure – Property Relations. In: Ciardelli F, Penczek S (eds) Modification and Blending of Synthetic and Natural Macromolecules. Springer Netherlands, Dordrecht, pp 155–199

49. Jung HS, Choi MC, Chang Y-W, Kang P-H, Hong SC (2015) Facile preparation of thermoplastic elastomer with high service temperature from dry selective curing of compatibilized EPDM/polyamide-12 blends. European Polymer Journal 66:367–375

50. Banerjee SS, Bhowmick AK (2013) Novel nanostructured polyamide 6/fluoroelastomer thermoplastic elastomeric blends: Influence of interaction and morphology on physical properties. Polymer 54:6561–6571

51. Bhowmick AK, Chiba T, Inoue T (1993) Reactive processing of rubber–plastic blends: Role of chemical compatibilizer. J Appl Polym Sci 50:2055–2064

52. Chatterjee T, Basu D, Das A, Wiessner S, Naskar K, Heinrich G (2016) Super thermoplastic vulcanizates based on carboxylated acrylonitrile butadiene rubber (XNBR) and polyamide (PA12). European Polymer Journal 78:235–252

53. Prasath Balamurugan G, Maiti SN (2008) The influence of reactive compatibilization on uniaxial large strain deformation and fracture behavior of polyamide 6 and poly (ethylene-co-butyl acrylate) blends. Polymer Testing 27:752–764

54. Jha A, Bhowmick AK (1998) Thermal degradation and ageing behaviour of novel thermoplastic elastomeric nylon-6/acrylate rubber reactive blends. Polymer Degradation and Stability 62:575–586

55. Ma L-F, Wei X-F, Zhang Q, Wang W-K, Gu L, Yang W, Xie B-H, Yang M-B (2012) Toughening of polyamide 6 with β-nucleated thermoplastic vulcanizates based on polypropylene/ethylene–propylene–diene rubber grafted with maleic anhydride blends. Materials & Design 33:104–110

56. Drobny JG (2014) Processing Methods Applicable to Thermoplastic Elastomers. In: Handbook of Thermoplastic Elastomers. Elsevier, pp 33–173

57. Becker D (2019) Compounding of different kind of TPE in co-rotating twin screw extruders. Presented at the Thermoplastic Elastomers World Summit, Vienna

58. Beyer G, Hopmann C (eds) (2018) Reactive extrusion: principles and applications. Wiley-VCH, Weinheim

59. Giles HF, Wagner JR, Mount EM (2005) Extrusion: the definitive processing guide and handbook. William Andrew, Norwich, NY

60. Wu H, Tian M, Zhang L, Tian H, Wu Y, Ning N, Chan TW (2015) New Understanding of Morphology Evolution of Thermoplastic Vulcanizate (TPV) during Dynamic Vulcanization. ACS Sustainable Chem Eng 3:26–32

61. Gessler AM, Haslett JWH (1962) Process for preparing a vulcanized blend of crystalline polypropylene and chlorinated butyl rubber.

62. Coran AY, Patel RP (1997) Thermoplastic elastomers based on elastomer/thermoplastic blends dynamically vulcanized. In: Al-Malaika S (ed) Reactive Modifiers for Polymers. Springer Netherlands, Dordrecht, pp 349–394

63. Coran AY, Patel R (1980) Rubber-Thermoplastic Compositions. Part I. EPDM-Polypropylene Thermoplastic Vulcanizates. Rubber Chemistry and Technology 53:141–150

64. Coran AY, Patel R (1980) Rubber-Thermoplastic Compositions. Part II. NBR-Nylon Thermoplastic Elastomeric Compositions. Rubber Chemistry and Technology 53:781–794

65. Chatterjee T, Wiessner S, Naskar K, Heinrich G (2014) Novel thermoplastic vulcanizates (TPVs) based on silicone rubber and polyamide exploring peroxide cross-linking. Express Polym Lett 8:220–231

66. Chatterjee T, Basu D, Das A, Wiessner S, Naskar K, Heinrich G (2016) Super thermoplastic vulcanizates based on carboxylated acrylonitrile butadiene rubber (XNBR) and polyamide (PA12). European Polymer Journal 78:235–252

67. Drobny JG (2014) Thermoplastic Elastomers Prepared by Dynamic Vulcanization. In: Handbook of Thermoplastic Elastomers. Elsevier, pp 195–207

68. Ning N, Li S, Wu H, Tian H, Yao P, Hu G-H, Tian M, Zhang L (2018) Preparation, microstructure, and microstructure-properties relationship of thermoplastic vulcanizates (TPVs): A review. Progress in Polymer Science 79:61–97

69. George J, Neelakantan NR, Varughese KT, Thomas S (2006) Failure properties of thermoplastic elastomers from polyethylene/nitrile rubber blends: Effect of blend

ratio, dynamic vulcanization, and filler incorporation. J Appl Polym Sci 100:2912–2929

70. Nakason C, Jarnthong M, Kaesaman A, Kiatkamjornwong S (2009) Influences of blend proportions and curing systems on dynamic, mechanical, and morphological properties of dynamically cured epoxidized natural rubber/high-density polyethylene blends. Polym Eng Sci 49:281–292

71. Babu RR, Singha NK, Naskar K (2010) Interrelationships of morphology, thermal and mechanical properties in uncrosslinked and dynamically crosslinked PP/EOC and PP/EPDM blends. Express Polym Lett 4:197–209

72. Ning N, Li X, Tian H, Hua Y, Zuo H, Yao P, Zhang L, Wu Y, Hu G-H, Tian M (2017) Unique microstructure of an oil resistant nitrile butadiene rubber/polypropylene dynamically vulcanized thermoplastic elastomer. RSC Adv 7:5451–5458

73. Oderkerk J, Groeninckx G, Soliman M (2002) Investigation of the Deformation and Recovery Behavior of Nylon-6/Rubber Thermoplastic Vulcanizates on the Molecular Level by Infrared-Strain Recovery Measurements. Macromolecules 35:3946–3954

74. Oderkerk J, de Schaetzen G, Goderis B, Hellemans L, Groeninckx G (2002) Micromechanical Deformation and Recovery Processes of Nylon-6/Rubber Thermoplastic Vulcanizates As Studied by Atomic Force Microscopy and Transmission Electron Microscopy. Macromolecules 35:6623–6629

75. Sasdipan K, Kaesaman A, Vennemann N, Nakason C (2014) Influence of blend ratio on properties of novel thermoplastic vulcanizates based on copolyester/epoxidized natural rubber blends. Iran Polym J 23:965–977

76. Zhao Y, Liu Z, Su B, Chen F, Fu Q, Ning N, Tian M (2015) Property enhancement of PP-EPDM thermoplastic vulcanizates via shear-induced break-up of nano-rubber aggregates and molecular orientation of the matrix. Polymer 63:170–178

77. Ma P, Xu P, Zhai Y, Dong W, Zhang Y, Chen M (2015) Biobased Poly(lactide)/ethylene- *co* -vinyl Acetate Thermoplastic Vulcanizates: Morphology Evolution, Superior Properties, and Partial Degradability. ACS Sustainable Chem Eng 3:2211–2219

78. Zhou Z, Zhang X, Zhang W, Li J, Lu C (2013) Microstructure and properties of solvent-resistant fluorine-contained thermoplastic vulcanizates prepared through dynamic vulcanization. Materials & Design 51:658–664

79. Babu RR, Singha NK, Naskar K (2010) Interrelationships of morphology, thermal and mechanical properties in uncrosslinked and dynamically crosslinked PP/EOC and PP/EPDM blends. Express Polym Lett 4:197–209

80. Uthaipan N, Junhasavasdikul B, Nakason C, Thitithammawong A (2013) Assessment of Mixing Efficiency of Intermeshing Rotor Mixers on Morphological and Mechanical Properties and Crosslink Density of Dynamically Vulcanized EPDM/PP Blends. AMR 844:122–126

81. Wu H, Tian M, Zhang L, Tian H, Wu Y, Ning N, Hu G-H (2016) Effect of Rubber Nanoparticle Agglomeration on Properties of Thermoplastic Vulcanizates during Dynamic Vulcanization. Polymers 8:127

82. Wu H, Tian M, Zhang L, Tian H, Wu Y, Ning N, Chan TW (2015) New Understanding of Morphology Evolution of Thermoplastic Vulcanizate (TPV) during Dynamic Vulcanization. ACS Sustainable Chem Eng 3:26–32

83. Yao P, Wu H, Ning N, Zhang L, Tian H, Wu Y, Hu G, Chan TW, Tian M (2016) Properties and unique morphological evolution of dynamically vulcanized bromo-

isobutylene-isoprene rubber/polypropylene thermoplastic elastomer. RSC Adv 6:11151–11160

84. Sararoudi SS, Nazockdast H, Katbab AA (2004) Study on Parameters Affecting the Morphology Development of Dynamically Vulcanized Thermoplastic Elastomers Based on EPDM/PP in a Co-Rotating Twin Screw Extruder. Rubber Chemistry and Technology 77:847–855

85. Banerjee SS, Bhowmick AK (2015) Dynamic vulcanization of novel nanostructured polyamide 6/ fluoroelastomer thermoplastic elastomeric blends with special reference to morphology, physical properties and degree of vulcanization. Polymer 57:105–116

86. Wu H, Tian M, Zhang L, Tian H, Wu Y, Ning N, Hu G-H (2016) Effect of Rubber Nanoparticle Agglomeration on Properties of Thermoplastic Vulcanizates during Dynamic Vulcanization. Polymers 8:127

87. Ning N, Hu L, Yao P, Wu H, Han J, Zhang L, Tian H, Tian M (2016) Study on the microstructure and properties of bromobutyl rubber (BIIR)/polyamide-12 (PA12) thermoplastic vulcanizates (TPVs). J Appl Polym Sci 133:n/a-n/a

88. l'Abee RMA, van Duin M, Spoelstra AB, Goossens JGP (2010) The rubber particle size to control the properties-processing balance of thermoplastic/cross-linked elastomer blends. Soft Matter 6:1758

89. Nicolini A, de Campos Rocha TLÁ, Maldaner Jacobi MA (2008) Dynamically vulcanized PP/EPDM blends: Influence of curing agents on the morphology evolution. J Appl Polym Sci 109:3093–3100

90. Ma L, Bao R, Liu Z, Yang W, Yang M (2016) Effect of cross-linking degree of EPDM phase on the electrical properties and formation of dual networks of thermoplastic vulcanizate composites based on isotactic polypropylene (iPP)/ethylene–propylene–diene rubber (EPDM) blends. RSC Adv 6:74567–74574

91. Pechurai W, Sahakaro K, Nakason C (2009) Influence of phenolic curative on crosslink density and other related properties of dynamically cured NR/HDPE blends. J Appl Polym Sci 113:1232–1240

92. Babu RR, Singha NK, Naskar K (2009) Dynamically vulcanized blends of polypropylene and ethylene-octene copolymer: Comparison of different peroxides on mechanical, thermal, and morphological characteristics. J Appl Polym Sci 113:1836–1852

93. Babu RR, Singha NK, Naskar K (2010) Effects of mixing sequence on peroxide cured polypropylene (PP)/ethylene octene copolymer (EOC) thermoplastic vulcanizates (TPVs). Part. I. Morphological, mechanical and thermal properties. J Polym Res 17:657–671

94. Tang Y, Lu K, Cao X, Li Y (2013) Nanostructured Thermoplastic Vulcanizates by Selectively Cross-Linking a Thermoplastic Blend with Similar Chemical Structures. Ind Eng Chem Res 52:12613–12621

95. Nakason C, Wannavilai P, Kaesaman A (2006) Effect of vulcanization system on properties of thermoplastic vulcanizates based on epoxidized natural rubber/polypropylene blends. Polymer Testing 25:34–41

96. Babu RR, Singha NK, Naskar K (2009) Dynamically vulcanized blends of polypropylene and ethylene octene copolymer: Influence of various coagents on mechanical and morphological characteristics. J Appl Polym Sci 113:3207–3221

97. Nakason C, Jarnthong M, Kaesaman A, Kiatkamjornwong S (2009) Influences of blend proportions and curing systems on dynamic, mechanical, and morphological

properties of dynamically cured epoxidized natural rubber/high-density polyethylene blends. Polym Eng Sci 49:281–292

98. Soares BG, Santos DM, Sirqueira AS (2008) A novel thermoplastic elastomer based on dynamically vulcanized polypropylene/acrylic rubber blends. Express Polym Lett 2:602–613

99. Soares BG, de Oliveira M, Meireles D, Sirqueira AS, Mauler RS (2008) Dynamically vulcanized polypropylene/nitrile rubber blends: The effect of peroxide/bis-maleimide curing system and different compatibilizing systems. J Appl Polym Sci 110:3566–3573

100. Zhu S-H, Tzoganakis C (2010) Effect of interfacial strengthening in blends of reclaimed rubber and polypropylene. J Appl Polym Sci n/a-n/a

101. Ning N, Hu L, Yao P, Wu H, Han J, Zhang L, Tian H, Tian M (2016) Study on the microstructure and properties of bromobutyl rubber (BIIR)/polyamide-12 (PA12) thermoplastic vulcanizates (TPVs). J Appl Polym Sci 133:n/a-n/a

102. Wang C, Zhang Y, Zhang L, Liu Q, Wang Z (2016) Carbon black reinforced thermoplastic vulcanisates based on ethylene–vinyl acetate copolymer/styrene–butadiene rubber blends. Plastics, Rubber and Composites 45:415–422

103. Jolfaei AF, Gavgani JN, Jalali A, Goharpey F (2015) Effect of organoclay and compatibilizers on microstructure, rheological and mechanical properties of dynamically vulcanized EPDM/PP elastomers. Polym Bull 72:1127–1144

104. George J, Neelakantan NR, Varughese KT, Thomas S (2006) Failure properties of thermoplastic elastomers from polyethylene/nitrile rubber blends: Effect of blend ratio, dynamic vulcanization, and filler incorporation. J Appl Polym Sci 100:2912–2929

105. Lu K, Ye L, Liang Q, Li Y (2015) Selectively located aluminum hydroxide in rubber phase in a TPV: Towards to a halogen-free flame retardant thermoplastic elastomer with ultrahigh flexibility. Polym Compos 36:1258–1265

106. Cao X, Lu K, Li Y (2015) Isolated Protective Char Layers by Nanoclay Network: Significantly Improved Flame Retardancy and Mechanical Performance of TPV/MH Composites by Small Amount of Nanoclay. Ind Eng Chem Res 54:6912–6921

107. Wu H, Yao P, Ning N, Zhang L, Tian H, Wu Y, Tian M (2016) A novel dielectric elastomer by constructing dual-network structure of carbon nanotubes and rubber nanoparticles in dynamically vulcanized thermoplastic elastomer. RSC Adv 6:32932–32939

108. Hayichelaeh C, Nakason C, Thitithammawong A (2013) Mixing Methods Influencing on Properties of Epoxidized Natural Rubber/Polypropylene Thermoplastic Vulcanizates. AMR 844:109–112

109. Oderkerk J, Groeninckx G, Soliman M (2002) Investigation of the Deformation and Recovery Behavior of Nylon-6/Rubber Thermoplastic Vulcanizates on the Molecular Level by Infrared-Strain Recovery Measurements. Macromolecules 35:3946–3954

110. Oderkerk J, de Schaetzen G, Goderis B, Hellemans L, Groeninckx G (2002) Micromechanical Deformation and Recovery Processes of Nylon-6/Rubber Thermoplastic Vulcanizates As Studied by Atomic Force Microscopy and Transmission Electron Microscopy. Macromolecules 35:6623–6629

111. van Duin M (2006) Recent Developments for EPDM-Based Thermoplastic Vulcanisates. Macromol Symp 233:11–16

112. Babu RR, Naskar K (2010) Recent Developments on Thermoplastic Elastomers by Dynamic Vulcanization. In: Heinrich G (ed) Advanced Rubber Composites. Springer Berlin Heidelberg, Berlin, Heidelberg, pp 219–247

113. Oderkerk J, Groeninckx G, Soliman M (2002) Investigation of the Deformation and Recovery Behavior of Nylon-6/Rubber Thermoplastic Vulcanizates on the Molecular Level by Infrared-Strain Recovery Measurements. Macromolecules 35:3946–3954

114. Oderkerk J, de Schaetzen G, Goderis B, Hellemans L, Groeninckx G (2002) Micromechanical Deformation and Recovery Processes of Nylon-6/Rubber Thermoplastic Vulcanizates As Studied by Atomic Force Microscopy and Transmission Electron Microscopy. Macromolecules 35:6623–6629

115. Banerjee SS, Bhowmick AK (2017) HIGH-TEMPERATURE THERMOPLASTIC ELASTOMERS FROM RUBBER–PLASTIC BLENDS: A STATE-OF-THE-ART REVIEW. Rubber Chemistry and Technology 90:1–36

116. Mani S, Cassagnau P, Bousmina M, Chaumont P (2011) Morphology Development in Novel Composition of Thermoplastic Vulcanizates Based on PA12/PDMS Reactive Blends. Macromol Mater Eng 296:909–920

117. Chatterjee T, Wiessner S, Naskar K, Heinrich G (2014) Novel thermoplastic vulcanizates (TPVs) based on silicone rubber and polyamide exploring peroxide cross-linking. Express Polym Lett 8:220–231

118. Basuli U, Chaki TK, Naskar K (2008) Influence of Engage® copolymer type on the properties of Engage®/silicone rubber-based thermoplastic dynamic vulcanizates. Express Polym Lett 2:846–854

119. Padmanabhan R, Naskar K, Nando GB (2017) Influence of Octene Level in EOC–PDMS Thermoplastic Vulcanizates for Cable Insulation Applications. Polymer-Plastics Technology and Engineering 56:276–295

120. Padmanabhan R, Naskar K, Nando GB (2015) Investigation into the structure–property relationship and technical properties of TPEs and TPVs derived from ethylene octene copolymer (EOC) and polydimethyl siloxane (PDMS) rubber blends. Mater Res Express 2:105301

121. Basuli U, Chaki TK, Naskar K (2008) Mechanical properties of thermoplastic elastomers based on silicone rubber and an ethylene–octene copolymer by dynamic vulcanization. J Appl Polym Sci 108:1079–1085

122. Wang Y, Fang L, Xu C, Chen Z, Chen Y (2014) Morphology and properties of poly(vinylidene fluoride)/silicone rubber blends. J Appl Polym Sci 131:n/a-n/a

123. Xu C, Wang Y, Lin B, Liang X, Chen Y (2015) Thermoplastic vulcanizate based on poly(vinylidene fluoride) and methyl vinyl silicone rubber by using fluorosilicone rubber as interfacial compatibilizer. Materials & Design 88:170–176

124. Lei C-H, Li S-L, Xu R-J, Xu Y-Q (2012) Thermoplastic vulcanizates based on compatibilized polyurethane and silicone rubber blend. Journal of Elastomers & Plastics 44:563–574

125. Soares BG, Santos DM, Sirqueira AS (2008) A novel thermoplastic elastomer based on dynamically vulcanized polypropylene/acrylic rubber blends. Express Polym Lett 2:602–613

126. Li Y, Oono Y, Kadowaki Y, Inoue T, Nakayama K, Shimizu H (2006) A Novel Thermoplastic Elastomer by Reaction-Induced Phase Decomposition from a Miscible Polymer Blend. Macromolecules 39:4195–4201

127. Jha A, Bhowmick AK (2000) Mechanical and dynamic mechanical thermal properties of heat- and oil-resistant thermoplastic elastomeric blends of

poly(butylene terephthalate) and acrylate rubber. Journal of Applied Polymer Science 78:1001–1008

128. Soares BG, de Oliveira M, Meireles D, Sirqueira AS, Mauler RS (2008) Dynamically vulcanized polypropylene/nitrile rubber blends: The effect of peroxide/bis-maleimide curing system and different compatibilizing systems. J Appl Polym Sci 110:3566–3573

129. Le HH, Zia Q, Ilisch S, Radusch HJ (2008) Effect of extender oils on the stress relaxation behavior of thermoplastic vulcanizates. Express Polym Lett 2:791–799

130. Tian M, Han J, Wu H, Tian H, She Q, Chen W, Zhang L (2012) Effect of the compatibility on the morphology and properties of acrylonitrile-butadiene rubber/polypropylene thermoplastic vulcanizates. J Appl Polym Sci 124:1999–2006

131. Ning N, Li X, Tian H, Hua Y, Zuo H, Yao P, Zhang L, Wu Y, Hu G-H, Tian M (2017) Unique microstructure of an oil resistant nitrile butadiene rubber/polypropylene dynamically vulcanized thermoplastic elastomer. RSC Adv 7:5451–5458

132. Tang Y, Lu K, Cao X, Li Y (2013) Nanostructured Thermoplastic Vulcanizates by Selectively Cross-Linking a Thermoplastic Blend with Similar Chemical Structures. Ind Eng Chem Res 52:12613–12621

133. Ning N, Hua Y, Wu H, Zhang L, Wu S, Tian M, Tian H, Hu G-H (2016) Novel heat and oil-resistant thermoplastic vulcanizates based on ethylene-vinyl acetate rubber/poly(vinylidene fluoride). RSC Adv 6:91594–91602

134. Wu W, Wan C, Wang S, Zhang Y (2014) Reactive processing of ethylene-vinyl acetate rubber/polyamide blends via a dynamic transesterification reaction. Polym Bull 71:1505–1521

135. Dutta J, Ramachandran P, Naskar K (2016) Scrutinizing the influence of peroxide crosslinking of dynamically vulcanized EVA/TPU blends with special reference to cable sheathing applications. J Appl Polym Sci. https://doi.org/10.1002/app.43706

136. Van Dyke JD (Jack), Gnatowski M, Koutsandreas A, Burczyk A (2003) A study of dynamic vulcanization for polyamide-12 and chlorobutyl rubber. J Appl Polym Sci 90:871–880

137. Yao P, Tian M, Zhang L, Tian H, Wu Y, Ning N (2014) Phase morphologies of vulcanized chlorobutyl rubber/polyamide 12 blends: The breakup of pre-crosslinked CIIR phase. J Appl Polym Sci 131:n/a-n/a

138. Yao P, Wu H, Ning N, Zhang L, Tian H, Wu Y, Hu G, Chan TW, Tian M (2016) Properties and unique morphological evolution of dynamically vulcanized bromo-isobutylene-isoprene rubber/polypropylene thermoplastic elastomer. RSC Adv 6:11151–11160

139. Van Dyke JD (Jack), Gnatowski M, Burczyk A (2008) Solvent resistance and mechanical properties in thermoplastic elastomer blends prepared by dynamic vulcanization. J Appl Polym Sci 109:1535–1546

140. Ning N, Hu L, Yao P, Wu H, Han J, Zhang L, Tian H, Tian M (2016) Study on the microstructure and properties of bromobutyl rubber (BIIR)/polyamide-12 (PA12) thermoplastic vulcanizates (TPVs). J Appl Polym Sci 133:n/a-n/a

141. Ismail SMRS, Chatterjee T, Naskar K (2017) Superior heat-resistant and oil-resistant blends based on dynamically vulcanized hydrogenated acrylonitrile butadiene rubber and polyamide 12: Thermoplastic Vulcanizate based on HNBR/PA12. Polym Adv Technol 28:665–678

142. Mohammed Reffai SIS, Chatterjee T, Naskar K (2018) Exploring the influence of radiation crosslinking on high-performance hydrogenated acrylonitrile butadiene

rubber and polyamide 12 based blends with special reference to heat and oil resistance. Radiation Physics and Chemistry 148:50–59

143. Banerjee SS, Kumar KD, Bhowmick AK (2015) Distinct Melt Viscoelastic Properties of Novel Nanostructured and Microstructured Thermoplastic Elastomeric Blends from Polyamide 6 and Fluoroelastomer: Distinct Melt Viscoelastic Properties of Novel. Macromol Mater Eng 300:283–290

144. Banerjee SS, Bhowmick AK (2015) Dynamic vulcanization of novel nanostructured polyamide 6/ fluoroelastomer thermoplastic elastomeric blends with special reference to morphology, physical properties and degree of vulcanization. Polymer 57:105–116

145. Zhou Z, Zhang X, Zhang W, Li J, Lu C (2013) Microstructure and properties of solvent-resistant fluorine-contained thermoplastic vulcanizates prepared through dynamic vulcanization. Materials & Design 51:658–664

146. Banerjee SS, Bhowmick AK (2013) Novel nanostructured polyamide 6/fluoroelastomer thermoplastic elastomeric blends: Influence of interaction and morphology on physical properties. Polymer 54:6561–6571

147. Banerjee SS, Bhowmick AK (2015) Tailored Nanostructured Thermoplastic Elastomers from Polypropylene and Fluoroelastomer: Morphology and Functional Properties. Ind Eng Chem Res 54:8137–8146

148. Banerjee SS, Bhowmick AK (2016) Viscoelastic properties and melt rheology of novel polyamide 6/fluoroelastomer nanostructured thermoplastic vulcanizates. J Mater Sci 51:252–261

149. Khan AS, Baig M, Hamid S, Zhang H (2010) Thermo-mechanical large deformation responses of Hydrogenated Nitrile Butadiene Rubber (HNBR): Experimental results. International Journal of Solids and Structures 47:2653–2659

150. Tao Z, Viriyabanthorn N, Ghumman B, Barry C, Mead J (2005) Heat Resistant Elastomers. Rubber Chemistry and Technology 78:489–515

151. ARLANXEO_Therban_brochure. In: http://arlanxeo.com/fileadmin/user_upload/ARLANXEO/Brochures/2017/ARLANXEO_Therban_brochure_EN.pdf.

Chapter 2

General conclusions

The major aim of this thesis is to advance on the design of high-performance thermoplastic vulcanizates for vibration damping applications. For that, TPE blends of HNBR with PA6 have been developed and the relationship between their microstructure and properties investigated. The main conclusions of this research work are summarized below.

Reactive compatibilization of PA6/HNBR TPE blends

In the first part of the thesis, the reactive blending approach has been explored as an effective technique for improving the compatibility of PA6/HNBR TPE blends. For that, four TPEs have been prepared by melt-blending PA6 with HNBR, adding different amounts of XHNBR as compatibilizer: 40/60/0, 40/42/18, 40/30/30 and 40/18/42 (PA6/HNBR/XHNBR).

With the addition of XHNBR, the adhesion between the rubber and thermoplastic phases was enhanced and thus a decrease of the rubber particle size was noted in the TPE sample containing 18% XHNBR. Curiously, a reactively compatibilized TPE blend with co-continuous morphology has been obtained with the addition of 42% of XHNBR. Melt-linear rheological measurements demonstrated that the generation of a co-continuous morphology was mainly caused by the increase of the elasticity of the rubber phase with the addition of XHNBR. The reactively compatibilized blend with co-continuous morphology demonstrated lower PA6 crystallinity degree and improved elastomeric properties, which correspond to enhanced interfacial interactions. The elongation at break of the TPE with 42% of XHNBR was 16 times higher than the uncompatibilized

PA6/HNBR blend. Moreover, a curious double T_g increase phenomenon was noted with the introduction of 42% XHNBR, which has been attributed to a decrease in the mobility of the amorphous domains, of both the PA6 and the rubber phase, caused by the interfacial interactions between the phases.

Summarizing, a novel approach based on the reactive compatibilization of PA6/HNBR blends by adding XHNBR has been presented. This approach was shown to be very promising for the development of TPE blends with superior properties. The obtained results showed that the control of the interfacial interactions and the morphology represents a key strategy to develop TPE blends with tailored properties. Moreover, melt-linear rheology has been identified as a strong tool to provide information about the morphological changes and the enhanced interfacial interactions. Two new methodologies have been proposed:

1) <u>Methodology to control the phase morphology of TPE blends</u>

The proposed methodology to control the morphology of TPE blends is based on the use of viscous and elastic models to predict the change of the morphology during melt-blending. This methodology has been shown to be very effective to determine the effects of viscous and elastic effects that caused the change of morphology from droplet-matrix to co-continuous when adding 42% of XHNBR. Melt-linear rheology tests revealed that the elastic effects (characterized by the storage modulus $G\acute{}$) become more important than the viscous ones (characterized by the complex viscosity η^*) when increasing the XHNBR content, which favoured the formation of a reactive blend with co-continuous morphology. Therefore, the strategy we propose in order to control the phase morphology is to test the rubber and thermoplastic components of the blends by melt-linear rheology and evaluate the viscosity (η^*) and elasticity ($G\acute{}$) ratios at the melt-blending temperature and shear rate condition.

2) <u>Methodology to control the interfacial interactions in TPE blends</u>

The methodology proposed to control the interfacial interactions in TPE blends is based on the measurement of the critical stress, which is a parameter that is sensible to the adhesion between blend components. The critical stress is defined as the value of stress when the modulus is equal to the 95% of the plateau modulus. Melt-linear rheology tests have showed that, when measuring the variation of the storage modulus

of the blends as a function of the stress at the melt-blending temperature, critical stress increases with XHNRB content, which is indicative of the enhanced interfacial interactions between the phases. Consequently, the strategy we propose to control the interfacial interactions is to tests the TPE blends by melt-linear rheology and evaluate the critical stress value at the melt-blending temperature.

Novel strategy to design TPVs with improved vibration damping properties

In the second part of the thesis, the reactively compatibilized PA6/HNBR blend with co-continuous morphology, i.e. the one with 42% of XHNBR, was subjected to dynamic vulcanization by using mixed crosslink systems of peroxide with metal oxides and hindered phenolic antioxidants. The selected metal oxides were zinc oxide (ZnO) and magnesium oxide (MgO), whereas the selected hindered phenolic antioxidants were Irganox 1010 and Irganox 1098.

Scanning electron microscopy (SEM) studies showed a droplet-matrix morphology with crosslinked rubber particles in the micron level for all developed TPV compounds. Besides, Fourier Transform Infrared (FTIR) spectroscopy measurements revealed the creation of carbon-carbon (C-C) crosslinks in all of them. FTIR measurements showed also that Irganox 1098 acts mainly as an inorganic filler, not being coupled with the carboxyl functionalities present in the rubber phase, whereas Irganox 1010 forms hydrogen bonds with XHNBR. The TPV compounds with MgO and ZnO showed an additional relaxation transition corresponding to the relaxation transition of ionic bonds. This ionic transition was particularly evident for the TPV system containing the higher amount of MgO. The TPV systems containing 5 phr of both Irganox 1010 and MgO showed the lowest crystallinity degrees together with greater elastomeric properties, which is further evidence of the strong hydrogen bonding and ionic interactions formed with the carboxylic rubber phase. These two TPV compounds exhibited the highest loss tangent (*tan δ*) values and so the most promising vibration damping properties.

In summary, the investigation of the effect of the rubber network structure on the damping performance of the PA6/XHNR TPV systems by DMA showed that high-performance TPVs with good damping properties can be developed by controlling the type and magnitude of the different crosslinking interactions. The achieved results

highlighted that the generation of ionic crosslinks, via the addition of metal oxides, represents a very promising way to develop high-performance TPVs with enhanced vibration damping properties within a wide range of temperature and frequencies, which is very interesting for electric vehicle applications, where challenges in broad range of temperatures and frequencies exist.

Physical mechanisms involved in the mechanical behaviour of TPVs

The third part of the thesis was focused on the study of the relationship between microstructural features of TPVs and their non-linear quasi-static and dynamic mechanical behaviour. This study has been carried out in the two peroxide cured TPV compounds that showed the best vibration damping properties, i.e. the ones containing 5 phr of Irganox 1010 and MgO. Thus, one of the analysed TPVs contains a rubber network structure based on C-C and hydrogen bonds, while the other possess a rubber network structure formed by C-C and ionic bonds.

Correlation between mechanical and microstructural analysis indicated that the nonlinear quasi-static and dynamic mechanical behaviour of both TPV samples is mainly influenced by the rubber network structure. Cyclic tensile stress-strain measurements revealed a similar cyclic stress softening (also known as Mullins effect), hysteresis loss and permanent set for both TPV samples below 30% strain level. This has been attributed to the similar PA6 phase crystallinity degree and crystalline lamellae thickness that both TPVs possess, which was demonstrated by means of differential scanning (DSC) calorimetry measurements. Above 30% of strain level the TPV sample containing C-C and ionic bonds exhibited a less significant stress softening, which has been ascribed to the better elastic recovery capacity of the rubber network structure formed by a higher amount of covalent C-C linkages and stronger non-covalent bonds. The differences in the mechanical deformation behaviour, observed by quasi-static mechanical test, were confirmed by SEM analysis. SEM micrographs proved that in the TPV containing C-C and ionic bonds the development of plastic voids and rubber cavitation was suppressed.

On the basis of the observed phenomena, a physical interpretation for the deformation mechanism has been introduced. The observed micromechanical processes have been interpreted in terms of the yielding, buckling and bending of thin PA6 ligaments at low

strain levels and the rupture of covalent and non-covalent bonds presented in the rubber network at high strain levels. This research work opens new prospects for the micromechanical modelling of TPV materials.

2.1. Future works

This research work represents a first approximation for the development of new methods to design and fabricate TPV systems with high-performance properties and improved vibration damping performance. Hence, there is a great deal of room for improvements and new investigations. For future work, the investigation could be continued in the following research fields:

Optimize the formulation

Experimental results reveal the possibility of obtaining high-performance TPVs with customized viscoelastic vibration damping properties by melt blending PA6 with XHNBR and using mixed crosslink systems. Further research work will deal with the application of the melt-linear rheology characterization approach studied in the thesis as a method to optimize the formulations based carboxylic TPVs with rubber network structures with C-C and ionic bonds.

Processability by injection moulding

The obtained results indicated that the shear applied during melt-blending strongly influences the microstructure of TPE blends due to viscous and elastic effects. Therefore, in near future the TPV systems revealing the most promising damping characteristics will be further injection moulded to study their processability and the effect of subsequent shear on their microstructure.

Another interesting research field to cover would be the industrial scalability of the TPV systems developed in the thesis. For that, a comparison of the long-term heat resistance and mechanical properties of the injection moulded TPVs and commercial high-performance PA6/AMC TPVs (Zeotherm) could be performed.

Passive solutions to suppress the vibrations of lightweight polymeric composites

The experimental finding demonstrated the potential of the designed TPV systems as passive solutions to suppress the structural vibrations. Further investigations will address the ability of the designed TPV materials to suppress vibrations of fibre reinforced polymeric composite materials by evaluating their applicability as free vibration damping treatments. The free-layer damping treatment is widely employed in automotive applications due to the simplicity of its structure and is based on the attachment of a damping material on the base panel whose vibration needs to be suppressed.

Process-microstructure relationship: anisotropy

The results obtained in the thesis pointed out the importance of understanding how the microstructural features influences the properties of TPV materials. When processing immiscible polymer blends by injection moulding, the blend components experience high shear forces and temperature gradients that typically lead to different orientation and dispersion phenomena along the flow direction and across the thickness of the part, which could result in anisotropic materials properties. Even though the process induced anisotropic behaviour of TPVs has been proven experimentally, no unanimous agreements for the cause and influencing factors exists to date.

In composite materials based on thermoplastics with fibres, the microstructural evolutions that take place during injection moulding are well correlated using commercial process simulation software's such as Moldflow or Moldex3D. Nevertheless, these commercial software's do not have the ability to provide the viscoelastic effects that occur when processing TPV materials, i.e. physical mixtures of thermoplastic with rubber.

Due to the lack of commercial technical resources that are able to consider the anisotropic character of TPVs, the process effect is not considered properly during the material design strategy. Therefore, the modelling of the microstructural evolution during processing represents a research field to be explored. Future research work will be focused in the development of methodologies to characterize and model the flow induced anisotropic behaviour of TPVs.

Appendix:

Published works

Bibliographic references of the publications presented in the thesis:

o Aizeti Burgoa*, Ricardo Hernandez and Jose L Vilas. Toward superior applications of thermoplastic. elastomer blends: double T_g increase and improved ductility. Polym Int 2019; 68: 1130–1139. doi.org/10.1002/pi.5803.

   • Impact Factor JCR: 2.574
   • CiteScore Rank in the category of Polymer and Plastics (Scopus): 31/154
   • CiteScore Percentile in Polymer and Plastics category (Scopus): 80th (Q1)

o Aizeti Burgoa*, Ricardo Hernandez and Jose L Vilas. New ways to improve the damping properties in high-performance thermoplastic vulcanizates. Polym Int 2020; 69: 467–475. doi.org/10.1002/pi.5977.

   • Impact Factor JCR: 2.574
   • CiteScore Rank in the category of Polymer and Plastics (Scopus): 31/154
   • CiteScore Percentile in Polymer and Plastics category (Scopus): 80th (Q1)

o Aizeti Burgoa*, Aitor Arriaga, Kepa Zulueta, Eva Maria Acuña, Jose Manuel Laza, Ricardo Hernandez, Jose Luis Vilas. Experimental investigation of the nonlinear quasi-static and dynamic mechanical behaviour of novel PA6/XHNBR thermoplastic vulcanizates: Linking mechanical nonlinearities to microstructural features. Materials Today Communications 2020, 25: 101395. doi.org/10.1016/j.mtcomm.2020.101395

   • Impact Factor JCR: 2.678
   • CiteScore Rank in the category Mechanics of Materials (Scopus): 152/367
   • CiteScore Percentile in Mechanics of Materials category (Scopus): 58th (Q2)

The **Impact Factor** measures the average number of citations received in a particular year by papers published in the journal during the two preceding years; **CiteScore Rank** indicates the absolute standing of a serial in its field; **CiteScore Percentile** indicates the relative standing of a journal in its subject field. A CiteScore Percentile of 98% means the journal is in the top 2% of its subject field.

Toward superior applications of thermoplastic elastomer blends: double Tg increase and improved ductility

Aizeti Burgoa[1*], Rikardo Hernandez[1] and Jose Luis Vilas[2,3]

[1] Leartiker S. Coop, Xemein Etorbidea, 12-A E-48270, Markina-Xemein, Bizkaia (Spain).

[2] Macromolecular Chemistry Research Group (labquimac), Department of Physical Chemistry, Faculty of Science and Technology, University of the Basque Country (UPV/EHU), 48940 Leioa, Spain.

[2] BCMaterials, Basque Center for Materials, Applications and Nanostructures, UPV/EHU Science Park, 48940 Leioa, Spain.

E-mail: aburgoa@leartiker.com

Abstract

With the aim to curb air pollution and address climate change, the use of low density thermoplastic elastomers (TPEs) in transportation could be a useful way to lighten the vehicle weight. For that, melt blending of high performance rubber and thermoplastics is an attractive way of preparing high performance TPEs. In this work, several TPEs have been prepared by melt blending of hydrogenated acrylonitrile butadiene rubber (HNBR) with polyamide 6 (PA6), adding different amounts of carboxylated HNBR (XHNBR) as compatibilizer: 40/60/0, 40/42/18, 40/30/30 and 40/18/42 (PA6/HNBR/XHNBR). The resulting blends were investigated using melt rheological measurements, morphological observations (scanning electron microscopy and polarized optical microscopy), dynamic mechanical analysis, differential scanning calorimetry analysis and mechanical tests. A biphasic morphology was noted for all TPEs. The increase of XHNBR amount changes the morphology from dispersed to co-continuous. This evolution was explained by the change of the melt rheological properties of the HNBR/XHNBR rubber phase. Moreover, the introduction of 42 % of XHNBR resulted in an increase of the glass transition temperature of both rubber and PA6 phases. This double T_g increase phenomena was attributed to the interfacial interactions between the carboxyl groups in XHNBR and amine end groups in

1

PA6. Additionally, thermal analysis revealed a reduced crystallinity of PA6 in the blend, which corresponds to the enhanced interfacial interactions. The interfacial adhesion and the co-continuous morphology resulted in an improved ductility. This study reveals the possibility of obtaining TPE blends with tunable thermal and mechanical properties by controlling both interfacial interactions and morphology.

Introduction

Thermoplastic elastomers (TPEs) are rubbery materials that possess elastomeric behaviour with the advantage that can be melt processed like thermoplastics [1]. Therefore, they are recyclable and offer an alternative to natural or synthetic rubbers [2,3]. The unique feature of TPEs is their biphasic morphology, in which one phase is soft and rubbery in nature and the other phase is generally continuous, hard, and semicrystalline. Both phases are thermodynamically immiscible and consequently act as individual phases [4].

Greening of transportation is one of the major actual challenges worldwide. The objective set-up by the EU to reduce transport greenhouse gas emissions to 60% below 1990 levels by 2050 (European Commission (https://ec.europa.eu/clima/policies/strategies/2050_en)) has led to a growing trend to vehicle lightweighting. The automotive industry employs a large number of rubber components. The lower density of TPEs, as compared to rubbers, contributes to reduced part weight. Therefore, the substitution of some rubber parts by TPEs would help in the transformation of the classical transport systems into greener transport systems. However, most of the TPEs available in the market do not possess the high temperature resistance and tensile set properties required for automotive parts [5,6].

Blending of different rubbers and thermoplastics is a particularly attractive way of preparing TPEs [7–9]. The commercial availability of so many polymers with the desired properties for blending allows the development of TPE blends with upgraded performance properties [10–13]. The final properties of TPE blends strongly depend on the properties of the individual

2

phases, the adhesion between them and the phase morphology of the system [14]. Particularly, the glass transition temperature (T_g) is one of the most important properties that govern the performance characteristics of polymer blends, being directly related with fields of potential application [15–17]. The design temperature range of a TPE blend is bounded by the glass transition temperature of the rubbery phase and the glass transition or melt temperature of the thermoplastic phase.

Several studies reveal the possibility of shifting the glass transition temperature of polymers by blending. Bates et al. [18] reported a depression of rubber T_g in systems consisting of microspherical inclusions of polybutadiene in polystyrene matrix. Qui et al. [19] found that both PLLA and POM showed an apparent T_g depression in the blends, as compared with the neat PLLA and POM. This double T_g depression phenomena was attributed to the differential contraction due to the thermal shrinkage mismatch. Richard et al. [20] studied PMMA films on native oxide of silicon and on evaporated gold. They observed an increase of PMMA T_g when deposited on native oxide of silicon. This was attributed to the restriction of mobility due to the formation of hydrogen bonding at the interface. These works demonstrate the possibility of shifting the glass transition temperature in polymer blends by tailoring the phase morphology and the interaction between components. Thus, a thorough understanding of the relationship between morphology as well as phase interaction and glass transition behaviour is of particular interest and can greatly aid the tailoring of novel TPE blends with tunable properties.

Therefore, the main objective of this work is to analyse the effect of phase morphology and phase interaction in the glass transition behaviour of TPE blends. A TPE system based on nylon 6 (PA6) and hydrogenated acrylonitrile butadiene rubber (HNBR) has been selected for this study. Both HNBR and PA6 are well known for their excellent chemical, wear and heat resistant properties [21,22]. Therefore, blending HNBR and PA6 would be encouraging in the field of high performance TPEs. However, PA6 and HNBR are not compatible and so it is necessary to use a compatibilizer to enhance the interfacial properties between these polymers. In this work, a carboxylated hydrogenated acrylonitrile butadiene rubber (XHNBR) has been considered as potential compatibilizer for PA6/HNBR blends. XHNBR

3

is miscible with HNBR and its inherent carboxylic functionalities can react with the amine end groups on PA6 during melt-mixing, improving the compatibility between the two phases [23]. Moreover, the presence of carboxylic functionalities in XHNBR enhances the abrasion and heat resistance. The effect of XHNBR concentration with regard to morphology and interfacial interaction has been investigated. We have observed the novel phenomena that both the rubber phase and the thermoplastic phase show an apparent increase of their glass transition temperatures, as compared with the neat rubber and thermoplastic. Furthermore, we found that the addition of XHNBR leads to a superior ductility.

Experimental

Materials

PA6, Durethan® B 30 S 000000, (density 1.14 g cm^{-3}, melting point 222 °C) was supplied by Lanxess. HNBR, Therban® AT 3904 VP, (specific gravity 0.96, acrylonitrile content 39 wt%, mooney viscosity ML (1+4) at 100 °C 40, residual double bonds 0.5%) and XHNBR, Therban® XT VP KA 8889, (specific gravity 0.97, acrylonitrile content 33 wt%, mooney viscosity ML (1+4) at 100 °C 74, residual double bonds 3.5%, carboxylic acid 5%) were supplied by Arlanxeo. Their chemical structures are shown in Fig. 1.
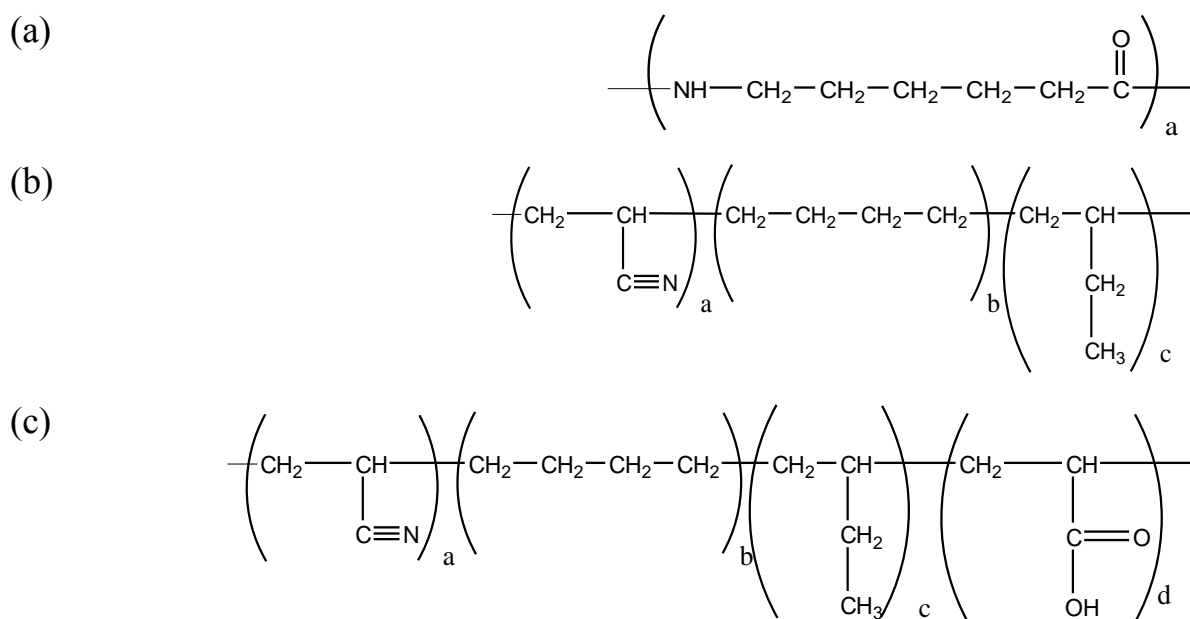
(a)

(b)

(c)

4

Fig. 1. Chemical structure of (a) PA6; (b) HNBR; (c) XHNBR.

TPE blends preparation

For the rubber phase HNRB and XHNBR were blended at three different blend ratios (70/30, 50/50 and 30/70 wt/wt). The HNBR/XHNBR blends were prepared in a two-roll mill. The rubber sheet obtained was extruded into strands for subsequent pelletization. Extrusion was carried out at 90 °C with a rotor speed of 15 rpm in a Gumix extruder with L/D ratio of 10. The ratio of both rubber and thermoplastic components in the systems is crucial for the main final properties of TPE blends. Banerjee et al [24,25] have shown that 40 PA6/60 FKM (wt/wt) blend composition exhibited best thermoplastic elastomeric properties. For that reason, the amount of rubber and PA6 in the blends was fixed to that particular ratio. PA6 was dried overnight at 80 °C before blending so as to minimize the effects of moisture. Four TPE blends were prepared by melt blending the rubber blends with PA6 in a Brabender DSE 20/40 corrotating twin screw extruder. The blending conditions were the same for all the blends. The temperature fixed during mixing was 240 °C and the rotor speed was 100 rpm. After extrusion, the blends were pelletized and compression molded in a hydraulic press at 240 °C increasing the pressure from 50 to 200 bar during 360 seconds in order to ensure the homogeneous filling of the mold, avoid air trapping and to obtain 1 mm thick plates. The composition of the prepared samples and their designation are presented in table 1. All samples were dried for 8 hours at 80 °C prior to any measurement.

Composition (PA6/HNBR/XHNBR)	Sample name
0/70/30	70H30X
0/50/50	50H50X
0/30/70	30H70X
40/60/0	P100H
40/42/18	P70H30X
40/30/30	P50H50X
40/18/42	P30H70X

Table 1. Composition of prepared samples and desigACK

.

Morphological characterization

5

The morphology of the blends was analysed using a field-emission scanning electron microscope with a Schottky type field-emission gun (JEOL JSM-7000F). SEM analysis was carried out by inspecting the cryofractured surface of the samples. The TPE blend containing 42 wt% of XHNBR, i.e. P30H70X, was selectively etched with acetone for 24 hours to remove the rubber phase. The surface of the samples was sputter coated with gold prior to the SEM observation.

ImageJ image analysis software was used to calculate the size of dispersed phase domains. The number average, d_n, and volume average, d_v, diameter of the dispersed phase domains that are reported in this study were calculated via the following relations:

$$\overline{d_n} = \frac{\sum d_i N_i}{\sum N_i} \tag{1}$$

$$\overline{d_v} = \frac{\sum d_i^4 N_i}{\sum d_i^3 N_i} \tag{2}$$

where Ni is the number of dispersed domains. In SEM micrographs 400 particles were measured for each sample.

The phase structure of the TPE blends was observed by means of Polarized Optical Microscopy (POM) using a Nikon ECLIPSE 80i microscope equipped with a LINKAM LTS420 hot stage. The samples were placed between two cover glasses and heated from room temperature to 240 °C; the temperature was then lowered to 160 °C allowing the material to crystallize with a cooling rate of 10 °C min^{-1}.

Melt rheological characterization

Melt rheological characterization was carried out using a Thermo Haake Mars III oscillatory rheometer. Characterization of the samples was carried out at 240 °C with a 20 mm parallel plate. Test were carried out in both frequency and stress sweeps. Frequency sweeps were performed from 0.1 to 100 rad s^{-1} at a constant strain of 0.1%. Stress sweeps were performed from 1 to 10^5 Pa at a constant frequency of 1 Hz.

6

Dynamic mechanical analysis (DMA)

Dynamic mechanical measurement were carried out on a Rheometrics Solids Analyzer (RSA II) in tensile mode. The temperature was swept from -50 to 140 °C at a heating rate of 3 °C min^{-1} with an oscillating frequency of 1 Hz. All the measurements were performed at the strain of 0.03%.

Differential scanning calorimetry (DSC)

The crystallization behaviour of samples was studied by differential scanning calorimetry (DSC). DSC measurements were performed in a DSC Q100 (TA Instruments) in a dry nitrogen atmosphere. Samples were heated and cooled from -50 to 250 °C with a rate of 10°C min^{-1}.

Mechanical testing

Tensile testing of the blends were performed according to ISO 37 test method by using dumbbell-shaped specimens. The test were carried out in a MTS Insight Universal Testing Machine at room temperature and with a crosshead speed of 5 mm min^{-1}. The hardness was tested according to ISO 868. The tensile and hardness results reported in this work are the average of at least five samples.

Results and discussion

Morphological investigation

Polarized optical microscopy (POM) has been used in order to distinguish the PA6 (light) and rubber (dark) phases. The biphasic morphology of P100H TPE blend is demonstrated in Fig. 2. As we expected, dispersed spherical droplets of HNBR in PA6 matrix are observed in the P100H blend. Moreover, the two-phase interface is clear and there is space between the

7

droplets and the matrix, demonstrating the weak compatibility between HNBR and PA6. As it can be seen in Fig. 3b the addition of 18 % XHNBR resulted in a smaller droplet size and narrower size distribution compared with that of P100H blend.

The final morphology of a polymer blend is a result of the competition between droplet deformation and break-up on the one side and shape recovery and coalescence on the other side [26]. In this case, the presence of XHNBR leads to smaller droplet size because lowers the interfacial tension which makes the droplet deformation and break-up easier, i.e., coalescence is reduced [27,28]. The number average and volume average diameter were calculated as 1.33 and 1.99 μm for P100H and 0.79 and 1.14 for P70H30X (Fig. 4). Moreover, as the XHNBR content is increased to 30% the rubber droplets start to coarse and the two-phase interface becomes uneven (Fig. 3c). Finally, the micrograph shown in Fig. 3d suggests that the addition of 42% of XHNBR induces a change in the morphology type from a dispersed to a co-continuous morphology (the rougher area belongs to PA6). Note that the droplets have completely disappeared for this composition. This is further revealed from the SEM micrograph of the cryofractured surface with rubber phase extracted (Fig. 5), where a continuous morphology can be observed.
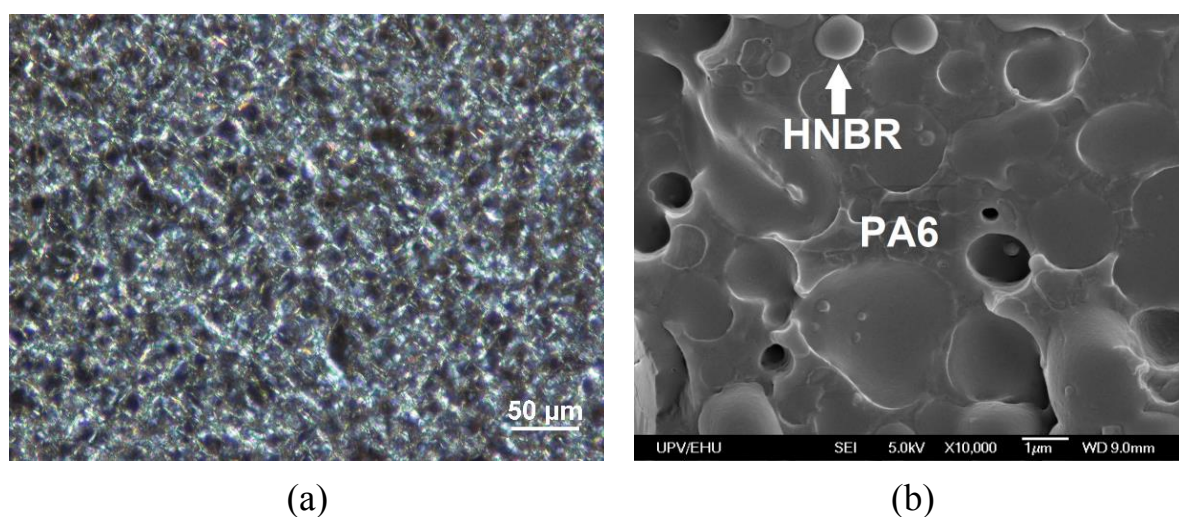

(a)   (b)

Fig. 2. (a) POM and (b) SEM micrographs of P100H.

8

(a)   (b)

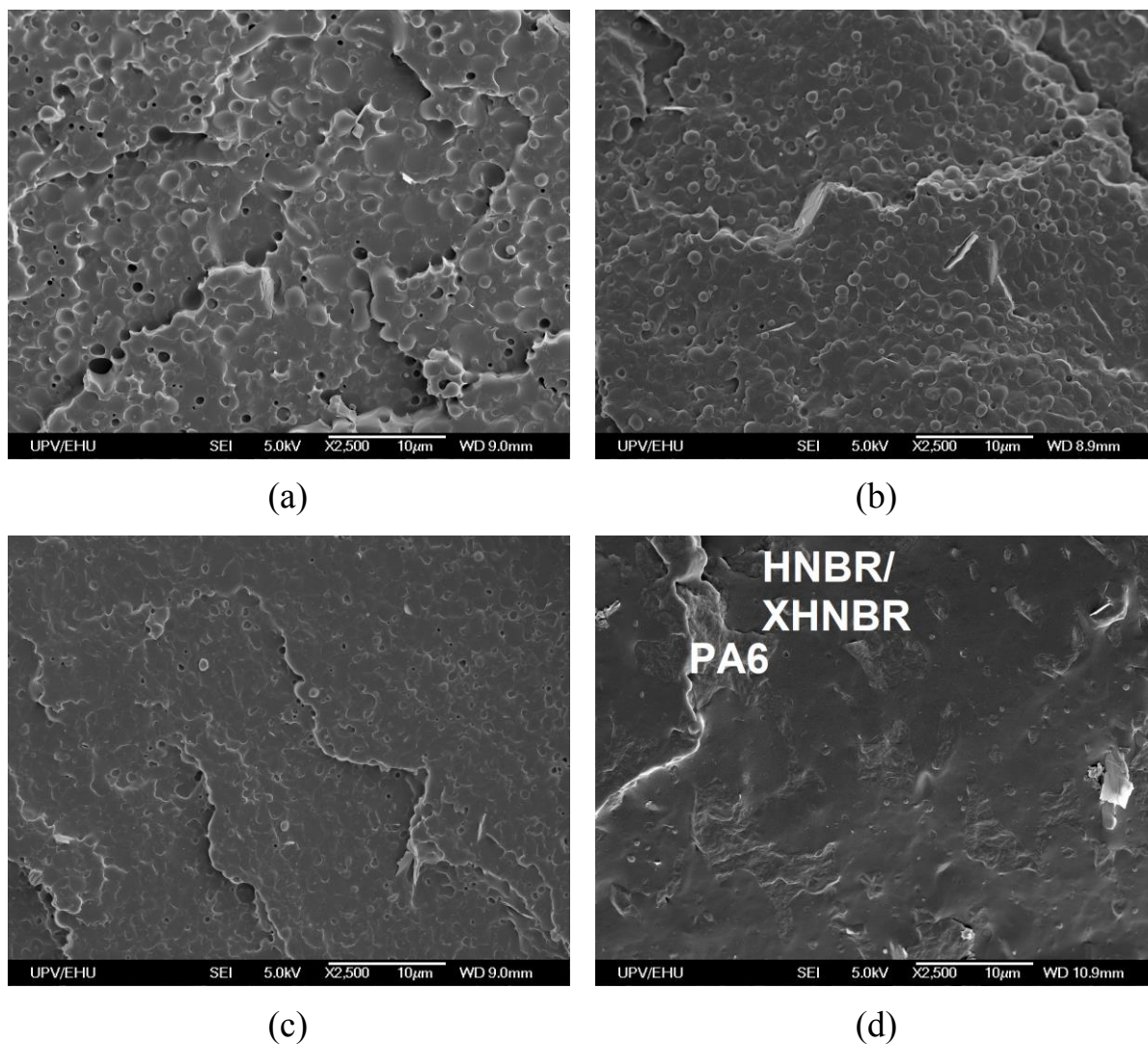(c)   (d)

Fig. 3. SEM micrographs of (a) P100H; (b) P70H30X; (c) P50H50X; (d) P30H70X.
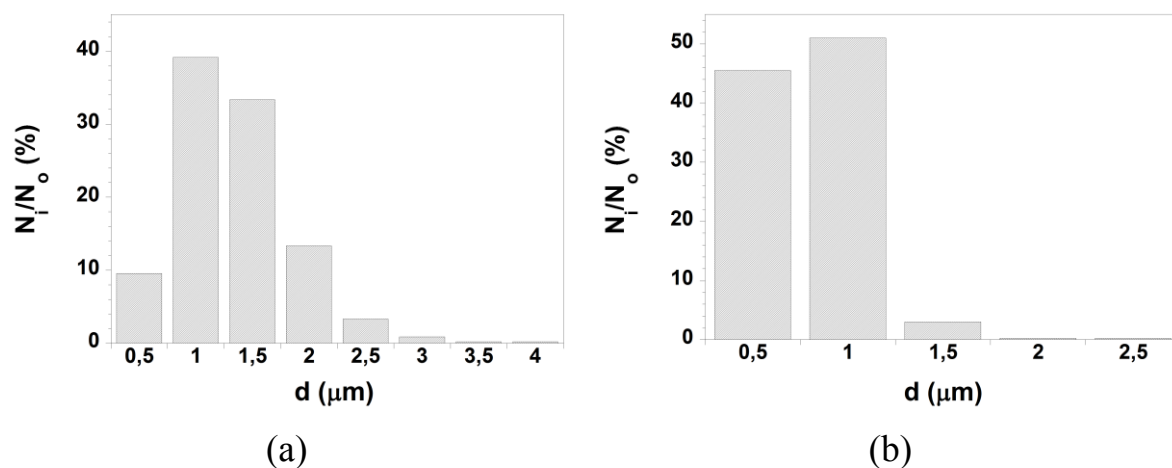
9

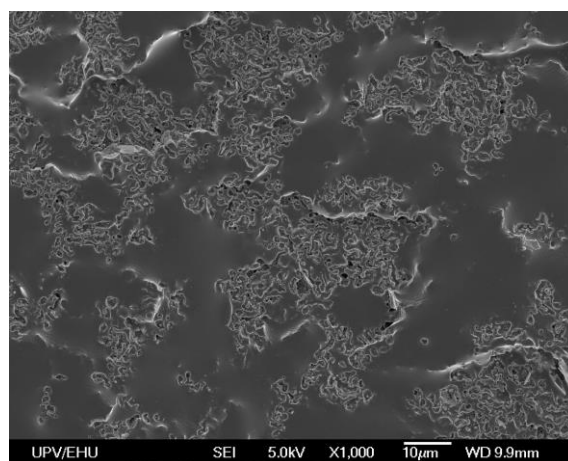Fig. 4. Particle size distributions of (a) P100H and (b) P70H30X.

Fig. 5. SEM micrograph of P30H70X after etching the rubber phase by acetone.

Melt linear rheological behaviour

The melt linear rheological properties of polymer blends strongly depend on the interaction between the components and their morphology [29]. Fig. 6a shows the variation of the complex viscosity (η^*) as a function of the angular frequency (ω) at 240 °C for the blends. All blends show a non-newtonian behaviour. Furthermore, by increasing the XHNBR content the yield phenomena becomes more apparent. Fig. 6b shows the curves of the storage modulus (G´) as a function of the angular frequency for the blends. Fig. 6b reveals that there is a well-developed dependence of the cross-over point of storage and loss

10

modulus on the XHNBR content: both the frequency and the storage modulus at which this cross-over appears increase with the XHNBR content. For the P30H70X blend, the values of storage modulus are higher than loss modulus in the entire range of frequencies examined, which is indicative of the morphological change from droplet-matrix to co-continuous morphology [30,31].
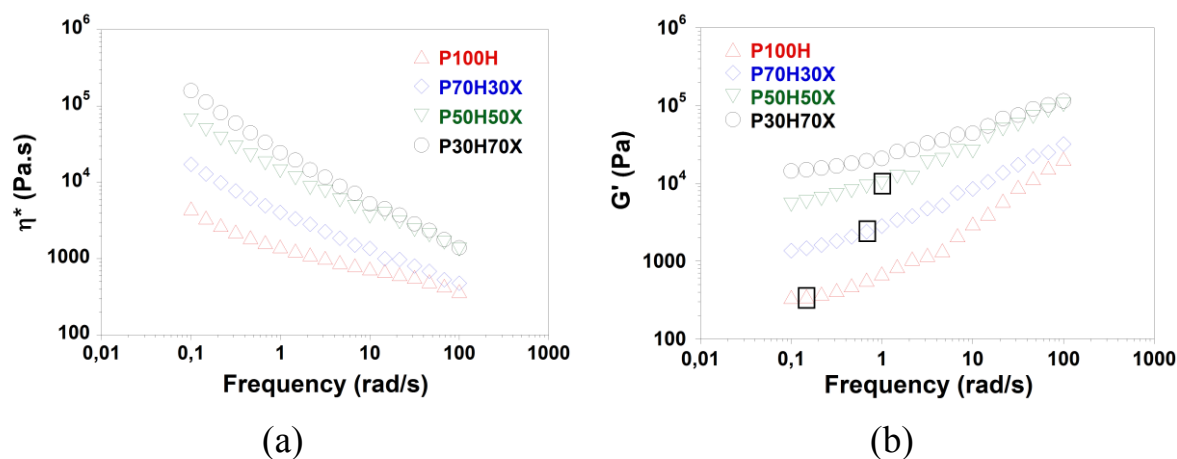

Fig. 6. Variation of (a) complex viscosity and (b) storage modulus of the blends as a function of the angular frequency at 240 °C. Cross-over points of the storage and loss modulus are framed.

So as to obtain a further insight on the effect of XHNBR content on the blend microstructure, the complex viscosity and storage modulus of the blend components are compared in Fig. 7a and b. PA6 shows a Newtonian behaviour whereas rubber blends show a linear increase in viscosity with decreasing the frequency. It is clearly seen that the addition of XHNBR increases both the viscosity and elasticity of the HNBR/XHNBR blends. Moreover, the viscosity and elasticity of the rubber blends are much higher than those of PA6 in the low angular region. Most of the models developed to predict the point at which the dispersed phase becomes continuous in a melt-mixed immiscible polymer blend have only considered the viscosity ratio of the blend components [32]. The most common empirical equation used to predict the phase inversion point is the one proposed by Paul and Barlow [33]:

$$\frac{\phi_A \eta_B}{\phi_B \eta_A} = 1 \tag{3}$$

11

where ϕ_A and ϕ_B are the volume fractions of phases A and B, and η_A and η_B their respective viscosities. If the ratio in equation (3) is lower than 1, phase A should form the dispersed phase in a continuous matrix of B, whereas B should be dispersed in A for values higher than 1. However, many authors have pointed out that the elasticity of the blend components plays also an important role in the co-continuity of binary blends [34–36]. Bourry and Favis [37] formulated an expression for the prediction of co-continuity as a function of the elasticity, represented by the storage modulus ratio of the two blend component:

$$\frac{\phi_A G'_A}{\phi_B G'_B} = 1 \tag{4}$$

So the model considering the viscosity ratio predicts that the less viscous phases will have the tendency to form the matrix and on the other hand the model based on elastic effects predicts that the more elastic phase will tend to form the matrix.

The variation of the viscosity and elasticity ratios of the TPE blends as a function of XHNBR content are shown in Fig. 8. The viscosity and elasticity ratios have been calculated using the values of complex viscosity and storage modulus of the blend components at 100 rad s^{-1} by applying Cox-Merz rule [38]. The twin-screw mixing speed of 100 rpm has been approximated to a shear rate of 100 s^{-1} [39] The results shown in Fig. 8 suggest that by increasing the XHNBR content the elastic effects become more important than the viscous ones. The increased elasticity of the rubber phase hinders the break-up and retraction phenomena of the elongated domains formed during melt-mixing, favouring the formation of the co-continuous morphology [40]. Therefore, the co-continuous morphology of the P30H70X blend is mainly caused by the increase of the elasticity of the rubber phase. The nonspherical shape of rubber domains of P50H50X blend is also a consequence of the increased droplet elasticity.

In order to further study the effect of XHNBR content in the adhesion between the phases, the variation of storage modulus of the blends as a function of stress has been studied at 240 °C and is shown in Fig. 9. It is observed that the onset of non-linearity shifts to higher stress values upon increasing the XHNBR content. This is shown in Fig. 10, which summarizes the critical stress, estimated as the value of the stress when the modulus is equal to 95% of the

12

plateau modulus [41] as a function of the XHNBR content. The critical stress can be related to the cohesive energy density, i.e., the energy needed to break the structure [42]. The critical stress increases with the XHNBR content, which is indicative of stronger adhesion between the rubber and PA6 phases.
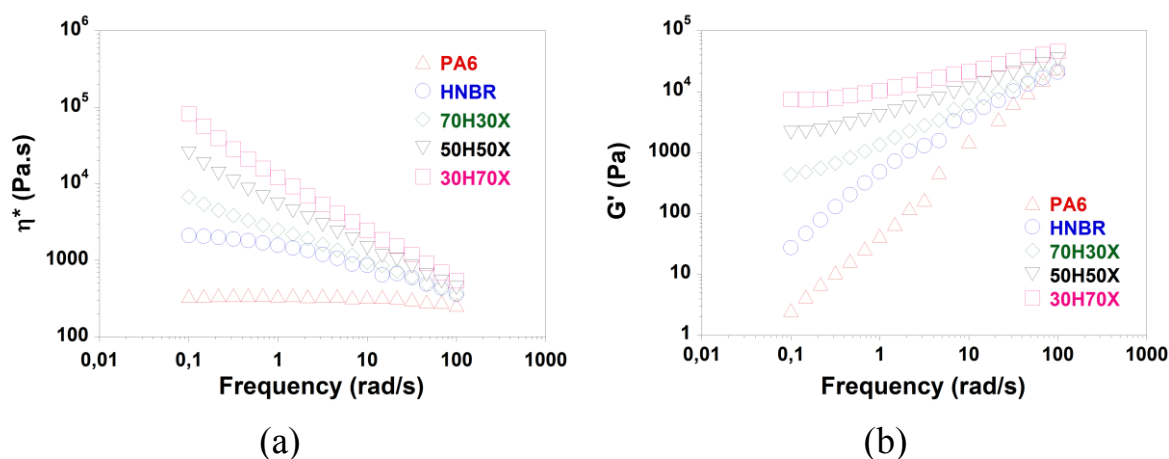

Fig. 7. Variation of (a) complex viscosity and (b) storage modulus of the blend components as a function of the angular frequency at 240 °C.
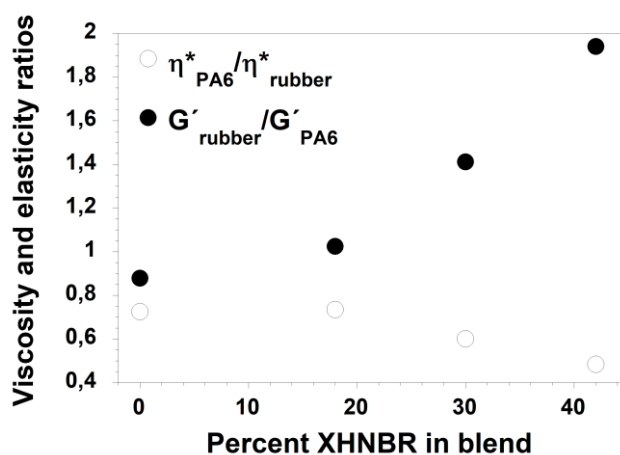

Fig. 8. Viscosity and storage modulus ratios as a function of XHNBR content, at 240 °C for an angular frequency of 100 rad s[-1].
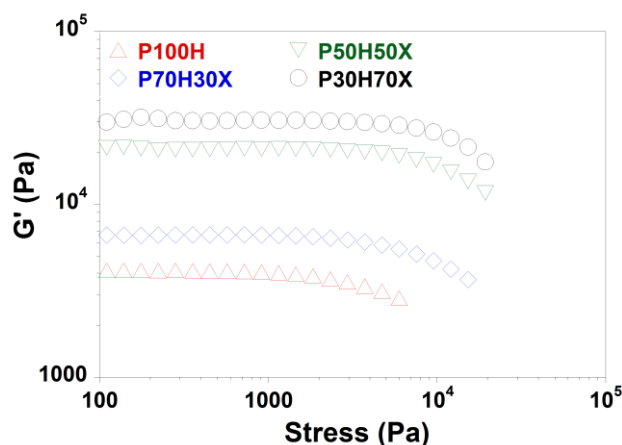
13

Fig. 9. Variation of storage modulus of the blends as a function of the stress at 240 °C.
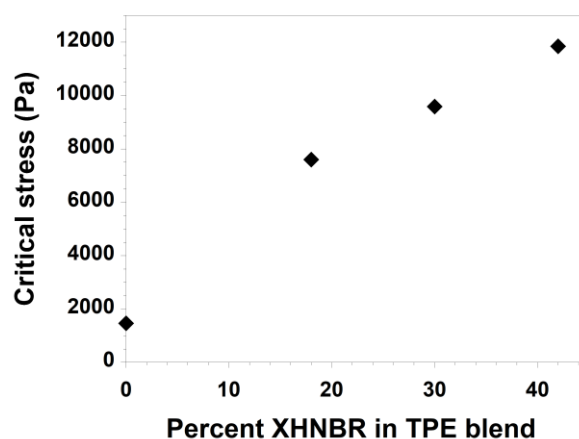

Fig. 10. Critical stress vs. XHNBR content.

Dynamic mechanical analysis

Fig. 11 shows the storage and loss modulus (E´ and E´´) of the blends and neat components as a function of temperature, obtained from the DMA measurements, in tensile mode. PA6 presents the maximum values of E´ at -50 °C whereas HNBR shows the minimum values. The blends show values of E´ that are in between those limits. Regarding the shape of the curves, it can be seen that the curves of the blends have two well defined drops related with the glass transition regions of the rubber phase and the PA6 phase. This observation can be explained on the basis of the two-phase morphological structure of the blends, typical of

14

immiscible systems. Furthermore, E′ values of P100H and P70H30X are near E′ values of PA6 at temperatures below the glass transition of the rubber phase. On the other hand, the E′ values corresponding to P50H50X and P30H70X get closer to those of the rubber blend components. This behaviour is related to the observed change from dispersed to co-continuous morphology. In blends with dispersed type morphology the E′ value is dominated by the matrix component, in our case by PA6, whereas in blends with co-continuous morphology the contribution of both components becomes greater [30]. Therefore, DMA results are in accordance with the change of morphology, from dispersed to co-continuous, observed in SEM images (Figs. 3 and 5).

The temperature dependence of loss modulus and loss tangent (tan δ) of the neat components and TPE blends are presented in Figs. 11b and 12, respectively. Two distinct relaxation peaks were observed for all the TPE blend samples that confirms the existence of a two phase-separated structure. It is therefore considered that the two peaks correspond to the T_gs of rubber and PA6 phases. DMA has been shown to be more sensitive than DSC to blend morphology [43,44]. For that reason, the glass transition temperatures have been evaluated by DMA. Fig. 13 illustrates the variation of the two T_gs with the XHNBR content in the blends. The glass transition temperatures have been considered as the peak values of the tan δ curve [45].
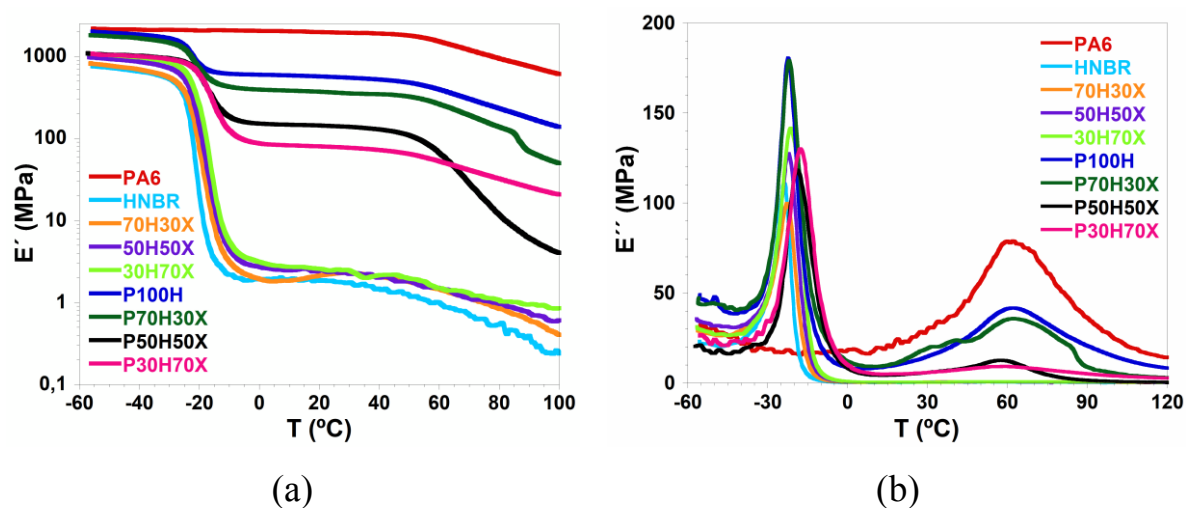

(a)   (b)

Fig. 11. Temperature dependence of storage modulus (a) and loss modulus (b) for pure components and TPE blends.

15

For the rubber phase an evident T_g depression has been observed in the P100H and P70H30X blends, where rubber is present in discrete domains. Many research works have reported the depression of rubber T_g in systems consisting of microspherical inclusions of a rubber in a rigid plastic matrix [46,47]. In such systems, the difference of the thermal contraction between the two phases would generate a negative pressure in the rubber phase, which results in an increase of the free volume and correspondingly a decrease of the T_g of the rubber phase.

Otherwise, a sharp increase in rubber T_g is observed at P50H50X blend approaching to the neat rubber T_g. Furthermore, it is interesting to note that the rubber T_g becomes slightly higher than the neat rubber T_g as the XHNBR content in the rubber blends phase is increased up to a 70% (Fig. 13a). The co-continuous morphology is characterized by frequent changes in the sign of curvature of the domain boundaries [48]. Besides, the pressure dependence of T_g [49] becomes more complicated. The co-continuous morphology is expected to show two rubber T_gs since some of the rubber is under compression and some is not. However, only one T_g is observed.

The rubber T_g increase in the P30H70X TPE blend is attributed to the interaction between phases which disturbs the molecular relaxation and cooperative mobility between structural units that is required during the glass transition process [50,51]. As the XHNBR content increases, more carboxyl groups exist in the rubber phase and this could result in a stronger interaction with PA6, thus generating a reduction of the molecular mobility of the amorphous domains located in the close vicinity of the crystals. Mucha [52] observed that the T_gs of both aPS and iPP changed due to phase interactions in aPS/iPP blends.

Another interesting point is that the addition of XHNRB leads to an increase of the glass transition temperature of PA6 (Fig. 13b). The measured T_g of neat PA6 was approximately 70 °C, whereas the T_g of PA6 in blends increases to 83 °C as the concentration of XHNBR in the TPE blend increases to 42%. Imre et al [53] observed an increase of the PLA T_g in PLA/PU blends prepared by reactive processing and they related this effect to the interfacial interactions. Recently, Fourati et al [39] reported an upward shift in the T_g of PBAT and TPS in PBAT/TPS blends in presence of PBATg-MA. They attributed the double T_g increase to

16

the strong adhesion between the two phases. Therefore, the measured PA6 T_g increase can be attributed to the enhanced interaction between PA6 and rubber as XHNBR content increases. It can be concluded that the interfacial interaction appears to explain the observed double T_g increase behavior in the P30H70X blend.
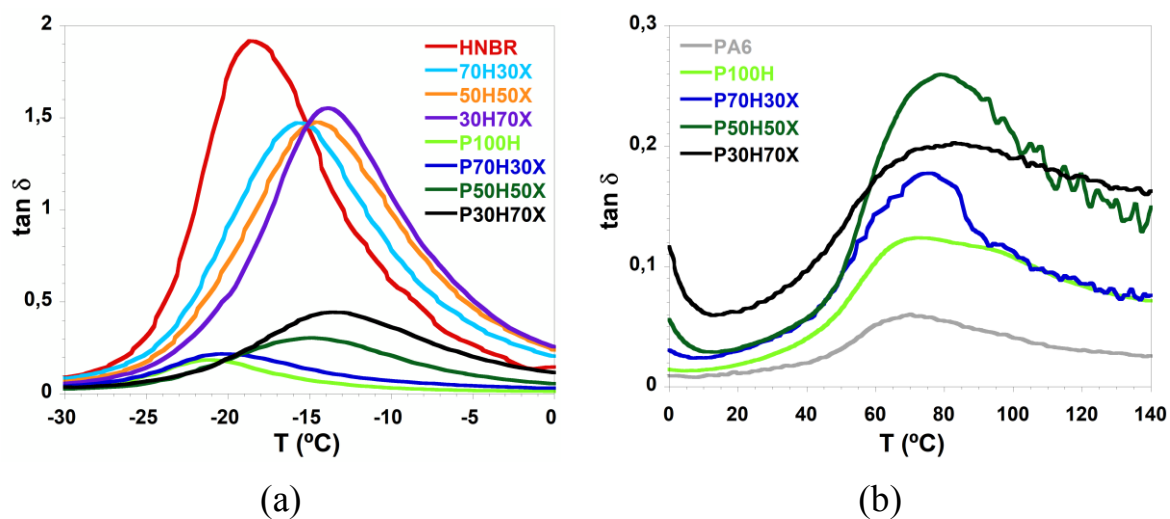

Fig. 12. Temperature dependence of loss tangent (tan δ) of pure components and TPE blends: (a) near loss peak of rubber phase and (b) near loss peak of PA6 phase.

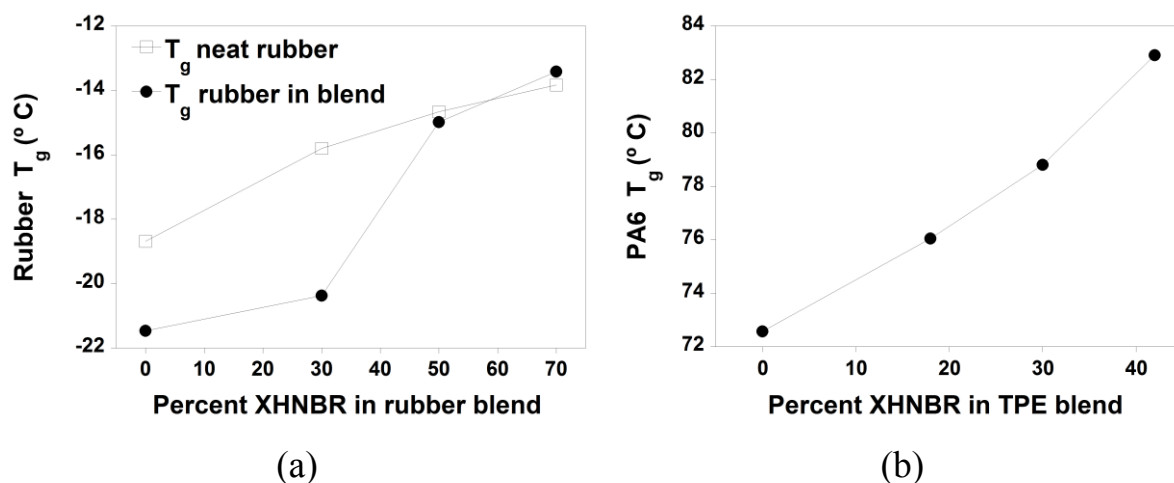Fig. 13. (a) Rubber T_g as a function of XHNBR wt% content in the rubber blend phase; (b) PA6 T_g as a function of XHNBR wt% in the TPE blend.

Differential scanning calorimetry analysis

The first heating and cooling DSC thermograms of PA6 and TPE blends are shown in Fig. 14, and the melting enthalpy (ΔH_m) and crystallinity degree (X_c) of PA6 are listed in Table 2. The degree of crystallinity was calculated from the heat of fusion during heating, considering a heat of fusion of 190 J/g for a 100% crystalline PA6 [54]. It is clearly seen that the content of XHNBR in the blend produces a big effect on the degree of crystallinity of PA6. The crystallinity of PA6 in the TPE blends decreased with the XHNBR content. As the content of XHNBR is increased, the crystallization peak became broader, as shown in Fig. 14b, which is attributed to reduced crystallinity of PA6 in the TPE blends [55]. Moreover, it can be observed that the crystallization peak of PA6 in the TPE blends shifted to lower temperatures as the XHNBR content increased, which clearly suggests enhanced interfacial interactions [56,57].

The crystallinity degree of the PA6 is strongly dependent on the capacity of the chains to package in an ordered way. Therefore, the remarkable decrease in crystallinity of PA6 is attributed to the interaction of the two phases that disturbs the mobility between structural units that is required during the crystallization of the PA6 [58,59]. Recently, Chen et al. [60] reported that the crystallinity of both PA6 and PVDF decreased in PA6/PVDF blends and they explained this effect considering the interaction between the two components.
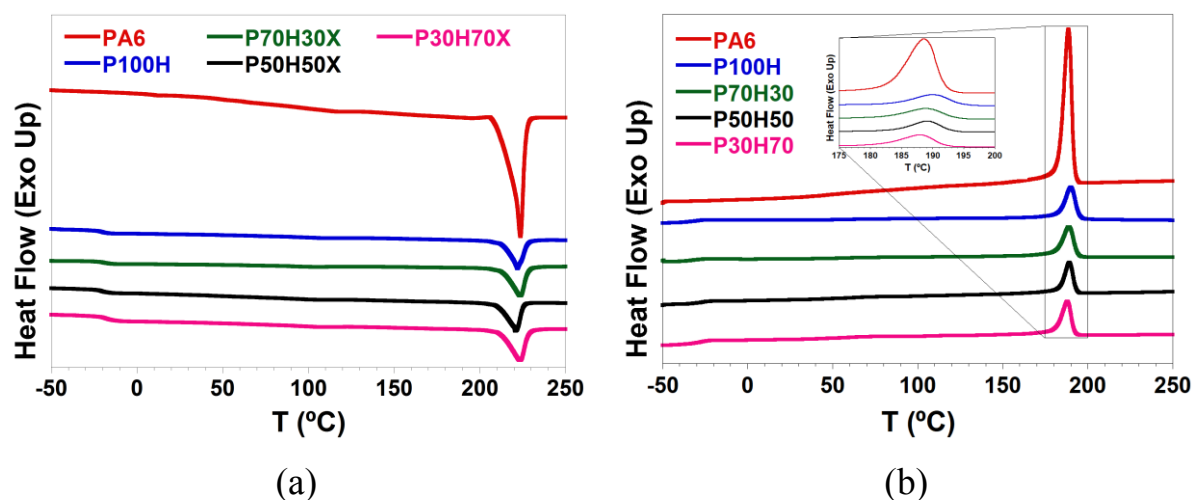

Fig. 14. DSC thermograms of PA6 and TPE blends: (a) first heating and (b) cooling.

Samples	ΔH_m (J/g)	X_c (%)
PA6	62.98	33.15

18

P100H	27.20	35.79
P70H30X	24.72	32.53
P50H50X	23.32	30.68
P30H70X	21.44	28.21

Table 2. Melting and crystallization results for PA6 and TPE blends, from DSC analysis.

Mechanical properties

The stress-strain curves at room temperature of TPE blends are presented in Fig. 15. It is found that while increasing the content of XHNBR and so decreasing the crystallinity (Table 2), the values of the stress at any strain decrease, indicating that the material deforms more easily. Fig. 16 illustrates the effect of XHNBR content on the tensile properties and the hardness of TPE blends. A remarkable brittle to ductile transition occurs with the addition of 42% of XHNBR. The P100H blend shows a limited elongation at break due to the poor interfacial adhesion between PA6 and HNBR [61]. The elongation at break of P30H70X blend reaches 180%, which is about 16 times higher than that of P100H. It has been proven by many authors that the elongation at break is sensitive to the morphological changes, and may exhibit a maximum in the co-continuous region [32]. Thus, the significant increment of the elongation at break with the addition of XHNBR is in line with the morphological results and suggests a better stress transmission capacity produced by the higher interfacial interaction between the rubber and PA6. Furthermore, unlike the elongation at break, the young modulus (Fig. 16b) of the blends decreases significantly with the addition of XHNBR. The decrease of the modulus by increasing XHNRB content may be caused by the change of morphology from dispersed to co-continuous together with the decrease of the crystallinity degree of the PA6. Regarding the hardness of the blends (Fig. 16c), there are no considerable differences among P100H, P70H30X and P50H50X blends. However, with the addition of 42% of XHNBR a reduction of the hardness is observed, which may be attributed to the existence of the co-continuous structure.
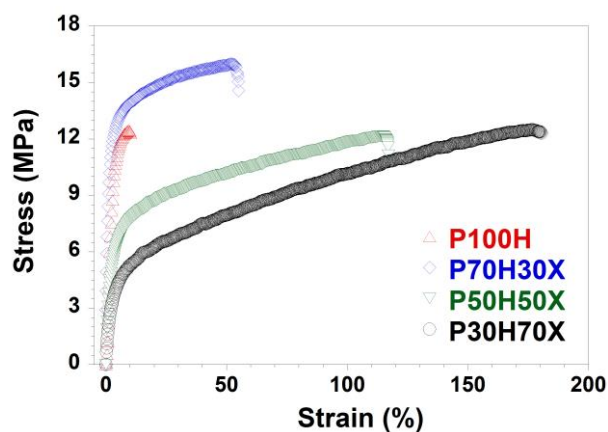
19

Fig. 15 Stress-strain curves at room temperature of the TPE blends.
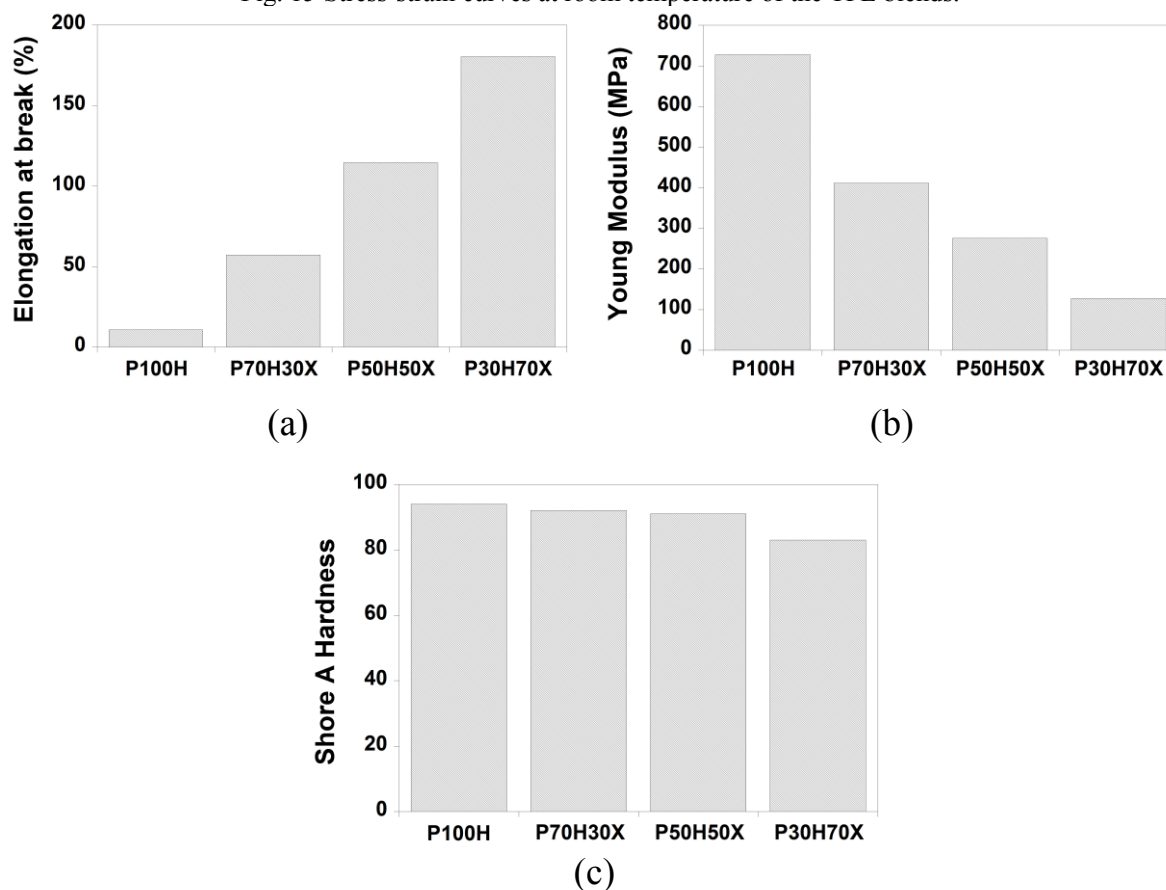

(a)

(b)

(c)

Fig. 16 Mechanical properties TPE blends: (a) Elongation at break; (b) Young Modulus and (c) hardness.

Conclusions

The four investigated PA6/HNBR/XHNBR TPE blend systems showed a biphasic morphology, indicating that the rubber and thermoplastic phases are immiscible. It was

20

found that the amount of XHNBR in the TPE blend influences the adhesion between the phases together with the viscosity and elasticity of the rubber phase. By the addition of XHNBR, the morphology of the TPE blends evolves from a droplet-matrix morphology with rubber particles in PA6 matrix to smaller-size rubber particles in PA6 matrix, then to string shape rubber particles in PA6 matrix, and finally to a co-continuous morphology when a 42% of XHNBR is introduced. The effects of the XHNBR content on the linear rheological properties of TPE blends were also investigated and correlated with the morphology and interfacial interaction. A decrease of PA6 crystallinity degree with the increase of XHNBR content was also observed. Moreover, when 42% of XHNBR was added the rubber as well as the PA6 phase showed a significant T_g increase, as compared with that of the neat components. It has been concluded that both the decrease in crystallinity and the double T_g increase phenomena may be due to the interfacial interactions between the phases, producing a decrease on the mobility of the amorphous domains of both the PA6 and the rubber phases. A fragile to ductile transition is also achieved by the addition of XHNBR. The TPE blend with 42% of XHNBR demonstrated 16 times the elongation at break of the blend without XHNBR. The enhanced interaction among the two phases, together with the change of morphology from matrix-dispersed to co-continuous, plays an important role in the improvement of ductile properties. Thus, the obtained changes in mechanical properties of the TPE blends are well corresponding to those obtained for morphology, viscoelastic and thermal properties.

This work opens new opportunities to develop TPE blends with superior ductility and increased glass transition temperatures of both rubber and thermoplastic phases by controlling the morphology and the interfacial interactions between the phases. Linear rheology has been identified as a strong tool to provide information about the morphological changes and the enhanced interfacial interactions.

Acknowledgements

21

References

1. Holden G, Kricheldorf HR, Quirt RP. Thermoplastic Elastomers. Eds. Hanser Publishers, Munich, Germany; 2004.

2. Nakajima K, Nishi T. Current topics in elastomers research. Bhowmick AK CRC Press N Y; 2008.

3. Bhowmick AK, Stephens H. Handbook of Elastomers. CRC Press; 2000.

4. Drobny JG. Handbook of thermoplastic elastomers. Elsevier; 2014.

5. Banerjee SS, Bhowmick AK. High-temperature thermoplastic elastomers from rubber–plastic blends: a state-of-the-art review. Rubber Chem Technol. 2017;90:1–36.

6. Smithers Rapra, Thermoplastic Elastomer Market to 2022. https://www.smithersrapra.com/market-reports/rubber-and-elastomer-industry/the-future-of-thermoplastic-elastomers-to-2022 [accessed 10 March 2017].

7. Donald PR, Bucknall CB. Polymer Blends: Formulation and Performance. John Wiley & Sons; 2000.

8. Das PK, Ambatkar SU, Sarma KSS, Sabharwal S, Banerji MS. Electron beam processing of nylon 6 and hydrogenated nitrile rubber (HNBR) blends: 1. Development of high strength heat- and oil-resistant thermoplastic elastomers. Polym Int. 2006;55:118–23.

9. Sarma AD, Padmanathan HR, Saha S, Banerjee SS, Bhowmick AK. Design and properties of a series of high-temperature thermoplastic elastomeric blends from polyamides and functionalized rubbers. J Appl Polym Sci. 2017;134:45353.

10. Saha S, Bhowmick AK. Computer aided simulation of thermoplastic elastomer from poly (vinylidene fluoride)/hydrogenated nitrile rubber blend and its experimental verification. Polymer. 2017;112:402–413.

11. Jung HS, Choi MC, Chang Y-W, Kang P-H, Hong SC. Facile preparation of thermoplastic elastomer with high service temperature from dry selective curing of compatibilized EPDM/polyamide-12 blends. Eur Polym J. 2015;66:367–75.

22

12. Hashim F, Ismail H, Rusli A. Comparison of properties of ethylene vinyl acetate/natural rubber/mengkuang leaf fibre (EVA/NR/MLF) and ethylene vinyl acetate/epoxidized natural rubber/mengkuang leaf fibre (EVA/ENR-50/MLF) thermoplastic elastomer composites. Polym Test. 2017;61:1–7.

13. Valerio O, Misra M, Mohanty AK. Statistical design of sustainable thermoplastic blends of poly(glycerol succinate-co-maleate) (PGSMA), poly(lactic acid) (PLA) and poly(butylene succinate) (PBS). Polym Test. 2018;65:420–8.

14. Xu C, Yuan D, Fu L, Chen Y. Physical blend of PLA/NR with co-continuous phase structure: Preparation, rheology property, mechanical properties and morphology. Polym Test. 2014;37:94–101.

15. Chaudhary V, Panyoyai N, Small DM, Shanks RA, Kasapis S. Effect of the glass transition temperature on alpha-amylase activity in a starch matrix. Carbohydr Polym. 2017;157:1531–1537.

16. Wang Y, Wang W, Zhang Z, Xu L, Li P. Study of the glass transition temperature and the mechanical properties of PET/modified silica nanocomposite by molecular dynamics simulation. Eur Polym J. 2016;75:36–45.

17. Zhao P, Wang M, Zhang J.Influence of chlorosulfonated polyethylene network structure on poly(acrylonitrile-styrene-acrylate)/poly(α-methylstyrene-acrylonitrile) blends: Mechanical properties, morphologies, glass transition behavior and heat resistance. Polym Test. 2017;57:175–83.

18. Bates FS, Cohen RE, Argon AS. Dynamic mechanical properties of polystyrene containing microspherical inclusions of polybutadiene: influence of domain boundaries and rubber molecular weight. Macromolecules. 1983;16:1108–14.

19. Qiu J, Xing C, Cao X, Wang H, Wang L, Zhao L, Li Y. Miscibility and double glass transition temperature depression of poly (l-lactic acid)(PLLA)/poly (oxymethylene)(POM) blends. Macromolecules. 2013;46(14):5806–5814.

20. Richard AL. Interface and surface effects on the glass-transition temperature in thin polymer films. Faraday Discuss. 1994;98:219–30.

21. Tao Z, Viriyabanthorn N, Ghumman B, Barry C, Mead J. Heat Resistant Elastomers. Rubber Chem Technol. 2005;78:489–515.

22. Kyriacos D. High-Temperature Engineering Thermoplastics. Brydsons Plast Mater. 2017;545–615.

23. Chowdhury R, Banerji MS, Shivakumar K. Polymer blends of carboxylated butadiene- acrylonitrile copolymer (nitrile rubber) and polyamide 6 developed in twin screw extrusion J Appl Polym Sci. 2007;104:372-7.

23

24. Banerjee SS, Bhowmick AK. Novel nanostructured polyamide 6/fluoroelastomer thermoplastic elastomeric blends: influence of interaction and morphology on physical properties. Polymer. 2013;54:6561–6571.

25. Banerjee SS, Bhowmick AK. Viscoelastic properties and melt rheology of novel polyamide 6/fluoroelastomer nanostructured thermoplastic vulcanizates. J Mater Sci. 2016;51:252–261.

26. Starý Z, Pemsel T, Baldrian J, Münstedt H. Influence of a compatibilizer on the morphology development in polymer blends under elongation. Polymer. 2012;53:1881–9.

27. Dedecker K, Groeninckx G. Reactive compatibilisation of A/(B/C) polymer blends. Part 1. Investigation of the phase morphology development and stabilisation. Polymer. 1998;39:4985–92.

28. Thomas S, Groeninckx G. Reactive compatibilisation of heterogeneous ethylene propylene rubber (EPM)/nylon 6 blends by the addition of compatibiliser precursor EPM-g-MA. Polymer. 1999;40:5799–819.

29. Jafari S., Pötschke P, Stephan M, Warth H, Alberts H. Multicomponent blends based on polyamide 6 and styrenic polymers: morphology and melt rheology. Polymer. 2002;43:6985–92.

30. Pötschke P, Paul DR. Detection of co-continuous structures in SAN/PA6 blends by different methods. Macromol Symp. 2003;198:69–82.

31. Abdolrasouli MH, Nazockdast H, Sadeghi GMM, Kaschta J. Morphology development, melt linear viscoelastic properties and crystallinity of polylactide/polyethylene/organoclay blend nanocomposites. J Appl Polym Sci. 2015;132.

32. Pötschke P, Paul DR. Formation of Co-continuous Structures in Melt-Mixed Immiscible Polymer Blends. J Macromol Sci Part C. 2003;43:87–141.

33. Paul DR, Barlow JW. Polymer Blends. J Macromol Sci Part C. 1980;18:109–68.

34. Chung O, Coran AY. The Morphology of Rubber/Plastic Blends. Rubber Chem Technol. 1997;70:781–97.

35. Steinmann S, Gronski W, Friedrich C. Cocontinuous polymer blends: influence of viscosity and elasticity ratios of the constituent polymers on phase inversion. Polymer. 2001;42:6619–29.

24

36. Lerdwijitjarud W, Sirivat A, Larson RG. Influence of dispersed-phase elasticity on steady-state deformation and breakup of droplets in simple shearing flow of immiscible polymer blends: J Rheol. 2004;48:843-62.

37. Bourry D, Favis BD. Cocontinuity and phase inversion in HDPE/PS blends: Influence of interfacial modification and elasticity J Polym Sci Part B Polym Phys. 1998;36:1889–1899.

38. Cox WP, Merz EH. Correlation of dynamic and steady flow viscosities. J Polym Sci. 1958;28:619–622.

39. Fourati Y, Tarrés Q, Mutjé P, Boufi S. PBAT/thermoplastic starch blends: Effect of compatibilizers on the rheological, mechanical and morphological properties. Carbohydr Polym. 2018;199:51–7.

40. Nuzzo A, Bilotti E, Peijs T, Acierno D, Filippone G. Nanoparticle-induced co-continuity in immiscible polymer blends − A comparative study on bio-based PLA-PA11 blends filled with organoclay, sepiolite, and carbon nanotubes. Polymer. 2014;55:4908–19.

41. Abbasi S, Carreau PJ, Derdouri A, Moan M. Rheological properties and percolation in suspensions of multiwalled carbon nanotubes in polycarbonate. Rheol Acta. 2009;48:943.

42. Bossard F, Moan M, Aubry T. Linear and nonlinear viscoelastic behavior of very concentrated plate-like kaolin suspensions: J Rheol. 2007;51:1253–1270.

43. Pinoit D, Prud'homme RE. DSC and DMTA characterization of ternary blends. Polymer. 2002;43:2321–2328.

44. Hunt BJ, James MI, editors. Polymer Characterisation. Dordrecht: Springer Netherlands; 1993.

45. Reghunadhan A, Stranskowski M, Datta J, Kalarikkal N, Thomas S. Recycled Polyurethane as a Second Phase in Thermoset Blends and Its Effect on Thermal Degradation Kinetics Studies. Macromol Symp. 2018;381:1800112.

46. Inoue T, Ogata S, Kakimoto M, Imai Y. Depression of glass transition temperature in aramid-polybutadiene multiblock copolymers. Macromolecules. 1984;17:1417–1419.

47. Hashima K, Usui K, Fu L, Inoue T, Fujimoto K, Segawa K, et al. Super-ductile PBT alloy with excellent heat resistance. Polym Eng Sci. 2008;48:1207–1213.

48. Thirtha V, Lehman R, Nosker T. Glass transition phenomena in melt-processed polystyrene/polypropylene blends. Polym Eng Sci. 2005;45:1187–1193.

25

49. Isayev AI. Encyclopedia of Polymer Blends, Volume 3: Structure. Vol. 3. John Wiley & Sons; 2016.

50. Donth E. The glass transition: relaxation dynamics in liquids and disordered materials. Vol. 48. Springer Science & Business Media; 2013.

51. Zachariah AK, Chandra AK, Mohammed PK, Parameswaranpillai J, Thomas S. Experiments and modeling of non-linear viscoelastic responses in natural rubber and chlorobutyl rubber nanocomposites. Appl Clay Sci. 2016;123:1–10.

52. Mucha M. Miscibility of isotactic polypropylene with atactic polystyrene. Colloid Polym Sci. 1986;264:859–865.

53. Imre B, Bedő D, Domján A, Schön P, Vancso GJ, Pukánszky B. Structure, properties and interfacial interactions in poly(lactic acid)/polyurethane blends prepared by reactive processing. Eur Polym J. 2013;49:3104–13.

54. Brandrup J, Immergut EH, Grulke EA. 1999, Polymer handbook. Wiley-Interscience, New York; 1989.

55. Joo YS, Cha JR, Gong MS. Biodegradable shape-memory polymers using polycaprolactone and isosorbide based polyurethane blends. Mater Sci Eng C. 2018;91:426–35.

56. Kar GP, Biswas S, Bose S. X-ray micro computed tomography, segmental relaxation and crystallization kinetics in interfacial stabilized co-continuous immiscible PVDF/ABS blends. Polymer. 101:291–304.

57. Salaeh S, Banda T, Pongdong V, Wießner S, Das A, Thitithammawong A. Compatibilization of poly(vinylidene fluoride)/natural rubber blend by poly(methyl methacrylate) modified natural rubber. Eur Polym J. 2018;107:132–42.

58. Talibuddin S, Wu L, Runt J, Lin JS. Microstructure of Melt-Miscible, Semicrystalline Polymer Blends. Macromolecules. 1996 ;29:7527–35.

59. Rim PB, Runt JP. Melting behavior of crystalline/compatible polymer blends: poly(iε-caprolactone)/poly(styrene-co-acrylonitrile). Macromolecules. 1983;16:762–768.

60. Chen N, Yao X, Zheng C, Tang Y, Ren M, Ren Y, et al. Study on the miscibility, crystallization and crystalline morphology of polyamide-6/polyvinylidene fluoride blends. Polymer. 2017;124:30–40.

61. Akhtar S, De PP, De SK. SEM studies of the tensile fracture surfaces of thermoplastic elastomers from blends of ldpe and natural rubber. Mater Lett. 1988;6:186–90.

26

New ways to improve the damping properties in high-performance thermoplastic vulcanizates

Aizeti Burgoa[1*], Ricardo Hernandez[1] and Jose Luis Vilas[2,3]

[1]Leartiker S. Coop, Xemein Etorbidea, 12-A E-48270, Markina-Xemein, Bizkaia (Spain).

[2]Macromolecular Chemistry Research Group (labquimac), Department of Physical Chemistry, Faculty of Science and Technology, University of the Basque Country (UPV/EHU), 48940 Leioa, Spain.

[3]BCMaterials, Basque Center for Materials, Applications and Nanostructures, UPV/EHU Science Park, 48940 Leioa, Spain.

E-mail: aburgoa@leartiker.com

Abstract

The incorporation of viscoelastic materials represents an effective strategy to reduce the vibratory level of structural components. Thermoplastic vulcanizates (TPVs) are a special type of viscoelastic materials that combine the elastomeric properties of rubbers with the ease processing of thermoplastics. In the present work, we propose innovative ways to improve the damping properties of high-performance TPVs by using rubbers with carboxylic functionalities. For that, TPVs from physical blends of carboxylated hydrogenated acrylonitrile butadiene rubber (XHNBR) and polyamide 6 (PA6) are prepared. The chain dynamics of different mixed crosslink systems containing peroxide, metal oxides and hindered phenolic antioxidants are investigated in order to find the most suitable strategy to design high-performance TPV system with upgraded damping properties. Results indicate that the damping performance of the TPV systems can be tailored by controlling the type and magnitude of the bonding interactions between the mixed crosslink systems and the XHNBR rubber phase. Therefore, this study demonstrates the potential of TPV systems containing carboxylic rubbers as high-performance damping materials.

Introduction

The reduction of vibration phenomena is one of the major criteria for achieving customer satisfaction in several industries, such as automotive, aeronautic and aerospace[1,2]. A fairly simple way to increase the vibration performance of lightly damped structures is based on the incorporation of viscoelastic materials[3]. The use of viscoelastic materials decreases the vibratory level transmitted and so the noise field generated[4]. Thermoplastic elastomers (TPEs) are a special class of viscoelastic materials that combine properties of thermoplastic and elastomers[5]. These viscoelastic materials possess elastomeric behavior with the advantage that can be melt-processed like thermoplastics[6].

Melt-mixing of different rubbers and thermoplastics is a particularly interesting way of making TPEs[7–9]. The TPE blends can be either simple blends with non-crosslinked rubber phase or blends with dynamically vulcanized rubber phase, i.e, thermoplastic vulcanizates (TPVs)[10]. The dynamic vulcanization refers to the crosslinking of the rubber phase during melt blending with the thermoplastic and promotes the achievement of superior properties[11–13]. Over the last few years, numerous researchers have reported different TPEs from various rubbers and thermoplastics[14]. In our recent publication, we have reported an effective strategy for the preparation of high-performance thermoplastic elastomer blends from polyamide 6 (PA6) and carboxylated hydrogenated acrylonitrile butadiene rubber (XHNBR)[15].

The exceptional damping properties of carboxylic rubbers, such as XHNBR, have generated an extensive interest in the design and preparation of such elastomers[16–18]. The addition of different crosslink types can improve the damping properties of carboxylic rubbers within a wide range of temperature and frequency ranges[19]. One of the most conventional ways to improve the damping properties of carboxylic rubbers is based on the use of metallic oxides in order to create ionic crosslinks[20]. The ionic crosslinking reaction occurs through the formation of the corresponding salt of the metal ion[21,22]. These ionic bonds tend to associate and form an independent microphase, which is immersed in the elastomeric matrix[23].

Zinc oxide (ZnO) is one of the most commonly used metallic oxides for carboxylic rubbers[24]. However, the use of ZnO presents some problems. The most important ones are related to its precocity and toxic effects[25]. To find an alternative to ZnO Ibarra et al. explored the ionic crosslinking of XNBR with MgO[26]. They reported that ionic associations are formed between XNBR and MgO, which lead to the formation of a segregated structure that generates an additional relaxation at high temperatures apart from the glass transition of XNBR.

Mixing different crosslink systems represents an effective approach to obtain damping elastomers with upgraded properties[27]. Carboxylic rubbers crosslinked only with metal oxides show poor properties at high temperatures due to the low bond energy of ionic crosslinks. In order to overcome this disadvantage, Ibarra et al.[28] studied the vulcanization of XNBR by a mixed crosslink system of zinc oxide and zinc peroxide. The combination of metal oxides and peroxides produces not only ionic bonds but also covalent ones. These combination improves the properties of XNBR at high temperatures without altering the thermo-reversible nature of the ionic structure[29].

Addition of hindered phenolic compounds is also a quite new and useful method to improve the damping performance of carboxylic rubbers. This method is based on the design concept of organic hybrid damping materials[30,31]. Liu et al.[32] found that the addition of hindered phenolic antioxidants improves remarkably the damping properties of XNBR. They associated this effect to the formation of hydrogen bonds. Moreover, the damping capacity of XNBR is improved when the number of generated hydrogen bonds is increased.

Therefore, carboxylic rubbers are potential elastomeric segments to be used in order to obtain TPVs with superior damping performance properties. However, hardly any paper has been found in the literature that analyzes the use of carboxylated rubbers to develop damping TPV materials. Thus, in the present work peroxide-cured thermoplastic vulcanizates based on polyamide 6 (PA6) and carboxylated hydrogenated acrylonitrile butadiene rubber (XHNBR) containing different amounts of ZnO, MgO and hindered phenolic antioxidants were prepared. The chain dynamical properties of ZnO, MgO and

hindered phenolic antioxidants were investigated in order to find the most suitable high-performance system for damping applications.

Experimental

Materials

The hydrogenated acrylonitrile butadiene rubber HNBR and carboxylated hydrogenated acrylonitrile butadiene rubber XHNBR used in this study were respectively, Therban® AT 3904 VP (acrylonitrile content 39 wt%, residual double bonds 0.5%, specific gravity 0.96, mooney viscosity ML (1+4) at 100 °C 40) and Therban® XT VP KA 8889 (acrylonitrile content 33 wt%, residual double bonds 3.5%, carboxylic acid 5%, specific gravity 0.97, mooney viscosity ML (1+4) at 100 °C 74), supplied by Arlanxeo, Deutschland GmbH. The polyamide 6 PA6 Durethan® B 30 S 000000 (melting point 222 °C, density 1.14 g cm^{-3}) was obtained from Lanxess, Deutschland GmbH. The peroxide used was Trigonox 145, which was supplied by Akzo Nobel Polymer Chemicals, The Netherlands. Trimethylolpropane trimethacrylate (TMPTMA, Rhenofit TRIM/S) used as co-agent was provided by Rhein Chemie Additives, Lanxess Deutchland GmbH. The metallic oxides used were ZnO and MgO, which were obtained from Panreac Applichem, Spain. The hindered phenolic antioxidants used were Irganox 1098 and Irganox 1010 from BASF, Switzerland (their chemical structures are given in table 1). All chemicals were used as were received.
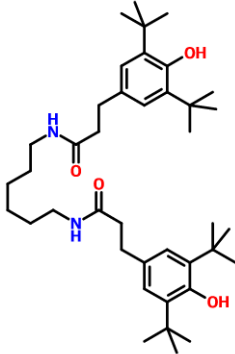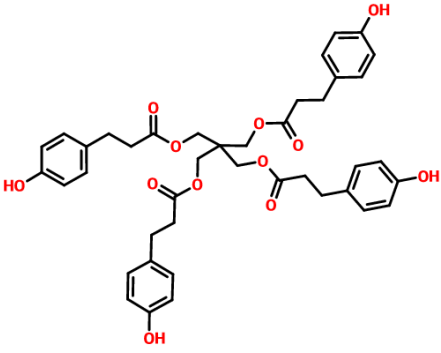
Commercial name	Chemical name	Chemical structure

Irganox 1098	N,N'-hexane-1,6-diylbis(3-(3,5-di-tert.-butyl-4-hydroxyphenylpropionamide))	
Irganox 1010	Pentaerythritol tetrakis(3-(3,5-di-tert-butyl-4-hydroxyphenyl)propionate)	

Table 1: Chemical structure of the hindered phenolic antioxidants used.

Preparation of TPVs

In our recent studies the effect of XHNBR content on the thermal and mechanical properties of TPE systems based on PA6 and HNBR have been analyzed. 40 PA6/18 HNBR/42 XHNBR blend composition showed a co-continuous morphology and the best elastomeric properties among the analyzed compositions[15]. For those reasons, this particular composition was subjected to dynamic vulcanization.

The TPV preparation process was done in three steps. In the first step HNRB and XHNBR gums were blended at 30/70 wt/wt blend ratio in a two-roll mill and different amounts of additives were added and mixed continuously. The compositions of the rubber compounds are shown in table 2. The compound additives are given as parts per hundred by weight of the rubber polymer, i.e., phr. In the second step the uncured rubber compound sheets

obtained in the two-roll mill were extruded into strands for subsequent pelletization. Extrusion was carried out at a rotor speed of 15 rpm at 90 °C in a Gumix extruder (L/D=10).

Finally, in the third step, the TPVs were prepared by melt-blending the rubber compounds with PA6 in a Brabender DSE 20/40 corrotating twin screw extruder. PA6 granules were dried at 80 °C for 8 hours prior to blending. Blending was carried out at a rotor speed of 200 rpm at 240 °C. Immediately after blending, the TPV pellets where compression moulded at 240 °C at a constant pressure of 200 bar for 2 minutes to form 1 mm thick sheets. All samples were dried at 80 °C for 8 hours prior to any characterization.

Sample name	Composition					
	Peroxide	Co-agent	Hindered phenolic antioxidants		Metallic Oxides	
	Trigonox 145	TRIM/S	Irganox 1098	Irganox 1010	ZnO	MgO
HXA0	3	2	0	0	2	3
HXA98	3	2	5	0	2	3
HXA10	3	2	0	5	2	3
HXZM	3	2	0	0	1	1
HXM	3	2	0	0	1	5
HXZ	3	2	0	0	5	1

Table 2: Formulation of the rubber compounds.

Scanning Electron Microscopy (SEM)

Morphological study of the samples was carried out using a field-emission scanning electron microscope with a Schottky type field-emission gun (JEOL JSM-7000F). The samples where brittle fractured in liquid nitrogen prior to SEM observation. The rubber phase in the

surface of the non-vulcanized TPE blend, i.e. the TPE blend with co-continuous morphology, was extracted by immersing the blend into acetone at room temperature for 24 hours. The cryofractured surfaces were sputter coated with a gold layer prior to microscopy.

Dynamic Mechanical Analysis (DMA)

Dynamic mechanical analysis (DMA) was performed by means of a Rheometrics Solids Analyzer (RSA II) in tension mode. Loss tangent (*tan δ*) as a function of temperature was measured at 1 Hz oscillating frequency while heating from -40 to 200 °C at a heating rate of 3 °C min^{-1}. All the measurements were performed at a strain of 0.03%.

Fourier Transform Infrared (FTIR) Spectroscopy

Fourier Transform Infrared (FTIR) measurements were performed by a Nicolet IS10 spectrometer. FTIR-ATR spectra were collected from 400 to 4000 cm^{-1} by performing 32 scans with a resolution of 4 cm^{-1}. All FTIR spectra were normalized by the intensity of the antisymmetric –CH$_2$– stretching band located at 2937 cm^{-1}.

Differential Scanning Calorimetry (DSC)

Differential scanning calorimetry (DSC) measurements were performed on the DSC Q100 (TA Instruments) calorimeter under nitrogen atmosphere. Samples were heated from room temperature to 250 °C, followed by cooling from 250 °C to -50 °C and heating again from -50 to 250 °C with a rate of 10°C min^{-1}. The first heating was conducted to remove the thermal history.

Mechanical testing

Tensile tests of the TPVs were carried out according to ISO 37 test method on dumbbell-shaped specimens using a MTS Insight Universal Testing Machine at a constant crosshead speed of 5 mm min^{-1} at room temperature.

Results and discussion

Morphological investigation

SEM micrographs of the TPVs are shown in Fig. 1. As we expected, dispersion of crosslinked rubber particles in a continuous PA6 matrix is observed in all TPVs. The dynamic vulcanization in presence of curing agents leads to selective crosslinking in the rubber phase that results in an increase of the rubber viscosity. The abrupt increase of the viscosity of the rubber phase promotes the phase inversion, i.e, the rubber phase tends to be encapsulated by the less viscous thermoplastic phase. Meanwhile, the applied high shear rate does not allow the crosslinked rubber phase to be coalesced into a continuous phase. At the end of the melt mixing process of the rubber compound with the molten thermoplastic, the rubber phase will be finely dispersed in the thermoplastic matrix[33]. From the SEM micrographs in Fig. 1 it can be concluded that the domain sizes of the crosslinked rubber particles are in the micron (µm) or submicron level for all TPV samples. The development of the dispersed phase morphology from the co-continuous phase is depicted in Fig. 2. The rubber phase on the surface of the non-vulcanized TPE blend was etched with acetone in order to reveal the co-continuous phase[34].
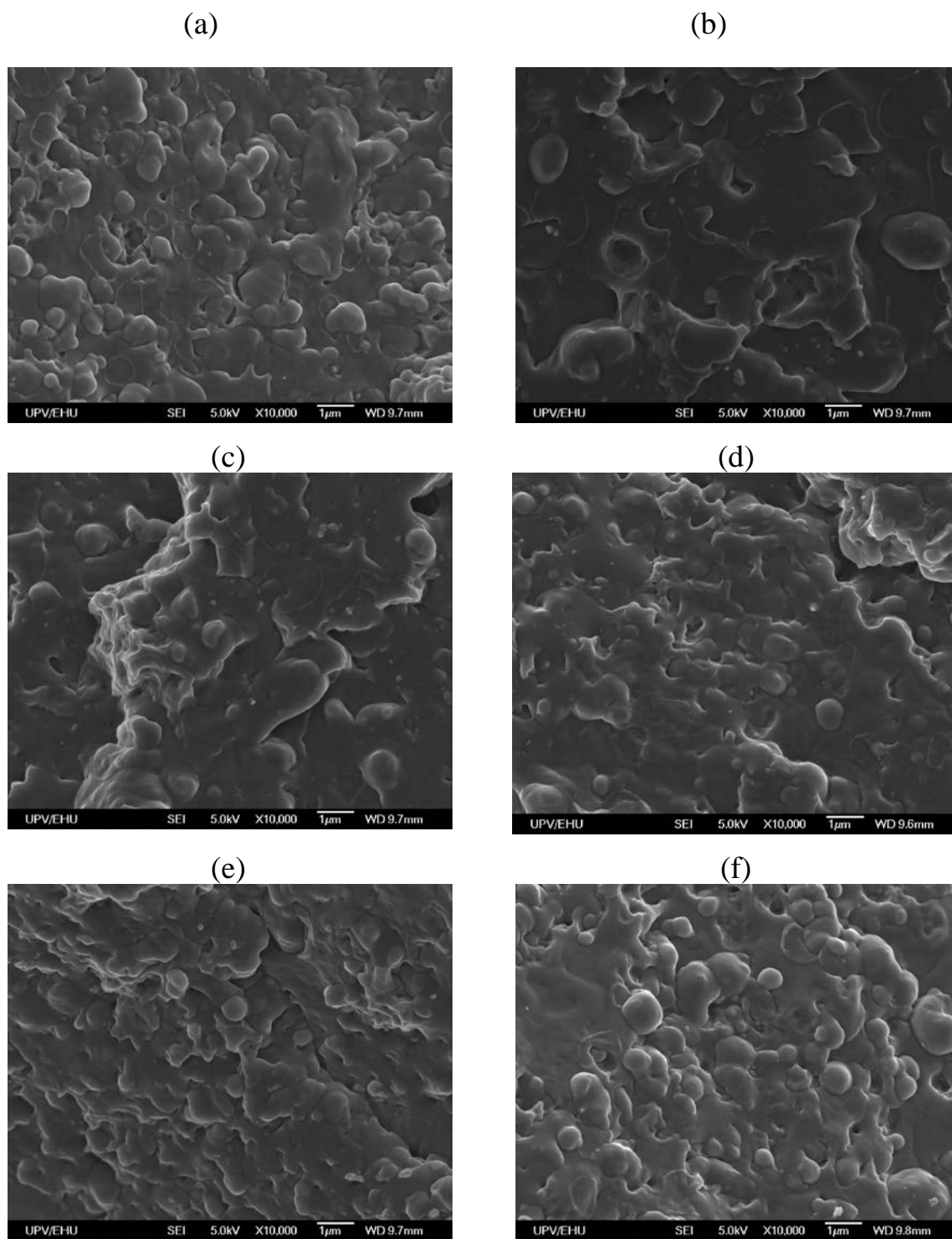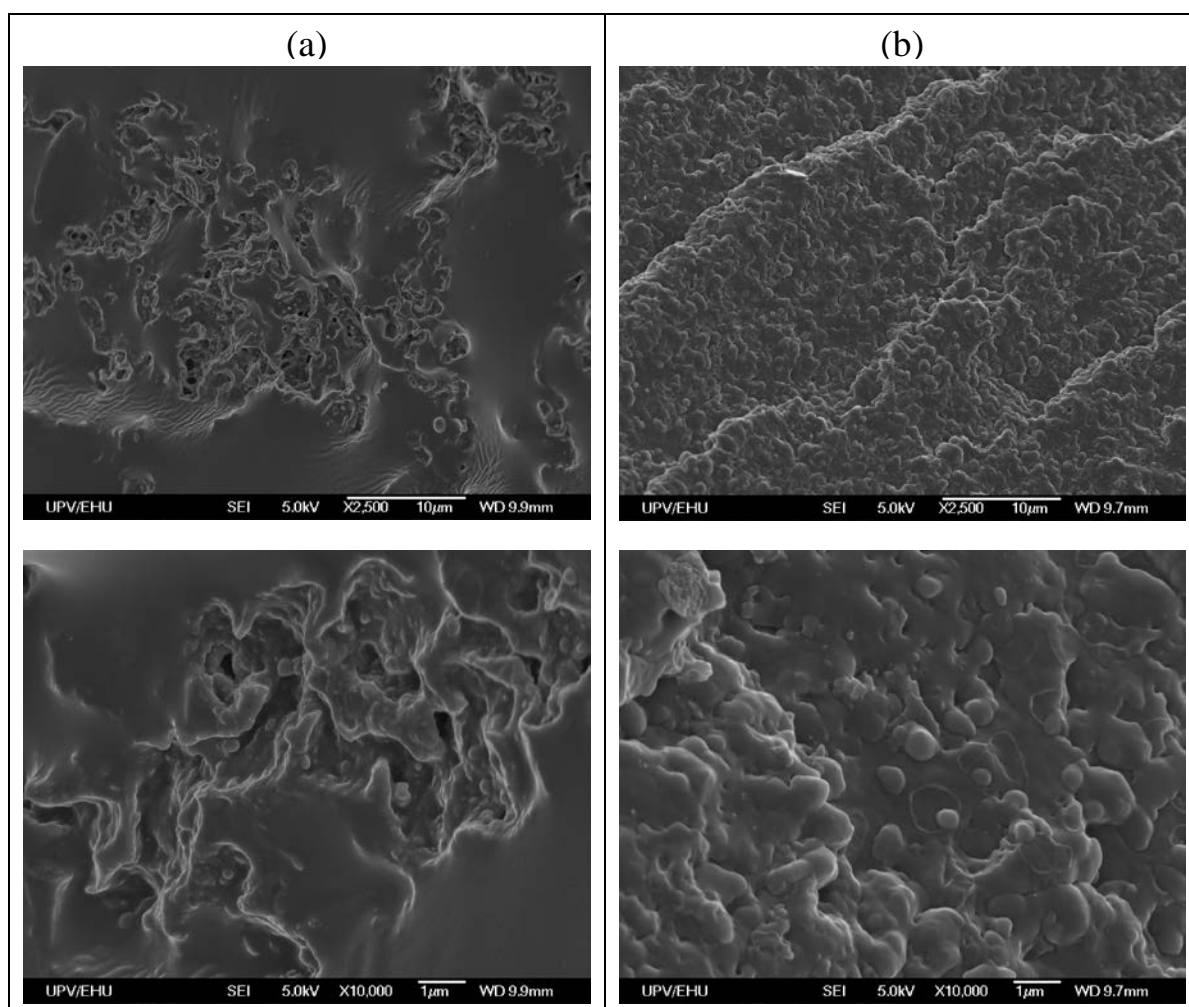
(a)

(b)

(c)

(d)

(e)

(f)

Figure 1. SEM micrographs of (a) PA6/HXA0; (b) PA6/HXA98; (c) PA6/HXA10; (d) PA6/HXZM; (e) PA6/HXM; (f) PA6/HXZ.

Dynamic vulcanization

Figure 2. Morphological transition from co-continuous to droplet-matrix morphology of the PA6/HNBR/XHNBR (40/18/42 wt/wt/wt) blend after dynamic vulcanization: (a) SEM images of the non-vulcanized TPE blend after etching the rubber phase with acetone and (b) SEM images of PA6/HXA0 TPV. Upper and lower images represent SEM images with different magnifications.

Dynamic mechanical analysis

The damping properties of TPVs are investigated by means of DMA analysis and loss tangent (*tan δ*) is used as a measure of damping. Fig. 3 shows the effects of hindered phenolic antioxidants on the damping properties of TPV samples. The effects of metallic oxides on damping properties of TPVs are shown in Fig. 4. The lower temperature peak can be assigned to the T_g of the rubber phase, whereas the damping peak at about 80 ºC is assigned to the PA6 amorphous phase T_g. Therefore, DMA results confirm the existence of a two phase-separated structure observed in SEM images.

Regarding the effect of hindered phenolic antioxidants, as shown in Fig. 3, the presence of Irganox 1010 increases the *tan δ* peak height of both rubber and PA6 phases. By contrast, the presence of Irganox 1098 decreases sharply the *tan δ* peak of the rubber phase. Moreover, the damping peak temperature (T_g) of the rubber phase in PA6/HXA10 increases slightly from -10 ºC to -7 ºC, while no shift was observed in PA6/HXA98. The peak shift and the growth of the *tan δ* peak demonstrate the existence of strong hydrogen bonding interaction between the Irganox 1010 and the rubber phase[35,36].

With respect to the TPVs containing different amounts of metallic oxides, the results shown in Fig. 4 clearly reveal an additional relaxation transition at about 40 ºC for PA6/HXM and PA6/HXZ, i.e, the TPV samples containing 5 phr of MgO and 5 phr ZnO, respectively. This relaxation transition can be associated with the formation of ionic clusters or associates between Zn or Mg ions and the carboxyl groups present in the rubbery phase, which behave as independent microphases inside the rubbery phase[37]. This phenomena is schematically represented in Fig. 5.

Interestingly, the PA6/HXM sample shows the highest *tan δ* values, whereas PA6/HXZ shows the lowest ones. The other TPV samples show values that are in between. Moreover, the PA6/HXM sample possess a much higher *tan δ* value in the ionic transition, and the ionic transition range is also broader. These results reflect that, for this particular TPV compounds, MgO is more effective than ZnO in neutralizing the carboxyl groups present in

the rubbery phase. The effect of different oxides and hydroxides of divalent metals in the mechanical properties of a carboxylic styrene butadiene rubber (XSBR) containing 1.5 wt% of carboxylic groups have been studied by Dolgoplost et al.[38]. They found that MgO gives better physical properties than ZnO. The mechanics of crosslinking in the carboxylic rubber phase of the TPV compounds as a function of the different crosslinking agents is shown in Fig. 6.
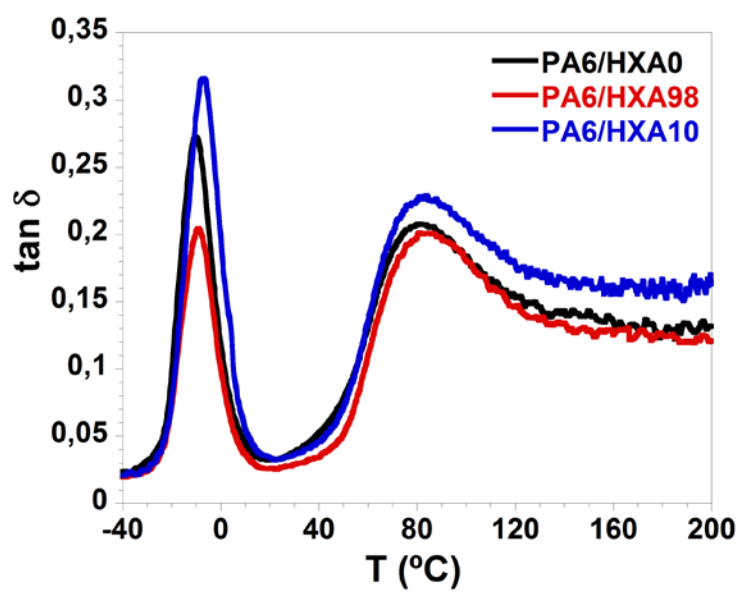

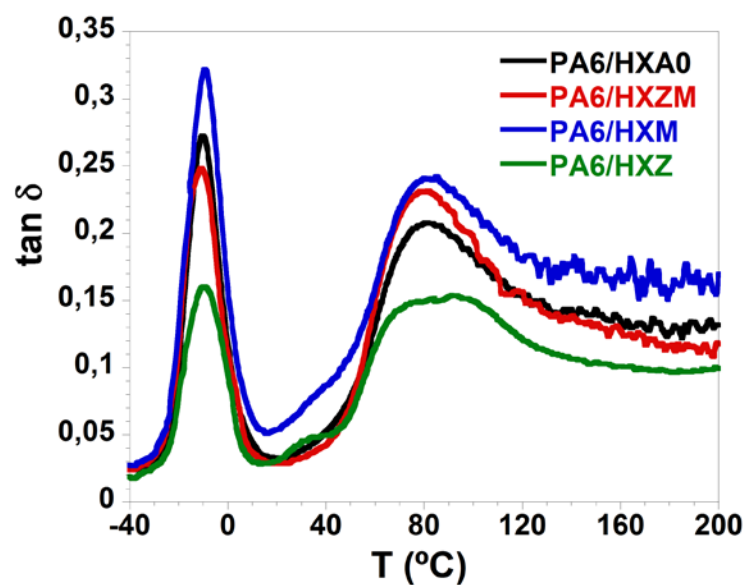**Figure 3.** Temperature dependence of tan δ for TPV samples containing different amount of phenolic antioxidants.

Figure 4. Temperature dependence of tan δ for TPV samples containing different amount of metallic oxides.
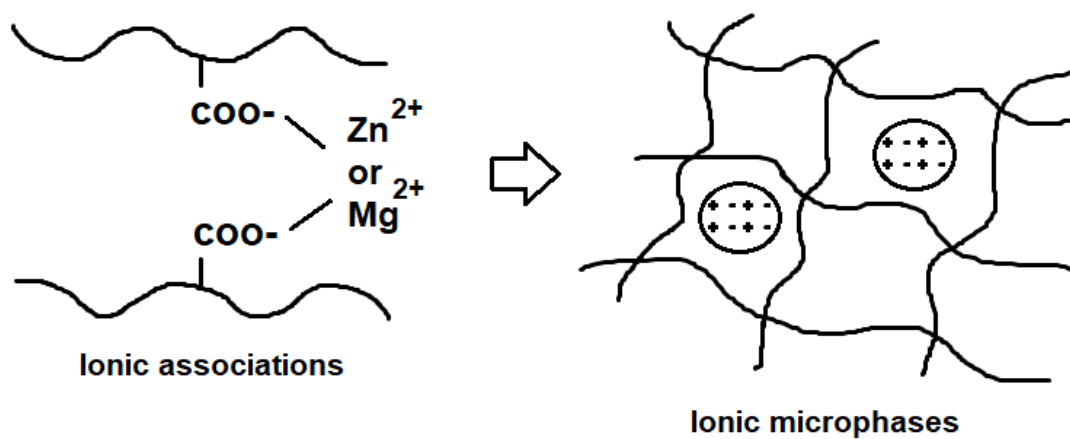

Figure 5. Schematic model showing the formation of ionic associations and ionic microphases comprising ZnO or MgO and carboxylate ions.
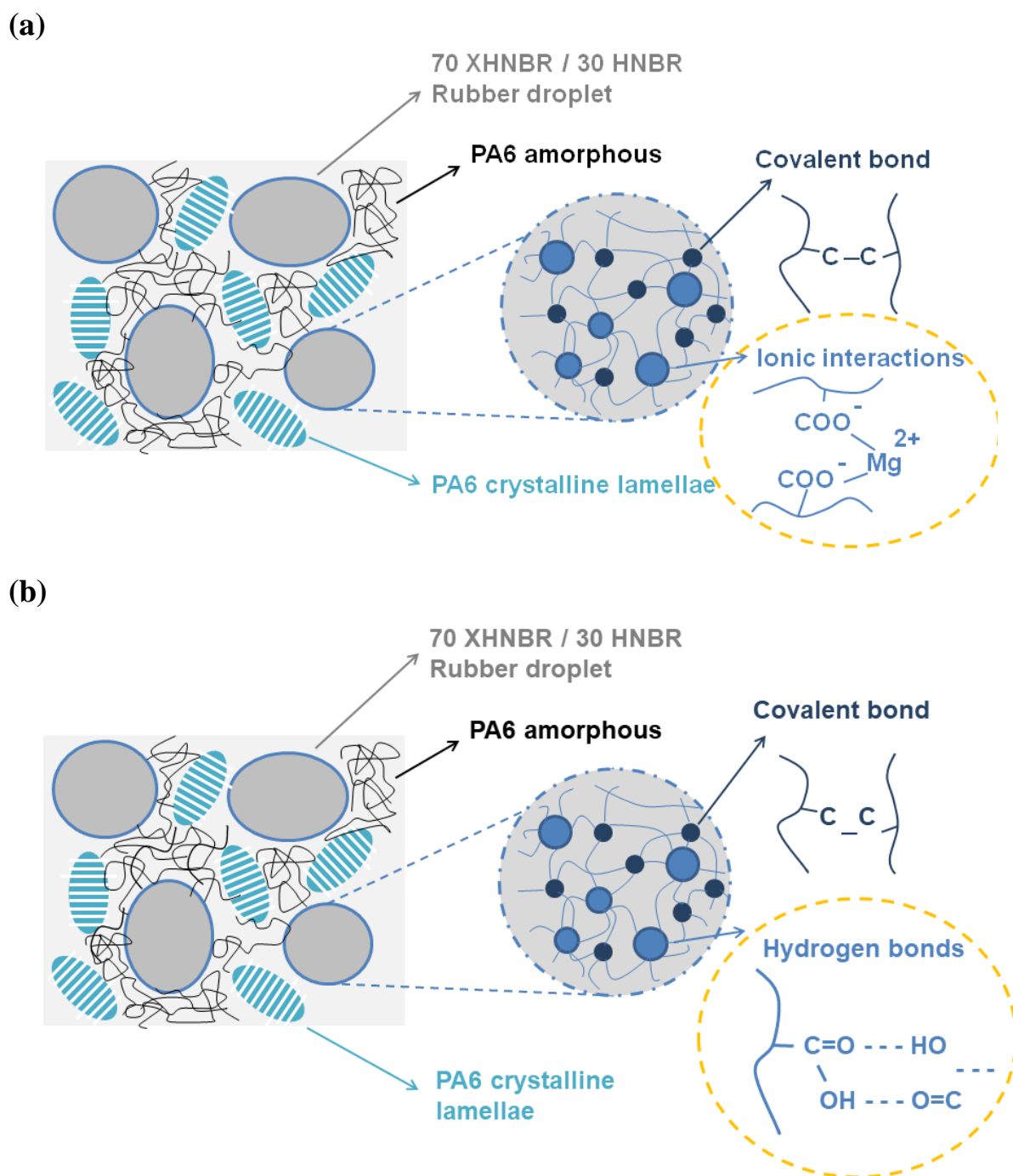
Figure 6. Mechanism of crosslinks in the carboxylic rubber phase of TPV compounds when (a) peroxide and MgO metal oxide and (b) peroxide and Irganox 1010 hindered phenolic antioxidant were used as crosslinking agents.

FTIR studies

Fig. 7 shows the FTIR spectra of the TPE blend (P30H70X), i.e, the sample without crosslinking, and the TPV samples in the out-of-plane deformation γ (=C-H) *cis* region, a region associated to peroxide crosslinking reaction[39]. The peroxide crosslinking reaction involves three consecutive steps. The first step involves the formation of free radicals. Next, these radicals remove hydrogen atoms from the polymer forming a polymer radical; and finally, two polymer radicals are combined to form carbon-carbon crosslinks. All TPV samples show a decrease in the γ (=C-H) *cis* band located at 728 cm^{-1}, demonstrating the creation of covalent structures[40].
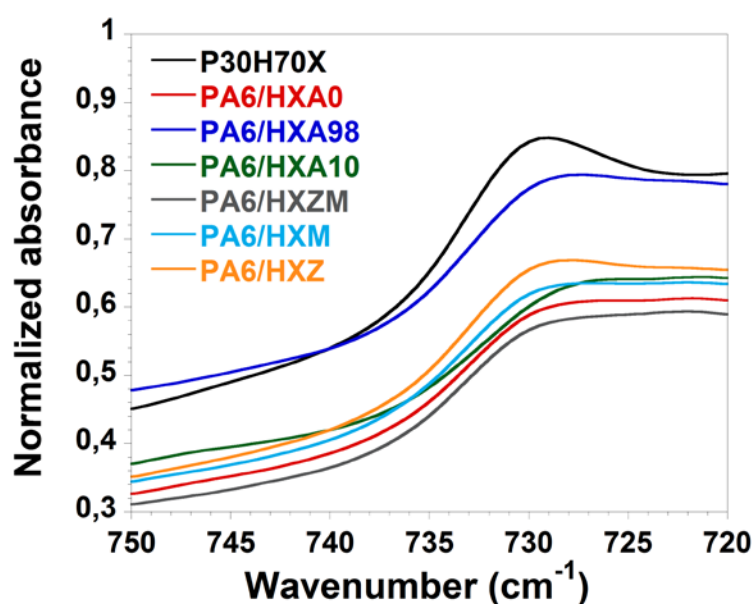

Figure 7: Infrared spectra of uncured TPE blend (P30H70X) and TPV samples in the out-of-plane deformation γ (=C-H) *cis* region.

In order to find further evidences to support the compatibility of Irganox 1010 with the rubber phase, the effectiveness of both Irganox 1010 and Irganox 1098 to form hydrogen bonding interactions were investigated by FTIR measurement. Fig. 8 shows the FTIR spectra of PA6/HXA0, PA6/HXA98 and PA6/HXA10 TPV samples in the hydroxyl group

(OH) stretching region (3500 cm^{-1}). A band at 3643 cm^{-1} exists in the infrared spectrum of the PA6/HXA98 TPV sample, which can be assigned to the free (non-hydrogen bonded) OH groups of Irganox 1098. This result suggests that the Irganox 1098 antioxidant acts more as a filler, not being coupled with other functional groups, and this leads to a decrease of the *tan δ* peak of the rubber phase (as shown in Fig 3).
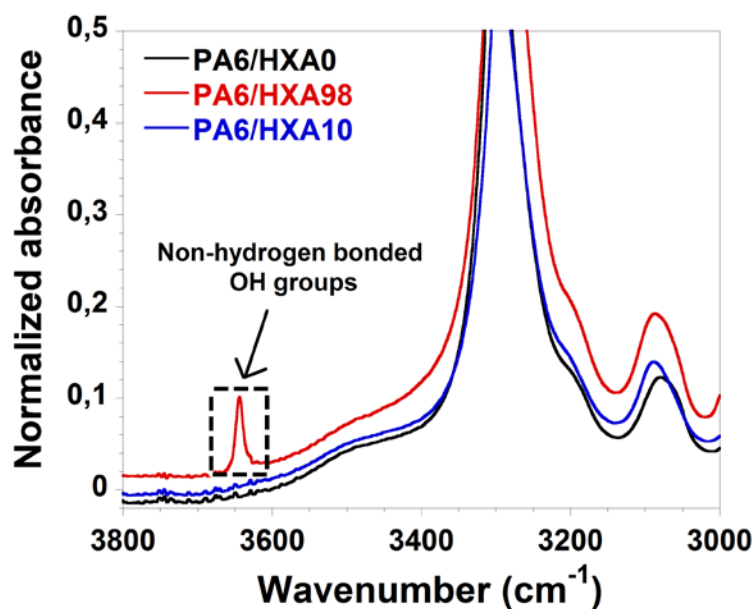

Figure 8: Infrared spectra in the OH stretching region for PA6/HXA0, PA6/HXA98 and PA6/HXA10 TPV samples.

Fig. 9 shows the FTIR-ATR spectra in the range 1000 to 3500 cm^{-1} for TPV compounds containing different amounts of metallic oxides and for the cured HXM rubber compound. The TPV compounds have two strong absorption bands at about 1645 cm^{-1} and 1545 cm^{-1}, corresponding to the amide I group (C=O stretch) and amide II group (in-plane N-H bend coupled with C-N stretch) of PA6[41,42]. The most important region of the FTIR spectrum related to the formation of ionic crosslinks is the one in between 1700 and 1500 cm^{-1}, where the peak related to the salt formation can be observed[43]. Therefore, the presence of the two peaks related to the amide groups of the PA6 phase in the TPV compounds complicates the analysis of ionic crosslink formation by FTIR measurements. For that reason, the ATR

spectra of the cured HXM rubber compound is added to the analysis. As it can be observed, XHM presents a peak at 1610 cm^{-1}. This peak is assigned to the carbonyl stretching of magnesium hydroxycarboxylate salt (-COOMgOH)[44]. This result confirms the creation of ionic crosslinks observed in the DMA analysis (see Fig. 4). Malmierca et al.[45] investigated the network structure and chain dynamics of ionic elastomers based on XNBR and MgO. They also found that the addition of MgO promoted the conversion of carboxylic groups presented in XNBR to the corresponding carboxylate salts.
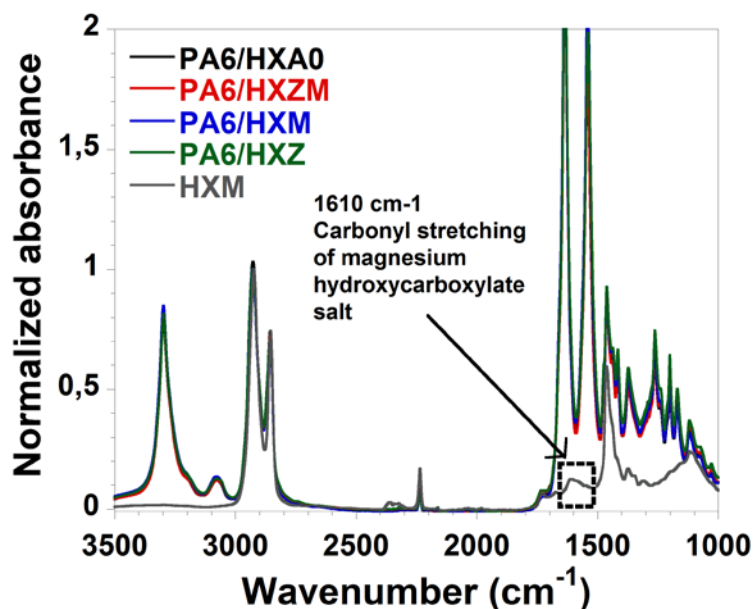

Figure 9: Infrared spectra of compounds containing different amounts of ZnO and MgO in the range 1000 to 3500 cm^{-1}.

Differential scanning calorimetry analysis

The heating and cooling DSC thermograms of PA6 and the TPV samples are shown in Fig. 10. The melting temperature (T_m), crystallization temperature (T_c), melting enthalpy (ΔH_m) and degree of crystallinity (X_c) of neat PA6 and TPV samples are listed in table 3. The degree of crystallinity was calculated as the ratio of the melting enthalpy to the weight fraction of PA6 (w_{PA6}) in the blend from the following equation:

$$X_c(PA6) = \frac{\Delta H_m}{\Delta H_m^0 w_{PA6}} \times 100$$

where ΔH_m is the measured enthalpy of melting and ΔH_m^0=190 J/g is the melting enthalpy of 100 % crystalline PA6[46].

The heating thermograms (Fig. 10(a)) reveal that the neat PA6 as well as the TPVs display two melting peaks. The low intensity melting peak at about 215 °C corresponds to the melting of γ-form crystalline structure whereas the high intensity melting peak at about 220 °C corresponds to the α-form crystalline structure of PA6[47]. The γ-form crystalline structure is considered an imperfect crystal formation while the α-form is considered a more stable crystal formation[48,49]. All TPV compounds present the same high intensity melting peak position, i.e., the same melting temperature. Moreover, it should also be noted from the cooling thermograms presented in Fig. 10(b) that all TPV samples show approximately the same crystallization temperature.

In regard to the crystallinity degree, we find that PA6/HXA10 and PA6/HXM TPV systems show the lowest crystallinity degree values. On the other hand, the PA6/HXA98 and PA6/HXZ TPV systems show an increase of the crystallinity degree. Therefore, from the DSC analysis we can confirm that the Irganox 1098 hindered phenolic antioxidant and the ZnO metallic oxide act as nucleating agents. Recently, Ling et al. have demonstrated that, the weaker are the hydrogen bond interactions between hindered phenols and XNBR, the easier is for the hindered phenol to crystallize[50]. Therefore, DSC results indicate that the interaction between Irganox 1098 and ZnO with the rubber phase is weak, resulting in a decrease of the damping performance properties, as observed in the DMA analysis (see Fig. 3 and Fig. 4).
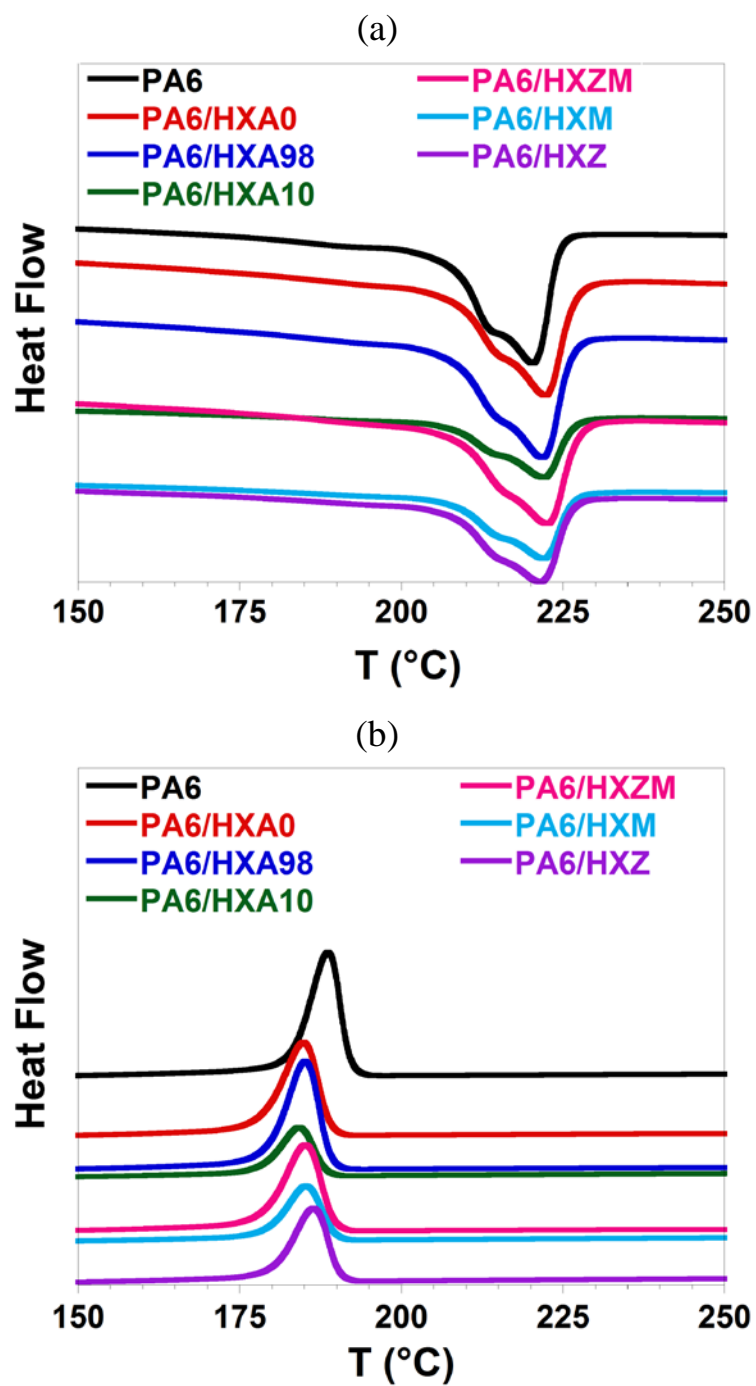
(a)

(b)

Figure 10: DSC thermograms of PA6 and TPV samples: (a) heating and (b) cooling.

Sample	T_m (°C)	T_c (°C)	ΔH_m (J/g)	X_c (%)
PA6	220	189	56	30
PA6/HXA0	222	185	35	46
PA6/HXA98	222	185	42	55
PA6/HXA10	222	184	23	30
PA6/HXZM	222	185	39	51
PA6/HXM	222	185	25	33
PA6/HXZ	222	186	32	42

Table 3. Melting and crystallization results for neat PA6 and TPV samples, from DSC analysis.

Mechanical properties

The stress–strain curves at room temperature of the TPV samples are presented in Fig. 11. The mechanical properties (i.e, young modulus, tensile strength and elongation at break) are summarized in table 4. It is found that, the addition of 5 phr of both Irganox 1098 and ZnO (PA6/HXA98 and PA6/HXZ, respectively) led to an increase of the young modulus and a drastic decrease of the elongation at break. Usually, the tensile strength and young modulus of TPV systems are increased with increasing the content of rigid fillers, whereas the elongation at break is decreased[33]. However, the use of the same amount of filler, i.e 5 phr, but in this case of Irganox 1010 and MgO (PA6/HXA10 and PA6/HXM, respectively) enhances the elongation at break, which is a further evidence of the strong interactions between Irganox 1010 and MgO with the rubber phase, as seen from the FTIR measurements (Fig. 8 and 9). Furthermore, PA6/HXA10 and PA6/HXM systems give the lowest young modulus values. This may be attributed to the low crystallinity degree that the PA6 phase possess in these two particular systems.
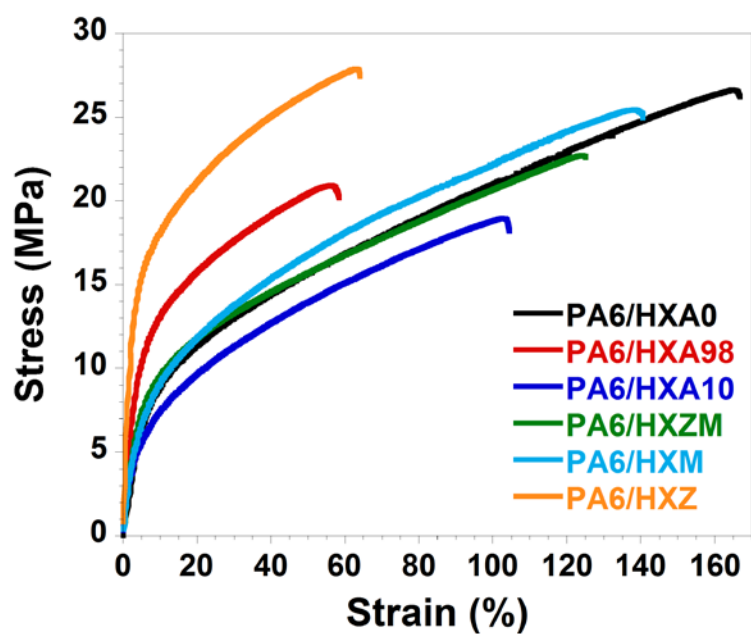
Figure 11: Stress–strain curves at room temperature of TPV samples.

Sample	Young modulus (MPa)	Tensile strength (MPa)	Elongation at break (%)
PA6/HXA0	223	27	166
PA6/HXA98	411	21	58
PA6/HXA10	163	19	103
PA6/HXZM	277	23	125
PA6/HXM	181	25	141
PA6/HXZ	630	28	64

Table 4. Mechanical properties of TPV samples.

Conclusions

In this study, the effect of adding metal oxides and hindered phenolic antioxidants on the damping properties of high-performance peroxide-cured TPVs based on PA6 and carboxylated HNBR were investigated, as novel strategies to improve the damping properties of carboxylic TPV systems. The selected metal oxides were ZnO and MgO, whereas the selected hindered phenolic antioxidants were Irganox 1010 and Irganox 1098. SEM studies revealed a droplet-matrix biphasic structure with the crosslinked rubber particles in the micron level for all the TPV systems investigated. Regarding the effect of hindered phenolic antioxidants, DMA results showed that the presence of Irganox 1010 increases the damping peak maximum value of both rubber and PA6 phases. In contrast, the addition of Irganox 1098 decreases remarkably the height of the damping peaks. FTIR investigations indicated that Irganox 1098 acts mainly as an inorganic filler, not being coupled with the carboxyl functionalities presented in the rubber phase, whereas Irganox 1010 forms hydrogen bonds with XHNBR. In the case of the metallic oxides, the dynamic mechanical properties revealed an additional relaxation transition corresponding to the temperature transition of the ionic microphases inside the rubber phase. The ionic transition was particularly evident for the TPV system containing 5phr of MgO. Therefore, MgO offers a higher effectiveness in interacting with the carboxyl functionalities presented in the TPVs rubber phase. This was also manifested in the FTIR analysis by the presence of an additional peak at 1610 cm^{-1}, attributed to the carbonyl stretching of magnesium hydroxycarboxylate salt. The TPV systems containing 5phr of both Irganox 1010 and MgO showed the lowest crystallinity degree values together with enhanced elastomeric properties, which is a further evidence of the strong hydrogen bonding and ionic interactions formed with the carboxylic rubber phase. This work revels new ways to improve the damping properties of high-performance TPV systems by using carboxylic rubbers and controlling the type and magnitude of different crosslinking interactions.

Acknowledgements

References

1. Rao MD. Recent applications of viscoelastic damping for noise control in automobiles and commercial airplanes. J Sound Vib. 2003 May 1;262(3):457–74.

2. Zhou XQ, Yu DY, Shao XY, Zhang SQ, Wang S. Research and applications of viscoelastic vibration damping materials: A review. Compos Struct. 2016 Feb 1;136:460–80.

3. Moreira RAS. Structural Dynamics and Viscoelastic Passive Damping Treatments. In: Davim JP, editor. Modern Mechanical Engineering: Research, Development and Education. Berlin, Heidelberg: Springer; 2014. p. 89–107. (Materials Forming, Machining and Tribology).

4. Rade DA, Deü J-F, Castello DA, de Lima AMG, Rouleau L. Passive Vibration Control Using Viscoelastic Materials. In: Jauregui JC, editor. Nonlinear Structural Dynamics and Damping. Cham: Springer International Publishing; 2019. p. 119–68. (Mechanisms and Machine Science).

5. Drobny JG. Handbook of Thermoplastic Elastomers. Elsevier; 2014. 465 p.

6. Bhowmick AK. Current topics in elastomers research. CRC press; 2008.

7. Paul DR, Bucknall CB. Polymer Blends: Formulation and Performance, Performance. Wiley; 2000. 610 p.

8. Das PK, Ambatkar SU, Sarma KSS, Sabharwal S, Banerji MS. Electron beam processing of nylon 6 and hydrogenated nitrile rubber (HNBR) blends: 1. Development of high strength heat- and oil-resistant thermoplastic elastomers. Polym Int. 2006 Jan 1;55(1):118–23.

9.   Sarma AD, Padmanathan HR, Saha S, Banerjee SS, Bhowmick AK. Design and properties of a series of high-temperature thermoplastic elastomeric blends from polyamides and functionalized rubbers. J Appl Polym Sci. 2017;134(39):45353.

10.   Holden G, Kricheldorf HR, Quirk RP. Thermoplastic elastomers. Munich, Germany; Cincinnati, Ohio: Hanser Publishers : Distributed by Carl Hanser Verlag ; Hanser Gardner Publications; 2004.

11.   Chatterjee T, Wiessner S, Naskar K, Heinrich G. Novel thermoplastic vulcanizates (TPVs) based on silicone rubber and polyamide exploring peroxide cross-link. Express Polym Lett. 2014;8(4).

12.   Chatterjee T, Basu D, Das A, Wiessner S, Naskar K, Heinrich G. Super thermoplastic vulcanizates based on carboxylated acrylonitrile butadiene rubber (XNBR) and polyamide (PA12). Eur Polym J. 2016;78:235–252.

13.   Huang H, Yang J, Liu X, Zhang Y. Dynamically vulcanized ethylene propylene diene terpolymer/nylon thermoplastic elastomers. Eur Polym J. 2002;38(5):857–861.

14.   Banerjee SS, Bhowmick AK. High-temperature thermoplastic elastomers from rubber–plastic blends: a state-of-the-art review. Rubber Chem Technol. 2016 Aug 1;90(1):1–36.

15.   Burgoa A, Hernandez R, Vilas JL. Toward superior applications of thermoplastic elastomer blends: double Tg increase and improved ductility. Polym Int. 2019;68(6):1130–9.

16.   Stöckelhuber KW, Das A, Klüppel M, editors. Designing of Elastomer Nanocomposites: From Theory to Applications. Springer International Publishing; 2017. (Advances in Polymer Science).

17.   Sasikumar K, Manoj NR, Mukundan T, Khastgir D. Hysteretic damping in XNBR – MWNT nanocomposites at low and high compressive strains. Compos Part B Eng. 2016 May 1;92:74–83.

18.   Manoj NR, Raut RD, Sivaraman P, Ratna D, Chakraborty BC. Sequential interpenetrating polymer network of poly(ethyl methacrylate) and carboxylated nitrile rubber: Dynamic mechanical analysis and morphology. J Appl Polym Sci. 2005;96(5):1487–91.

19.   Manoj NR, Chandrasekhar L, Patri M, Chakraborty BC, Deb PC. Vibration damping materials based on interpenetrating polymer networks of carboxylated nitrile rubber and poly(methyl methacrylate). Polym Adv Technol. 2002;13(9):644–8.

20. Gaca M, Pietrasik J, Zaborski M, Okrasa L, Boiteux G, Gain O. Effect of Zinc Oxide Modified Silica Particles on the Molecular Dynamics of Carboxylated Acrylonitrile-Butadiene Rubber Composites. Polymers. 2017 Nov 25;9(12).

21. Antony P, De SK. Ionic Thermoplastic Elastomers: A Review. J Macromol Sci Part C. 2001 Apr 28;41(1–2):41–77.

22. A. J. van der Mee M, M. A. l'Abee R, Portale G, Goossens JGP, Duin M. Synthesis, Structure, and Properties of Ionic Thermoplastic Elastomers Based on Maleated Ethylene/Propylene Copolymers. Macromolecules. 2008 Jun 21;41.

23. Ibarra L, Rodríguez A, Mora-Barrantes I. Crosslinking of unfilled carboxylated nitrile rubber with different systems: Influence on properties. J Appl Polym Sci. 2008;108(4):2197–205.

24. Hamed GR, Hua K-C. Effect of ZnO Particle Size on the Curing of Carboxylated NBR and Carboxylated SBR. Rubber Chem Technol. 2004 May 1;77(2):214–26.

25. Kołodziejczak-Radzimska A, Jesionowski T. Zinc Oxide-From Synthesis to Application: A Review. Mater Basel Switz. 2014 Apr 9;7(4):2833–81.

26. Ibarra L, Alzorriz M. Ionic elastomers based on carboxylated nitrile rubber and magnesium oxide. J Appl Polym Sci. 2007;103(3):1894–9.

27. Chakraborty SK, Bhowmick AK, De SK. Mixed cross-link systems in elastomers. J Macromol Sci Part C Polym Rev. 1981;21(2):313–332.

28. Ibarra L, Marcos-Fernández A, Alzorriz M. Mechanistic approach to the curing of carboxylated nitrile rubber (XNBR) by zinc peroxide/zinc oxide. Polymer. 2002 Mar 1;43(5):1649–55.

29. Mora-Barrantes I, Malmierca MA, Valentin JL, Rodriguez A, Ibarra L. Effect of covalent cross-links on the network structure of thermo-reversible ionic elastomers. Soft Matter. 2012 Apr 25;8(19):5201–13.

30. Zhang C, Wang P, Ma C, Sumita M. Damping properties of chlorinated polyethylene-based hybrids: Effect of organic additives. J Appl Polym Sci. 2006;100(4):3307–3311.

31. Zhao X-Y, Lu Y-L, Xiao D-L, Wu S-Z, Zhang L-Q. Thermoplastic Ternary Hybrids of Polyurethane, Hindered Phenol and Hindered Amine with Selective Two-Phase Dispersion. Macromol Mater Eng. 2009;294(5):345–351.

32. Liu Q, Zhang H, Yan X. Preparation of High-performance Damping Materials Based on Carboxylated Nitrile Rubber: Effects of Organic Fillers. Iran Polym J Engl Ed. 2009 May 1;18.

33. Ning N, Li S, Wu H, Tian H, Yao P, Hu G-H, et al. Preparation, microstructure, and microstructure-properties relationship of thermoplastic vulcanizates (TPVs): A review. Prog Polym Sci. 2018 Apr 1;79:61–97.

34. Zhang L, Hua J, Wang Z. Dynamically vulcanized polylactide/nitrile butadiene rubber blends with continuous cross-linked rubber phase. J Polym Res. 2019;26(1):11.

35. Li C, Cao D, Guo W, Wu C. The Investigation of Miscibility in Blends of ENR/AO-80 by DMA and FT-IR. J Macromol Sci Part B. 2007 Dec 1;47(1):87 –97.

36. Lu X, Li X. Broad temperature and frequency range damping materials based on epoxidized natural rubber. J Elastomers Plast. 2014 Feb 1;46(1):84–95.

37. Bieliński DM, Stępkowska A. Mechanical properties and friction of rubber vulcanizates: Aspects of crosslink structure. Arch Civ Mech Eng. 2013;13(2):192–198.

38. Dolgoplosk BA, Reǐkh VN, Tinyakova EI, Kalaus AE, Koryushenko ZA, Sladkevich EG. Carboxylic Rubbers. II. Properties of Cured Stocks. Rubber Chem Technol. 1959 Mar 1;32(1):328–36.

39. González L, Rodríguez A, Marcos A, Chamorro C. Crosslink Reaction Mechanisms of Diene Rubber with Dicumyl Peroxide. Rubber Chem Technol. 1996 May 1;69(2):203–14.

40. Valentín JL, Rodríguez A, Marcos-Fernández A, González L. Dicumyl peroxide cross-linking of nitrile rubbers with different content in acrylonitrile. J Appl Polym Sci. 2005;96(1):1–5.

41. Urbański J. Handbook of analysis of synthetic polymers and plastics. E. Horwood; 1977. 504 p.

42. Rusu E, Rusu G, Dorohoi D-O. Influence of temperature on structures of polymers with ε-caprolactam units studied by FT-IR spectroscopy. Polimery. 2009;54(5):347–352.

43. Tungchaiwattana S, Musa MS, Yan J, Lovell PA, Shaw P, Saunders BR. The role of acrylonitrile in controlling the structure and properties of nanostructured ionomer films. Soft Matter. 2014 Jun 11;10(26):4725–34.

44. Laskowska A, Zaborski M, Boiteux G, Gain O, Marzec A, Maniukiewicz W. Ionic elastomers based on carboxylated nitrile rubber (XNBR) and magnesium aluminum layered double hydroxide (hydrotalcite). Express Polym Lett. 2014;8(6).

45. Malmierca MA, González-Jiménez A, Mora-Barrantes I, Posadas P, Rodríguez A, Ibarra L, et al. Characterization of Network Structure and Chain Dynamics of Elastomeric Ionomers by Means of 1H Low-Field NMR. Macromolecules. 2014 Aug 26;47(16):5655–67.

46. Brandrup J, Immergut EH, Grulke EA, Abe A, Bloch DR. Polymer handbook. Vol. 89. Wiley New York; 1999.

47. Ogunsona EO, Misra M, Mohanty AK. Influence of epoxidized natural rubber on the phase structure and toughening behavior of biocarbon reinforced nylon 6 biocomposites. RSC Adv. 2017 Jan 27;7(15):8727–39.

48. Murthy NS. Hydrogen bonding, mobility, and structural transitions in aliphatic polyamides. J Polym Sci Part B Polym Phys. 2006;44(13):1763–1782.

49. Li T-C, Ma J, Wang M, Tjiu WC, Liu T, Huang W. Effect of clay addition on the morphology and thermal behavior of polyamide 6. J Appl Polym Sci. 2007;103(2):1191–9.

50. Zhang L, Chen D, Fan X, Cai Z, Zhu M. Effect of Hindered Phenol Crystallization on Properties of Organic Hybrid Damping Materials. Materials. 2019;12(7):1008.

Journal Pre-proof

Experimental investigation of the nonlinear quasi-static and dynamic mechanical behaviour of novel PA6/XHNBR thermoplastic vulcanizates: linking mechanical nonlinearities to microstructural features

Aizeti Burgoa, Aitor Arriaga, Rikardo Hernandez, Jose Luis Vilas, Kepa Zulueta, Eva Maria Acuña, Jose Manuel Laza

Please cite this article as: Burgoa A, Arriaga A, Hernandez R, Vilas JL, Zulueta K, Acuña EM, Laza JM, Experimental investigation of the nonlinear quasi-static and dynamic mechanical behaviour of novel PA6/XHNBR thermoplastic vulcanizates: linking mechanical nonlinearities to microstructural features, *Materials Today Communications* (2020), doi: https://doi.org/10.1016/j.mtcomm.2020.101395

This is a PDF file of an article that has undergone enhancements after acceptance, such as the addition of a cover page and metadata, and formatting for readability, but it is not yet the definitive version of record. This version will undergo additional copyediting, typesetting and review before it is published in its final form, but we are providing this version to give early visibility of the article. Please note that, during the production process, errors may be discovered which could affect the content, and all legal disclaimers that apply to the journal pertain.

Experimental investigation of the nonlinear quasi-static and dynamic mechanical behaviour of novel PA6/XHNBR thermoplastic vulcanizates: linking mechanical nonlinearities to microstructural features

Aizeti Burgoa[1*], Aitor Arriaga[1], Rikardo Hernandez[1], Jose Luis Vilas[2,3], Kepa Zulueta[1], Eva Maria Acuña[1] and Jose Manuel Laza[2]

[1] Leartiker S. Coop, Xemein Etorbidea, 12-A E-48270, Markina-Xemein, Bizkaia (Spain).

[2] Macromolecular Chemistry Research Group (labquimac), Department of Physical Chemistry, Faculty of Science and Technology, University of the Basque Country (UPV/EHU), 48940 Leioa, Spain.

[3] BCMaterials, Basque Center for Materials, Applications and Nanostructures, UPV/EHU Science Park, 48940 Leioa, Spain.

E-mail: aburgoa@leartiker.com

Abstract

Driven by the need to design environmentally friendly and sustainable polymeric materials that achieve superior mechanical properties, this work is centred on the relationship between the microstructure and the nonlinear quasi-static and dynamic mechanical behaviour of novel polyamide 6 (PA6)/carboxylated hydrogenated acrylonitrile butadiene rubber (XHNBR) thermoplastic vulcanizates (TPVs). In particular, with the aim to contribute to the further understanding of the physical mechanisms involved in the complex nonlinear mechanical behaviour of TPV compounds, the impact of different microstructural features of the PA6 matrix and the rubber network on the mechanical behaviour has been investigated. Interestingly, stronger rubber network interactions and so better elastic recovery capacity of the rubber network can hinder the growth of voids more efficiently. The observed micromechanical deformation processes are interpreted in terms of the role of the yielding, buckling and bending of thin PA6 ligaments at low strain levels and the rupture of covalent and non-covalent bonds presented in the rubber network at high strain levels.

1

Keywords: nonlinear, quasi-static, dynamic, thermoplastic vulcanizate, microstructure

Introduction

In the field of "green" elastomeric materials, thermoplastic elastomers (TPEs) are considered one of the most promising candidates for thermoset elastomers replacement due to their physico-mecanical properties, design flexibility, ease of processability, light weight and cost effective productivity [1–3]. The physical mixing of thermoplastic and rubber materials is a feasible approach of formulating TPEs with tailored properties [4,5]. TPE blends can be arranged in two main groups [6]. The first group is composed of simple blends of thermoplastics with non-crosslinked rubbers. The second group consist of blends of a thermoplastic with a rubber phase that has been dynamically vulcanized, i.e., thermoplastic vulcanizates (TPVs) [7]. The dynamic vulcanization describes the process of crosslinking the rubber phase during the melt-mixing with the thermoplastic. Dynamically vulcanized blends have superior properties than simple blends [8–10]. Due to their upgraded properties, TPVs are attracting a growing interest in many demanding engineering applications such as automotive and aeronautic components.

The microstructure of TPVs is characterized by crosslinked rubber particles dispersed in a continuous thermoplastic matrix [11,12]. In addition to the crosslinking agents, other kind of fillers can be added into the rubbery phase in order to enhance the engineering properties of TPV compounds [13–17]. The addition of fillers may alter the microstructure of the TPV compound generating a multiple-network structure [18–21]. This complex heterogeneous microstructure generates a highly nonlinear mechanical behaviour that depends on stress, strain history, time, temperature and frequency [22–24], characterized by remarkable inelastic effects and viscoplastic behaviour [25–28]. In order to ensure a competitive application of TPV materials, the complexity of their mechanical properties must be taken into account. Moreover, the mechanical nonlinearities intervene not only in the static level but also in the dynamic one.

In the quasi-static state, one of the most important mechanical nonlinearities that needs to be taken into account in TPV materials is the stress softening phenomena. When an elastomer is subjected to cyclic loading-unloading conditions, the stress to a given strain decreases over the cycles. The stress softening phenomena has been reported in filled and non-filled rubber-like materials and has been intensively investigated by Mullins and his co-workers [29–34], hence it is widely known as the "Mullins effect". Other important phenomena that appear when a TPV material is subjected to cyclic loading-unloading conditions are the hysteresis loss and the permanent deformation [35–37].The hysteresis loss represents the dissipated energy and is shown by the loop of strain-stress path due to the different stresses that a given strain presents at the loading and unloading curves [38]. The permanent deformation is a consequence of the viscoplastic nature, and represents the unrecoverable deformations when a strain threshold is reached [39].

In the dynamic state, TPV materials exhibit a highly nonlinear behaviour. One of these nonlinearities is the dependence of the storage modulus on the amplitude of the dynamic strain, which is known as the "Payne effect" [40]. The Payne effect refers to the phenomena that, above a threshold dynamic strain amplitude, the storage modulus decreases rapidly with increasing the amplitude. The Payne effect characterization is essential for the modelling of elastomeric components. Moreover, a static predeformation superimposed by a small harmonic oscillation can be found in many elastomeric applications where the elastomeric segment is used to attenuate the vibrations of industrial structures. Therefore, another interesting nonlinearities to consider are the dependence of TPV systems on the static predeformation and frequency.

Even though the deformation behaviour of TPV compounds has been the focus of several experimental and theoretical studies, there are no unanimous explanations of the physical origin of the complex nonlinear behaviour and so, a complete physical picture remains elusive. Therefore, in order to ensure a competitive and confident application of TPV compounds, detailed knowledge about the correlation between the nonlinear behaviour and the microstructural features need to be well stablished. Furthermore, linking the mechanical

performance to the microstructure would encourage the micromechanical modelling of TPV materials, an evolving field where different researchers continue developing new models every year.

In this scenario, the present work focuses on the analysis of nonlinear effects in the quasi-statical and dynamical states, trying to offer explanations for the deformation behaviour based on microstructural features. To this aim, two novel TPV compounds containing different microstructural features have been developed by melt-blending polyamide 6 (PA6) and carboxylated hydrogenated acrylonitrile butadiene rubber (XHNBR) and using mixed crosslink systems of peroxide, ZnO, MgO and hindered phenolic antioxidants.

Experimental

Materials

PA6, Durethan® B 30 S 000000, was provided by Lanxess. HNBR, Therban® AT 3904 VP, and carboxylated HNBR (XHNBR), Therban® XT VP KA 8889, rubbers were purchased from Arlanxeo. Trigoxox 145 from Akzo Nobel Polymer Chemicals was used as the vulcanization agent for the rubber phase in the TPVs. The co-agent trimethylolpropane trimethacrylate (TMPTMA, Rhenofit TRIM/S) was purchased from Rhein Chemie Additives. ZnO and MgO metallic oxides were provided by Panreac Applichem, Spain. Irganox 1010 hindered phenolic antioxidant was supplied by BASF, Switzerland. All chemicals were used as were received.

Preparation of thermoplastic elastomer blends

For the rubber phase, a premix of the XHNBR/HNBR (70/30 wt/wt) rubber phase with different additives was prepared in a two-roll mill. The obtained uncured rubber compound sheets were extruded into strands and subsequently pelletilized. Extrusion was performed at 90 °C and 15 rpm in a Gumix Extruder with a length to diameter ratio of 10.

The premixed rubber compounds and PA6 were melt-blended at a fixed weight ratio, 60/40 wt/wt, in a Brabender DSE 20/40 co-rotating twin screw extruder at a temperature of 240 °C and a rotor speed of 200 rpm. The PA6 pellets were dried at 80 °C for 8 hours before melt-blending. Table 1 presents the composition and designation of the prepared samples. PA6/HXM and PA6/HXA10 are the two particular peroxide-cured TPV compounds, analysed in our previous article, that showed the best thermoplastic elastomeric and damping properties [41]. In the case of the PA6/HXA10 TPV compound, the addition of 5 phr Irganox 1010 hindered phenolic antioxidant resulted in upgraded damping properties due to the formation of hydrogen bond interactions with the carboxyl functionalities presented in the rubber. Furthermore, PA6/HXM TPV compound showed improved damping behaviour as a result of the ionic interactions formed between ZnO and the carboxylic rubber.

Table 1. Composition and designation of the prepared samples.

Sample	Composition							
	Thermoplastic phase	Rubber phase		Peroxide	Co-agent	Hindered phenolic antioxidant	Metallic oxides	
	PA6	XHNBR	HNBR	Trigonox 145	TRIM/S	Irganox 1010	ZnO	MgO
PA6/HXM	40	42	18	3	2	0	1	5
PA6/HXA10	40	42	18	3	2	5	2	3

Compression moulding of the samples

The thermoplastic elastomer samples taken from the Brabender DSE 20/40 corrotating twin screw extruder were compression moulded at 240 °C to prepare sheets of 1 mm thick for the following quasi-static and dynamic mechanical testing. Drying of samples was performed before any testing. Morphology of the thermoplastic elastomer samples was measured from the compression moulded sheets in order to obtain the correct structure-property relationship.

5

Scanning Electron Microscopy (SEM)

Morphology of TPV samples was studied employing a JEOL JSM-7000F field-emission scanning electron microscope. Samples were immersed in liquid nitrogen and brittle fractured. The brittle fractured surface was sputter coated with gold prior to SEM measurements.

Differential Scanning Calorimetry (DSC)

Thermal transitions of the samples were investigated by performing DSC measurements on a DSC Q100 (TA Instruments) in a dry nitrogen atmosphere. Samples were heated up from -50 to 250 °C at a constant heating rate of 10 °C min^{-1}.

Quasi-static mechanical behaviour

The monotonic tensile properties of the blends were measured in accordance with the ISO 37 test method at 5 mm min^{-1} crosshead speed and room temperature. Measurements were performed in a MTS Insight Universal Testing Machine. The monotonic tensile results reported in this work are the average of three samples. Cyclic tensile stress-strain curves of the samples were also obtained by using the MTS Insight Universal Testing Machine at a constant strain rate of 100% min^{-1}. Six strain levels were applied (10, 20, 30, 50, 70 and 100%) and five cycles of loading-unloading were applied for each level of strain. A new loading stroke was started once a zero stress state was obtained in the tensile sample. The permanent set of the samples was considered as the residual strain when the tensile stress gets to zero [42]. The hysteresis loss of the samples was measured by estimating the ratio between the areas of loading-unloading cycles and the areas below the loading curves [43]. The values reported are of the engineering stress and strain.

Dynamic mechanical behaviour

The dynamic mechanical behaviour of the blends was analysed in a Mettler-Toledo DMA/SDTA 861^{e} in shear and tension mode. Disc samples of 8 mm diameter were cut from the 1 mm thick compression moulded sheets for the dynamic mechanical measurements in

6

shear mode. Rectangular samples of length 30 mm and section 4 mm ×1 mm were used for the measurements in tension mode.

To identify the frequency-dependent behaviour of the materials, dynamic frequency sweep tests from 1 to 200 Hz at -10, 25 and 80 °C were conducted in shear mode. The dynamic strain amplitude was set at 0.1%, in order to avoid the Payne effect. To investigate the Payne effect, dynamic strain sweep tests from 0.01 to 10 % at a constant frequency of 10 Hz were applied to the samples. The variation of the dynamic mechanical properties with temperature were also analysed by performing temperature sweeps from -40 to 120 °C at a heating rate of 3 °C min^{-1} with an oscillating frequency of 1 Hz in tension mode. In order to prevent sample buckling, a low static prestrain of 0.1% was applied in both dynamic strain sweep and temperature sweep tests conducted in tensile mode.

To consider the static prestrain effect on the dynamic properties, the experimental procedure consisted on superimposing a static tensile prestrain to the small sinusoidal dynamic strain applied to the sample. The experimental procedure can be expressed as follows:

$$\varepsilon(t) = \varepsilon_s + \varepsilon_d \sin(wt) \tag{1}$$

where ε_s denotes the static prestrain and ε_d the dynamic strain. The tests were performed with a frequency of 10 Hz and a small dynamic strain of 0.01% so that the Payne effect was avoided. Different levels of static prestrain from 0.1% to about 4% were reached. After each static prestrain has been applied the samples were allowed to relax for two minutes to reduce the effects of stress relaxation on the tests.

Results and discussion

Microstructural investigation

SEM images of the TPV samples are presented in Figure 1. The SEM images reveal a droplet-matrix morphology for both samples. The final morphology of a melt-mixed blends is derived from the competition of the deformation and break-up of droplets with the shape

recovery and coalescence [44]. For TPV compounds, the selectively crosslinked rubber gets encapsulated by the thermoplastic due to the increase of the rubber phase viscosity. This effect is known as phase inversion phenomena. At the same time, the employed high shear rate hinders the coalescence of the crosslinked rubber phase and facilitates the fine dispersion of the crosslinked rubber phase in the thermoplastic matrix [45]. The morphology developed during the TPV preparation process is schematically shown in Figure 1c. From the Figures 1a and 1b, it can be concluded that finely dispersed rubber particles are obtained for both TPV compounds, obtaining rubber particles sizes in the micron (μm) level.
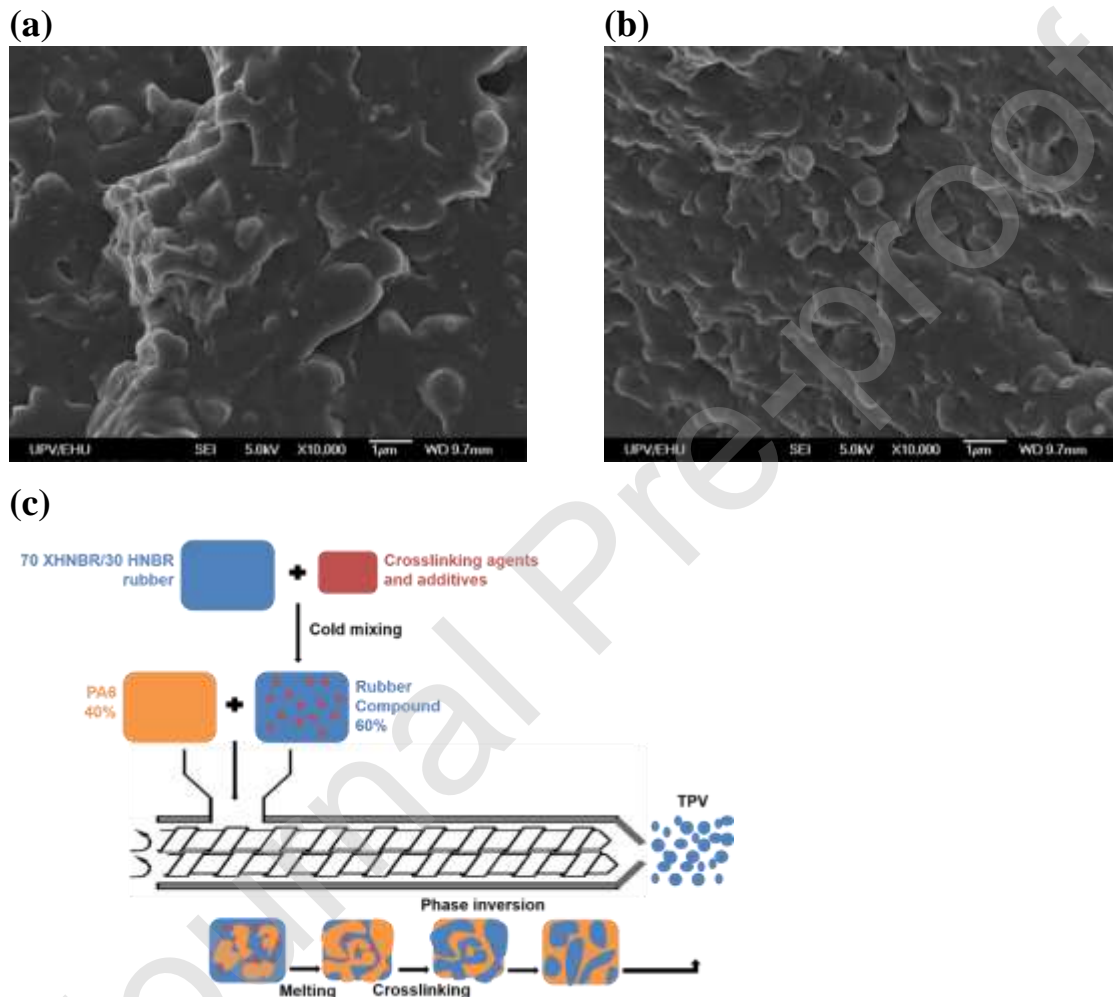
(a)

(b)

(c)

Figure 1. SEM images of (a) PA6/HXA10 and (b) PA6/HXM, and (c) schematic representation of the morphology developed during TPV preparation.

Microstructural features of TPVs where also investigated by DMA. Figure 2 displays the temperature dependence of storage modulus (E') and loss tangent ($tan\ \delta$), of both PA6/HXM and PA6/HXA10, measured in tension mode. $tan\ \delta$ is the ratio of the loss (E'') to storage modulus and indicates the ability of materials to absorb energy. Therefore, provides information about the different relaxation transitions that happen in the TPV compounds. Two glass transitions (T_gs) are observed in both samples (Figure 2b), confirming the biphasic microstructure observed in the SEM images (Figure 1). The T_g of the rubber phase is observed at around -8 ºC, while the T_g related to the PA6 amorphous phase is observed at about 80 ºC. Furthermore, it is interesting to note that, PA6/HXM presents an additional $tan\ \delta$ peak near room temperature, which appears as a small shoulder in Figure 2b. This additional peak corresponds to the microdomains formed by ionic linking of MgO with the carboxylic rubber phase [46,47]. The formation of ionic interactions is also supported by the lower storage modulus of PA6/HXM near room temperature (Figure 2a).
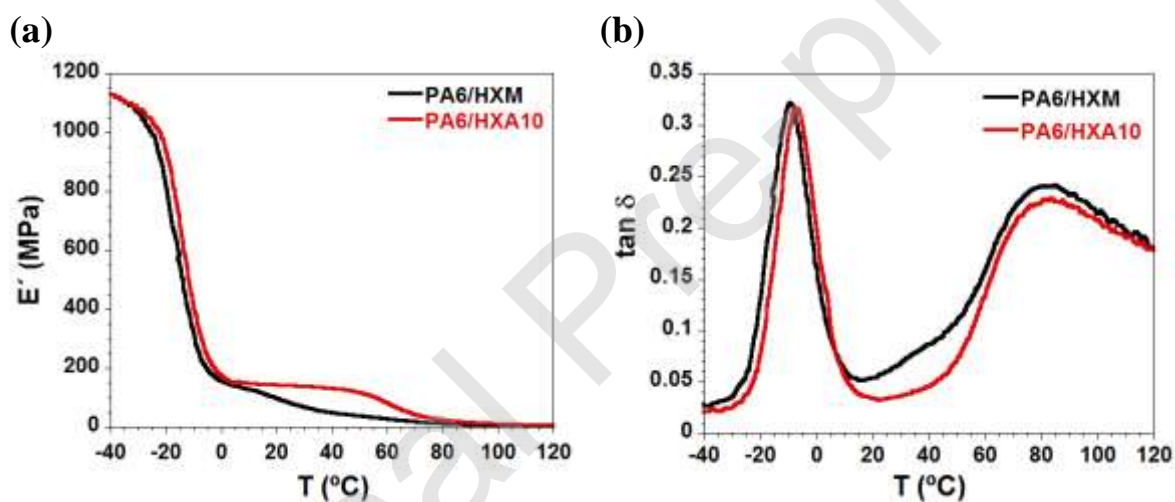
(a)   **(b)**

Figure 2. Temperature dependence of (a) storage modulus and (b) tan δ measured in tension mode.

As discussed in our earlier publication [41], PA6/HXM and PA6/HXA10 TPV samples possess different rubber network structures. The rubber network structure of PA6/HXM is based on peroxide cured C-C linkages and ionic bonds, while the PA6/HXA10 compound

9

exhibits C-C linkages and hydrogen bonds. The multiple-network morphology of the TPV compounds is schematically represented in Figure 3.
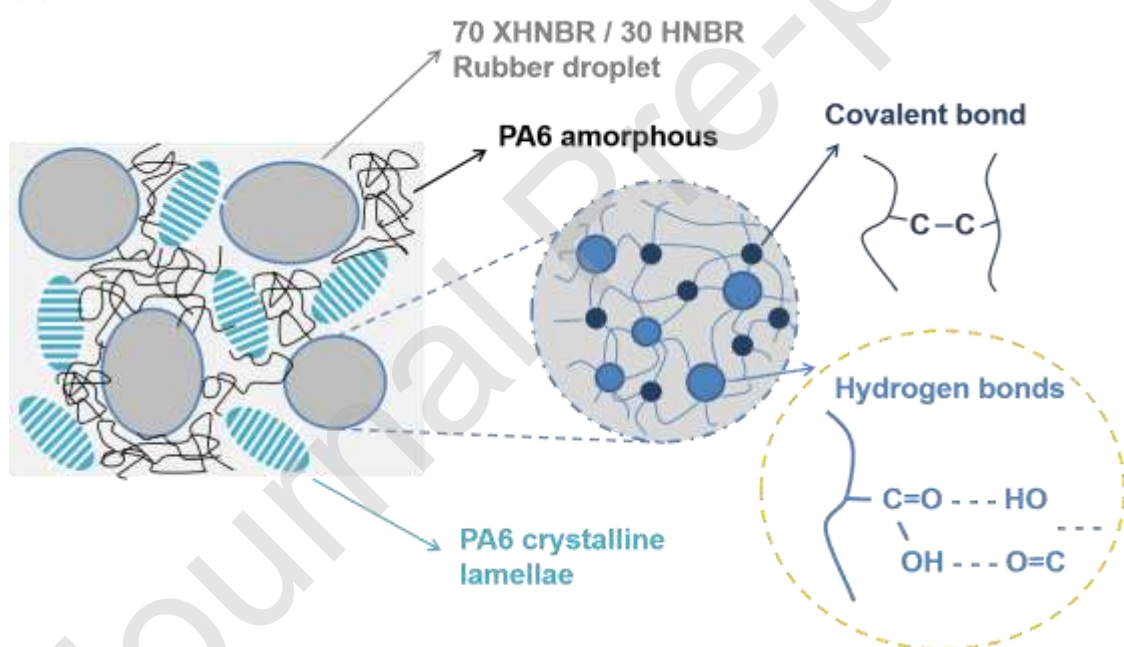
(a)
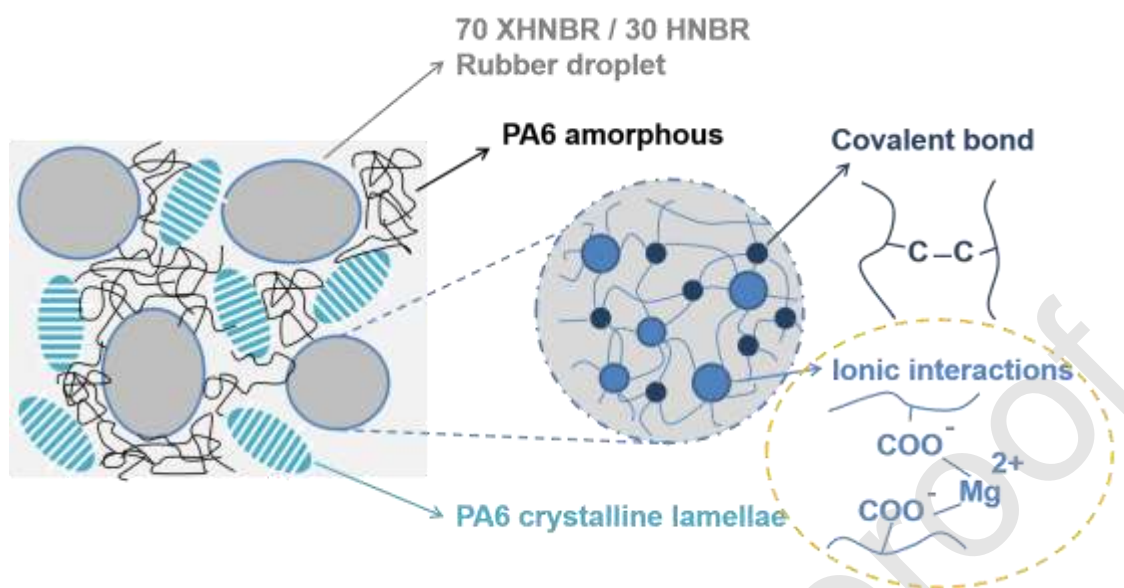
(b)

Figure 3. Schematic representation of the multiple-network morphology of (a) PA6/HXM and (b) PA6/HXA10 TPV compounds.

10

DSC data was used to evaluate the crosslinking densities of the rubber networks. Figure 4 shows the DSC thermograms of the TPV samples and the uncured rubber samples. Both TPVs present an exothermic reaction peak at about 120 °C. This peak is related to the reaction heat generated in the peroxide crosslinking reaction that takes place in the rubber phase of the TPVs. The crosslinking degree (CD) can be determined by comparing the crosslinking reaction enthalpy of the TPV samples with the crosslinking reaction enthalpy of the uncured rubber samples according to the following equation [48]:

$$CD \ (\%) = \frac{\Delta H_{(S0)} - \Delta H_{(SX)}}{\Delta H_{(S0)}} \tag{2}$$

where $\Delta H_{(S0)}$ is the crosslinking reaction enthalpy of the uncured rubber sample and $\Delta H_{(SX)}$ is the crosskinking reaction enthalpy of the TPV sample. The reaction enthalpies obtained by DSC measurements and the CD values calculated by equation 2 are depicted in Table 2. PA6/HXM sample presents a remarkable higher CD that PA6/HXA10. For the PA6/HXA10 TPV sample only a 85% of the peroxide curing agent is activated.
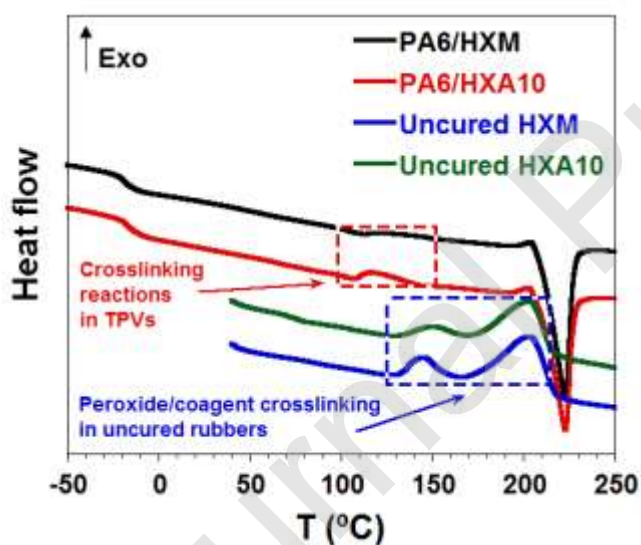

Figure 4. DSC thermograms of PA6/HXM and PA6/HXA10 TPV samples together with uncured HXM and HXA10 rubber samples.

11

Table 2. Crosslinking reaction enthalpies and related *CD* values of the TPV samples.

Sample	$\Delta H_{(S0)}$ (J/g)	$\Delta H_{(SX)}$ (J/g)	*CD* (%)
PA6/HXM	22.15	1.27	94
PA6/HXA10	18.11	2.71	85

Additionally, the microstructural properties of the PA6 thermoplastic phase that have an impact on the mechanical behaviour as the thickness of the crystalline lamellae and the crystallinity degree, have been monitored by DSC [49]. The melting temperature recorded by DSC (endothermic peak in Figure 4) can be transformed into lamellar crystals thickness by applying the Gibbs-Thomson equation [50]:

$$L = (\frac{T_m^0}{T_m^0 - T_m}) \frac{2\sigma_e}{\Delta H_m^0 \rho}$$ (3)

where L is the lamellar crystals thickness, T_m^0 is the equilibrium melting temperature of an infinite crystal, T_m is the experimental melting temperature, σ_e is the surface energy of the basal surface crystalline lamellae, ρ is the density and ΔH_m^0 is the melting enthalpy of the crystalline phase. The following PA6 constant values were utilized: $\sigma_e = 80.10 \times 10^{-7}$ J cm^{-2}, $\Delta H_m^0 = 190$ J g^{-1}, $T_m^0 = 259.85$ °C, $\rho = 1.23$ g cm^{-3} [51].

The crystallinity degree of the PA6 phase in the TPV samples can also be deduced from DSC measurements by applying the following equation:

$$X_C(PA6) = \frac{\Delta H_m}{\Delta H_m^0 w_{PA6}}$$ (4)

where ΔH_m is the measured enthalpy of melting, ΔH_m^0 is the melting enthalpy of 100 % crystalline PA6 and w_{PA6} is the weight fraction of PA6 in the blend. The values of crystalline lamellae thickness and crystallinity degree, calculated from equations 3 and 4, are presented in Table 3. Both TPV samples possess similar crystallinity degree and crystalline lamellae thickness.

Table 3. Melting temperature (T_m), enthalpy of melting (ΔH_m), thickness of lamellae and crystallinity degree (X_c) determined by DSC.

Sample	T_m (°C)	ΔH_m (J/g)	Crystalline lamellae thickness (nm)	Xc (%)
PA6/HXM	222.9	28.1	48.2	36.9
PA6/HXA10	223.1	26.0	48.5	34.2

Quasi-static mechanical characterization

The tensile curves of the TPVs, the pure PA6 thermoplastic and the pure rubber (vulcanized using 3 phr Trigonox 145 and 2 phr TRIM) are depicted in Figure 5. The tensile strength and elongation at break are listed in Table 4. The stress-strain curve of TPV compounds lies between the curve of pure PA6 and the curve of pure rubber. Additionally, the deformation behaviour of the TPV compounds can be divided in two main regions. At low strains, the stress increases considerably with the strain whereas at high strains there is a more gradual increase. Therefore, at low strain TPVs exhibit the deformation behaviour of the thermoplastic phase and that of the rubber phase at high strains.

In relation to the low strain behaviour, the stiffness shown by both samples is practically equal, which may be attributed to the fact that the PA6 phase of both TPVs possess similar crystallinity degree. Besides, PA6/HXM presents a much higher tensile strength and elongation at break values than PA6/HXA10. This result can be ascribed to the higher crosslink density of the rubber phase in the PA6/HXM sample [52]. Moreover, the formation of a rubber network structure consisting of C-C and ionic linkages contributes to a higher straining capacity of the rubber particles of the PA6/HXM TPV compound [53,54].
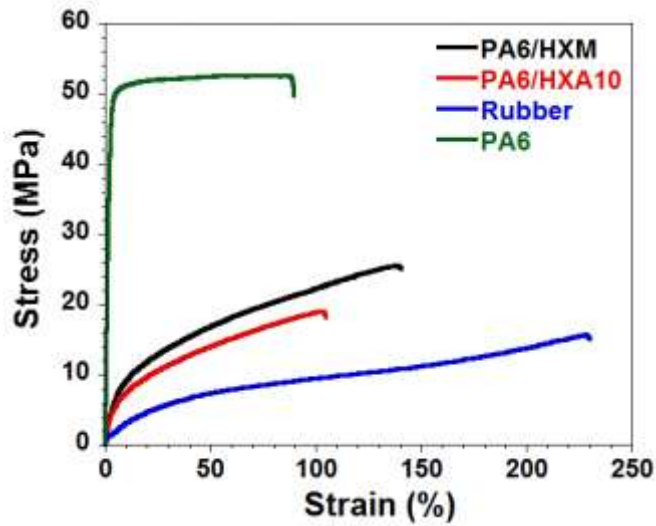
Figure 5. Monotonic stress-strain curves of the pure PA6 thermoplastic, pure rubber and TPE samples.

Table 4: Tensile strength and elongation at break of TPV samples.

Sample	Tensile strength (MPa)	Elongation at break (%)
PA6/HXM	24.86 ± 0.76	140.83 ± 9.94
PA6/HXA10	18.87 ± 0.45	102.72 ± 2.06

The cyclic stress-strain behaviour of the TPV samples which maximum strain level is increased sequentially from 10, 20, 30, 50, 70 and 100% is shown in Figure 6a. A stabilized state, characterized by a constant stress amplitude and constant hysteresis loop, was achieved after four cycles. As a result, the fifth cycle was considered as the stationary state. As shown in Figure 6a, both TPV samples exhibited a large hysteresis loss at the first loading-unloading cycles. Additionally, they also demonstrate a pronounced loss of hysteresis and stress during the cyclic deformation, suggesting a significant Mullins softening effect in both TPVs. The Mullins softening phenomena is schematically shown in Figure 6b [55]. Figure 7a presents the influence of the strain level on the stress softening during cyclic deformation, which has been characterized as follows:

14

$$Cyclic\ stress\ softening\ (\%) = (1 - \frac{\sigma_{max}^{stabilized\ cycle}}{\sigma_{max}^{first\ cycle}}) \times 100 \qquad (5)$$

where $\sigma_{max}^{stabilized\ cycle}$ and $\sigma_{max}^{first\ cycle}$ are the stress values for the maximum strain level at the stabilized cycle and first cycle, respectively [56]. The evolution of the hysteresis loss and the permanent set are depicted in Figures 7b and 7c. The evolution of these parameters gives evidences about the microstructural changes that the cyclic deformation under different strain levels causes in the TPV samples.

Quite a few models that describe the cyclic deformation and microstructural changes of PP/EPDM TPVs, which are one of the most commonly used general purpose TPVs, can be found in the literature [57–60]. Soliman *et al.* reported the deformation behaviour of a PP/EPDM TPV compound cured with a phenolic resin [61]. They performed combined infrared spectroscopy and tensile stress-strain tests in order to measure the orientation of the rubber and thermoplastic phases during the stretching of the sample. They found that the whole rubber phase was stretched, while only in a small portion of the thermoplastic phase was stretched. According to them, the plastic deformation of the thermoplastic phase is concentrated at the boundary between the rubber droplets. During the unloading process the previously deformed thermoplastic portion is pulled back to some extent owing to the elastic recovery capacity of the rubber. A schematic representation of the Soliman model is depicted in Figure 8. Based on the Soliman model, the cyclic deformation behaviour of TPV samples may be mainly driven by the yielding, buckling and bending of the thin PA6 matrix ligaments and the elastic recovery ability of the rubber droplets. Similar deformation mechanism have been also reported for PA6/EPDM-*g*-MA TPV compounds [62,63].

At low strains both the PA6 matrix phase and the rubber droplets may deform elastically and so the cyclic stress softening, hysteresis loss and permanent set are quite minimal at the initial strain levels. With increasing the strain level, the semicrystalline PA6 matrix will start to yield in the regions where matrix ligaments are thinnest. Upon unloading, the elastic forces of the stretched interconnected rubber network are able to pull back the plastically deformed thin ligaments by either bending or buckling. The loss of stiffness during the

15

reloading step may be attributed to the damage generated by the bending or buckling of the thin plastic ligaments during the unloading. The thicker thermoplastic ligaments of the matrix will interconnect the rubber droplets, forming an elastic interconnected network structure of rubber droplets and slightly deformed thicker zones of the PA6 matrix. When the strain level is increased the thin matrix ligaments will continue to yield in order to continue to the elastic deformation of the rubber droplets.

Below 30% strain level both TPV compounds present similar cyclic stress softening, hysteresis loss and permanent set, which may be attributed to the similar PA6 phase crystallinity degree and crystalline lamellae thickness that both TPVs possess. Furthermore, as shown in Figure 7a, both TPV samples present a decrease of the cyclic stress softening at 30% strain level. In the cases of the hysteresis loss and the permanent set, a linear evolution is perceived up to this value (Figures 7b and 7c). From that point on, the increase of the strain level generates a more pronounced increment in the hysteresis loss and permanent set at the first cycles. Furthermore, the difference between the hysteresis loss and permanent set in the first and fifth cycle becomes higher. Therefore, these phenomena may indicate that above the 30% strain level the thin matrix ligaments are highly plastically deformed and so from that point on the deformation induced softening behaviour may be driven by elastic recovery capacity of the rubber network.

An abrupt increment of the hysteresis loss and permanent set at the first cycle is observed for both TPV samples when the applied strain level is increased up to 50%. Moreover, as seen in Figure 7b, the values of hysteresis loss at the first cycle are higher for PA6/HXM sample and displays a higher variation of hysteresis loss from the first to the fifth cycle. These results are consistent with the fact that rubber network interactions are stronger in the PA6/HXM TPV compound, which means that they are able to dissipate more strain energy in terms of viscous losses [64,65]. Furthermore, PA6/HXM demonstrates a less significant stress softening effect (see Figure 7a).

Several physical interpretations exist for the Mullins softening behaviour of rubber materials, however a general agreement for the cause of this effect at the microscopic level

16

is still absent. In this work, authors propose that, in order to interpret the different cyclic stress softening effects that both TPV compounds show above the 30% strain level, the rubber droplets must to be treated as a two-network structures formed by covalent and non-covalent bonds [66]. Both TPV compounds possess a rubber network structure formed by chains connected by covalent and non-covalent links, however their structure differs in the strength of the non-covalent links and in the amount of covalent the links. In the case of non-covalent links, ionic bonds are stronger than hydrogen bonds. Therefore, the less significant stress softening effect displayed by PA6/HXM sample may be attributed to the better elastic recovery capacity of the rubber network structure formed by a higher amount of covalent C-C linkages and stronger non-covalent bonds.
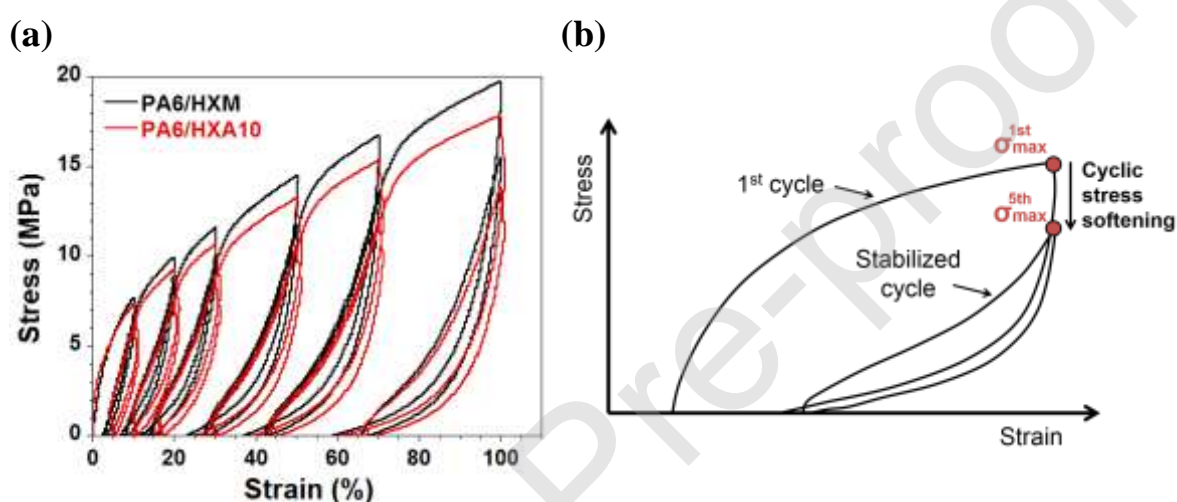
(a)   **(b)**

Figure 6. (a) Cyclic stretching stress-strain response of the TPV samples in uniaxial tension (first and 5th stabilized cycles for each strain level) and (b) schematic representation of the Mullins softening phenomena.
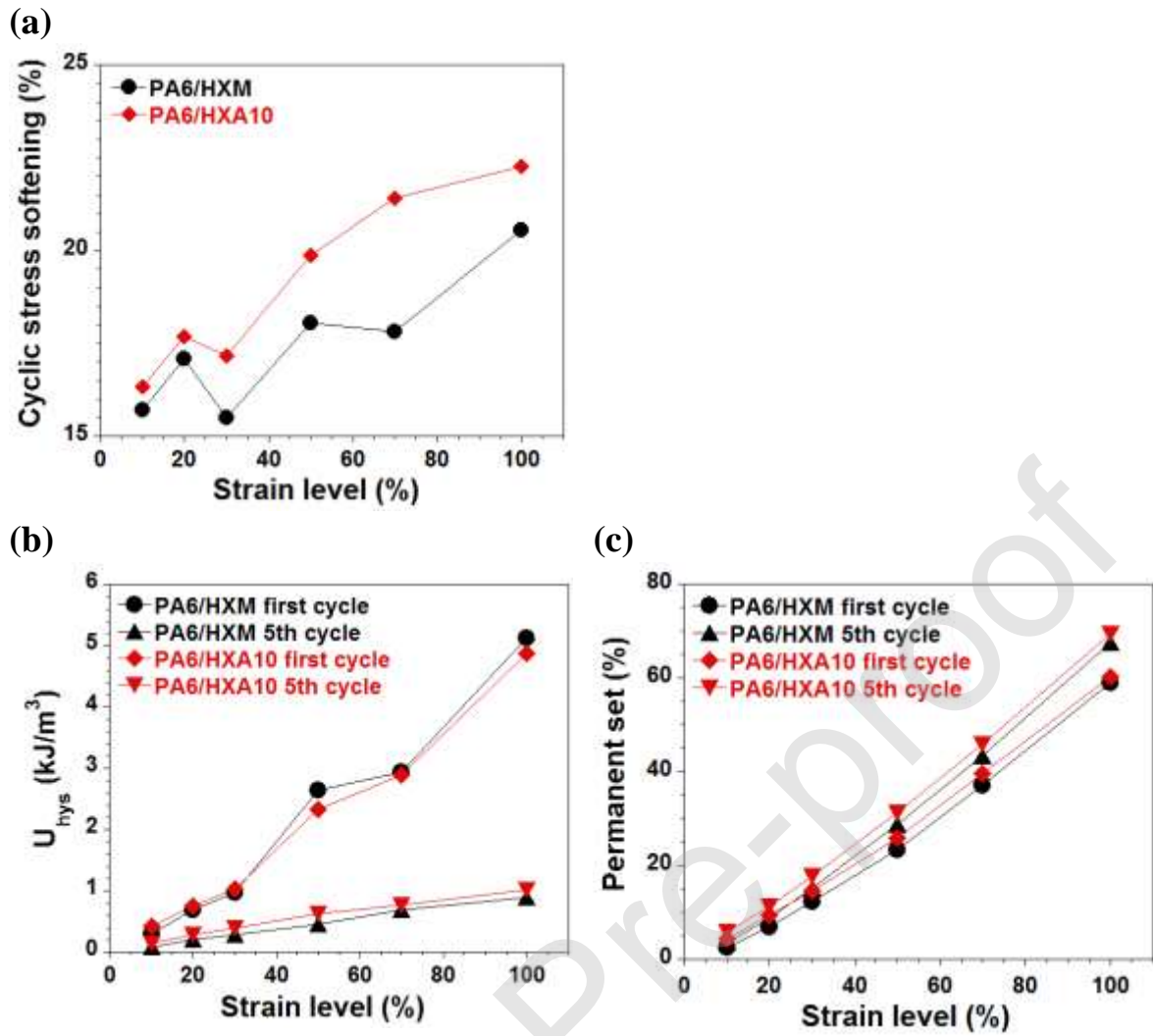
(a)

(b)

(c)

Figure 7. (a) Influence of strain level on cyclic stress loss response of the TPV samples, and evolution of the (b) hysteresis loss and (c) permanent set as a function of the strain level at the first and stabilized 5th cycle.
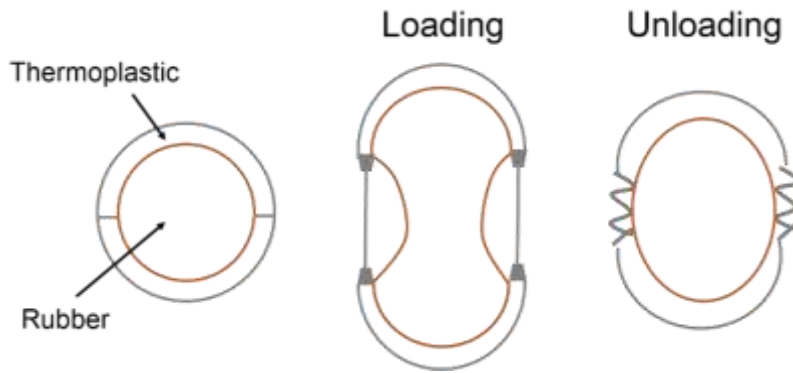
Figure 8. Schematic representation of the deformation mechanism of TPV materials suggested by Soliman et at. [61].

Micromechanical deformation analysis

To better understand the micromechanical processes that take place during the cyclic deformation of the TPV samples, SEM images of the tensile specimens of PA6/HXM and PA6/HXA10 after cyclic tensile tests up to 20 and 50% strain level were obtained. The results are shown in Figure 9. In Figure 9a it can be seen that both PA6/HXA10 and PA6/HXM present micro-voids in the PA6 matrix at 20% strain level. Thus, SEM images clearly point to the bending and buckling of PA6 thin plastic ligaments as the main deformation mechanism of the TPV compounds when applying strain levels below 30%. Interestingly, Figure 9b reveals that plastic voids in the PA6/HXA10 are much larger than in PA6/HXM at 50% strain level. Moreover, the cryofractured surface of PA6/HXA10 sample showed highly cavitated and plastically deformed PA6 phase containing debonded rubber dispersed domains. According to SEM images, the better elastic recovery capacity of PA6/HXM rubber network slows down the growth of voids and a large number of stable micro-voids are generated, which facilitates further deformation of the PA6 ligaments between the rubber droplets. On the other hand, the elastic forces of PA6/HXA10 rubber network are not sufficiently high to pull back the stretched thick PA6 ligaments and so void-fibrillar matrix structures are generated in the PA6/HXA10 compound.

19

When the TPV compounds are uniaxially stretched up to a stress threshold, the rubber droplets dispersed in the PA6 plastic matrix behave as stress concentration points. This phenomena is a consequence of the different Poisson´s ratio and modulus of PA6 and rubber [67,68]. Additionally, the concentration of the stress in rubber droplets causes a local stress state transition from uniaxial to a hydrostatic [63]. As the better elastic recovery capacity of PA6/HXM rubber network facilitates the deformation of PA6 ligaments, the critical hydrostatic stress in the rubber droplets is not achieved and so development of plastic voids and rubber cavitation is suppressed. Thus, the observed micromechanical processes by SEM analysis are consistent with the different nonlinear mechanical behaviours observed by cyclic tensile tests.

Figure 10 illustrates schematically the physical interpretation that authors propose for the deformation mechanisms of the TPV compounds under cyclic deformation at different strain levels. Below 30% strain level, the Mullins softening effect, and so the damage generated in the TPVs, is mainly driven by the buckling and bending of the thin plastic ligaments. Above the 30% strain level, once the thin plastic ligaments are highly plastically deformed, damage is mainly generated due to the bond rupture in the rubber network structure formed by covalent and non-covalent linkages.
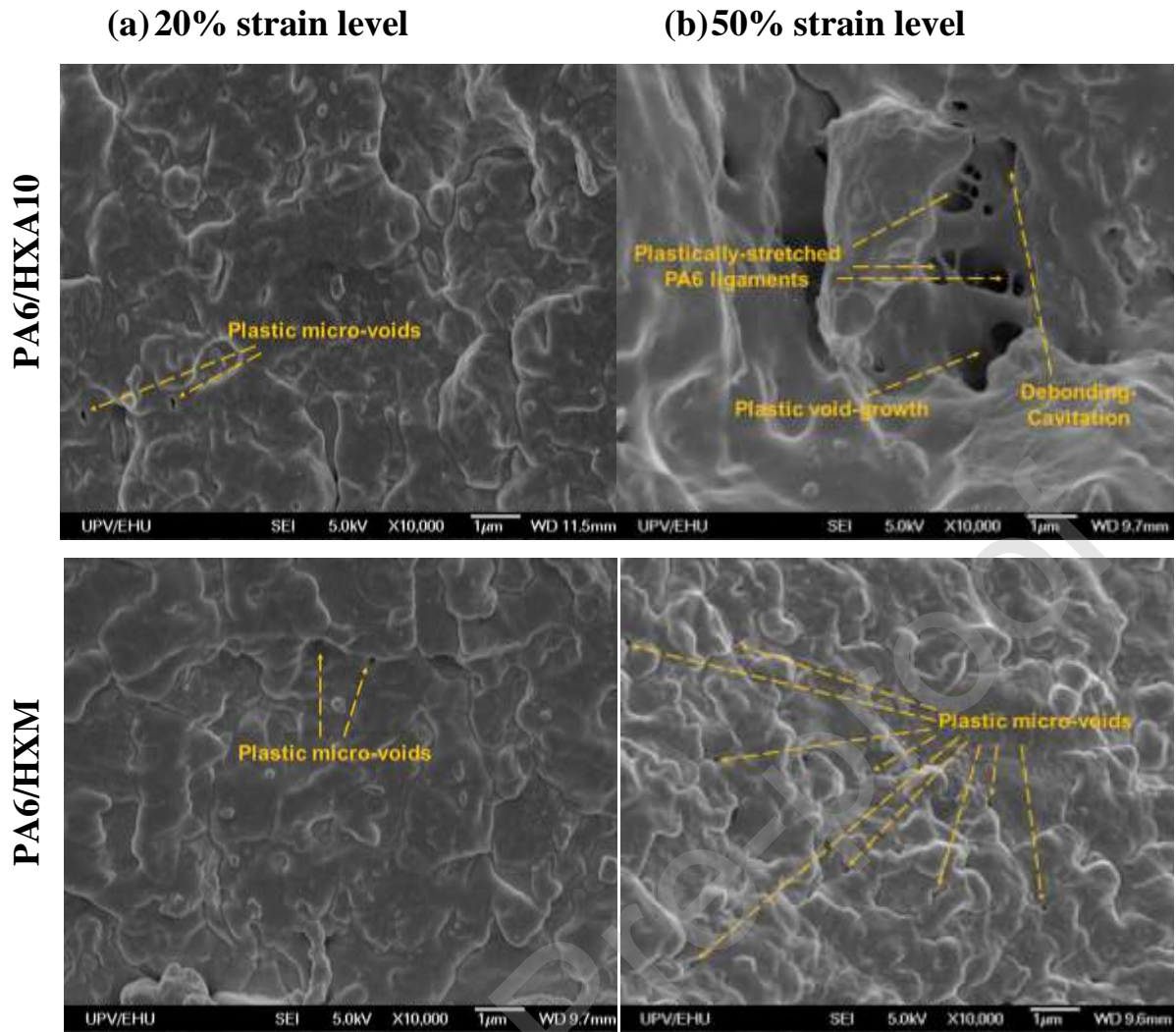
Figure 9. SEM micrographs of PA6/HXA10 and PA6/HXM TPV compounds as a function of strain level: (a) 20% strain level and (b) 50% strain level.
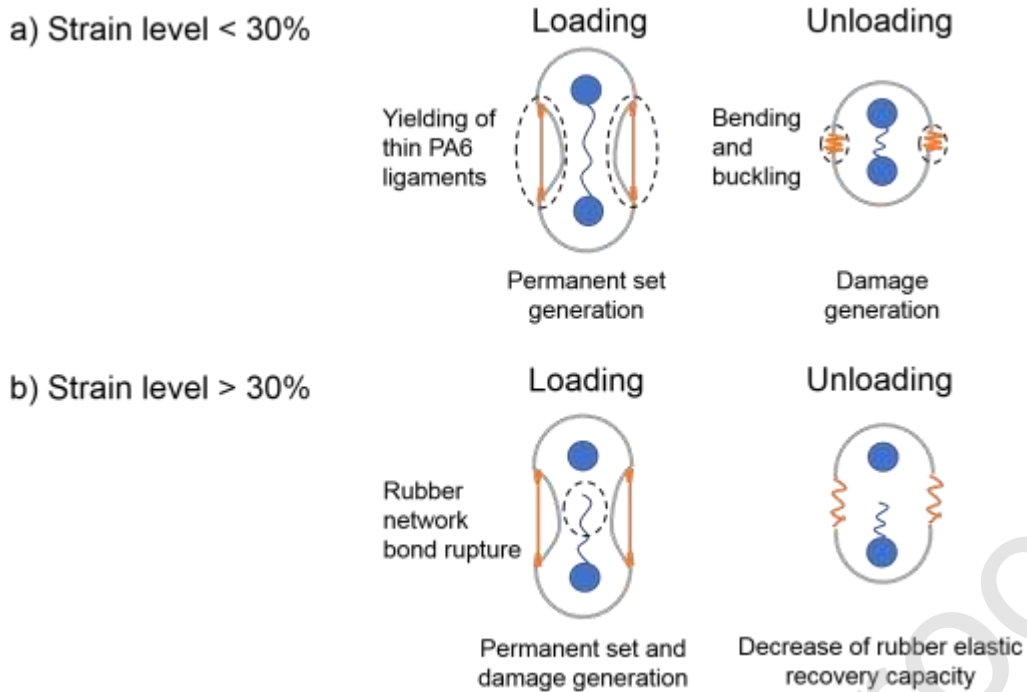
Figure 10. Proposed deformation mechanism of the PA6/XHNBR TPV compounds.

Dynamic mechanical behaviour

Dynamic strain sweeps were performed in order to investigate the dynamic strain softening phenomena, also known as Payne effect, in the TPV compounds. Figure 11a presents the dependence of the tensile storage modulus on the strain amplitude measured at ambient temperature and constant frequency of 10 Hz for both TPV compounds. The linear viscoelastic region is similar for both samples. Moreover, a large drop of E' with increasing dynamic strain amplitude was observed for both samples. As a measure for the Payne effect, the differences between the E' values at 0.01% and 10% has been calculated. The value of E' in the viscoelastic region drops 82% for PA6/HXM and 85% for PA6/HXA10, so the dynamic strain generates a similar softening phenomena in both samples.

A well-known approach to obtain a physical interpretation of the Payne effect in rubber-like materials is based on the micromechanical model of Kraus [69]. The micromechanical model proposed by Kraus states that the Payne effect is a consequence of the breakage and

recovery of weak physical bonds under a periodic strain. Here, in accordance with the observed quasi-static mechanical behaviour, authors propose that the initiation of dynamic strain softening phenomena may be ascribed to the damage generated during the bending and buckling of PA6 matrix ligaments when the TPV samples are subjected to increasing oscillatory strain amplitudes.

The frequency dependence of shear storage modulus (G') at ambient temperature is illustrated in Figure 11b. The G´ of PA6/HXA10 is higher than that of PA6/HXM in the whole frequency range studied, which is in line with the observed phenomena in the temperature sweep tests (Figure 2a), were PA6/HXM reveals a lower E´ modulus than PA6/HXA10 near room temperature. This is attributed to the ionic relaxation transition that the PA6/HXM sample possess near room temperature (Figure 2b). The storage modulus increases with the increase in frequency for both TPV samples. The increase of storage modulus with increasing frequency takes place due to the kinetic nature of the glass transition. As the frequency applied to the samples is increased the glass transition takes place at higher temperatures, i.e., molecular relaxations occur at higher temperatures [70]. Comparing the behaviour of both TPV compounds to the frequency, Figure 11b shows that the increase in storage modulus is larger for PA6/HXM. Precisely, the increase in storage modulus is of 23% for PA6/HXM and 18% for PA6/HXA10. That means that more energy is required to initiate the molecular movements in PA6/HXM, which confirms the stronger interaction forces presented in PA6/HXM compound [71].
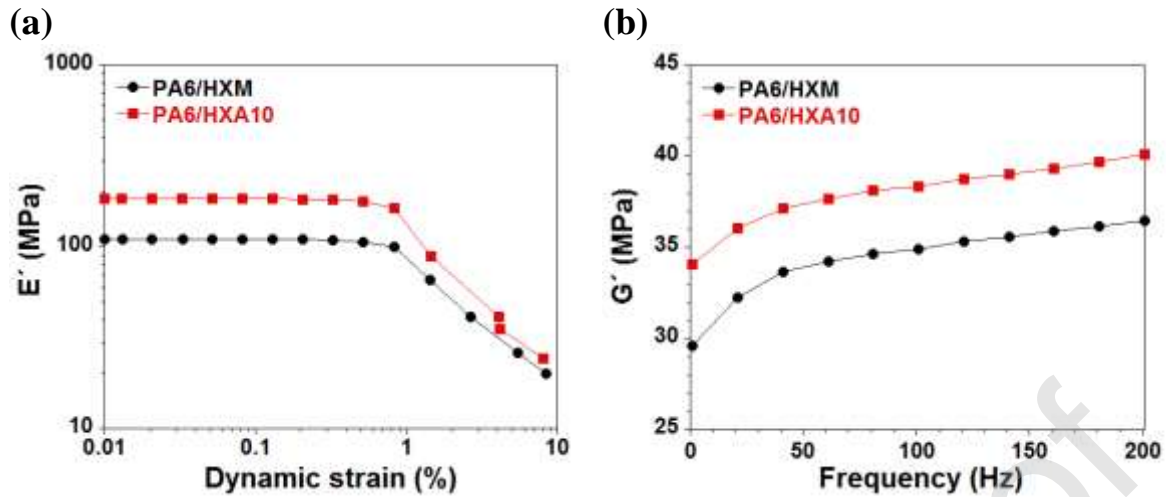
(a)

(b)

Figure 11. (a) Dynamic strain dependence of tensile storage modulus and (b) frequency dependence of shear storage modulus.

Figure 12 compares the effect of the static prestrain on the tensile storage ($E´$) and loss modulus ($E´´$) for PA6/HXM and PA6/HXA10. Both TPV samples exhibit a nonlinear behaviour exhibiting an increase of both storage and loss moduli that is started at low static prestrains. This phenomena has been observed and discussed previously on filled elastomers by several authors and has been ascribed to the finite extensibility of the network [72–74]. In the case of TPV compounds, authors suggest that the observed mechanical behaviour is associated to some deformation of the thin plastic ligaments in the direction of the applied strain. The alignment of the thin plastic ligaments between rubber droplets may modify the stress that is generated locally, which leads to the observed increase of storage and loss moduli with the static prestrain. Therefore, this phenomena could be well understood in terms of the previously presented physical interpretation for the deformation mechanism of TPV compounds (Figure 10).
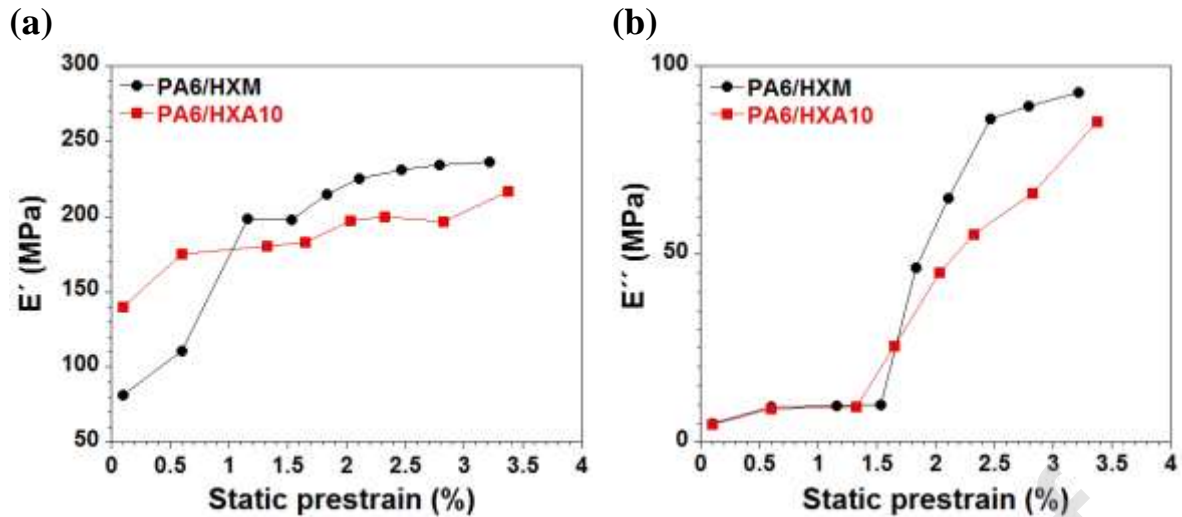
24

Figure 12. Static prestrain-dependence of (a) tensile storage and (b) loss modulus.

Conclusions

In this article, nonlinear quasi-static and dynamic mechanical effects of novel TPV compounds based on PA6 and XHNBR containing different rubber network structures based on covalent, ionic and hydrogen crosslinks have been experimentally investigated through monotonic tensile analysis, cyclic tensile tests and dynamic mechanical (DMA) measurements. The mechanical behaviour has been correlated with the microstructural evolution under cyclic deformations at different strain levels. Mechanical characterization showed a dependence on the rubber network structure. Additionally, the micrographs obtained from SEM study revealed that a stronger rubber network interaction and so a better elastic recovery capacity suppresses the development of plastic voids and rubber cavitation. Based on the observed phenomena a physical interpretation based on the yielding, buckling and bending of PA6 ligaments at low strain levels and the rupture of covalent and non-covalent bonds presented in the rubber network at high strain levels has been introduced.

Declaration of interests

25

Acknowledgements

References

[1] Spontak RJ, Patel NP. Thermoplastic elastomers: fundamentals and applications. Curr Opin Colloid Interface Sci 2000;5:333–40. https://doi.org/10.1016/S1359-0294(00)00070-4.

[2] Drobny JG. Handbook of thermoplastic elastomers. Elsevier; 2014.

[3] Hu X, Kang H, Li Y, Geng Y, Wang R, Zhang L. Preparation, morphology and superior performances of biobased thermoplastic elastomer by in situ dynamical vulcanization for 3D-printed materials. Polymer 2017;108:11–20. https://doi.org/10.1016/j.polymer.2016.11.045.

[4] Coran AY. Thermoplastic Elastomeric Rubber- Plastic Blends. Handb Elastomers 2000. https://doi.org/10.1201/9781482270365-17.

[5] Banerjee SS, Bhowmick AK. High-temperature thermoplastic elastomers from rubber–plastic blends: a state-of-the-art review. Rubber Chem Technol 2016;90:1–36. https://doi.org/10.5254/rct.16.83786.

[6] Naskar K, Babu RR. Thermoplastic Elastomers (TPEs) and Thermoplastic Vulcanizates (TPVs). Encycl Polym Nanomater 2015:2517–22.

[7] Babu RR, Naskar K. Recent Developments on Thermoplastic Elastomers by Dynamic Vulcanization. Adv Rubber Compos 2010:219–47. https://doi.org/10.1007/12_2010_97.

[8] Banerjee SS, Bhowmick AK. Dynamic vulcanization of novel nanostructured polyamide 6/ fluoroelastomer thermoplastic elastomeric blends with special reference to morphology, physical properties and degree of vulcanization. Polymer 2015;57:105–16. https://doi.org/10.1016/j.polymer.2014.12.016.

[9] Sun Z, Zhang Y, Shao H, He A. In situ reactive compatibilization of polypropylene/trans-1,4-poly(isoprene-co-butadiene) rubber (TBIR) blends with balanced toughness and stiffness via dynamic vulcanization. React Funct Polym 2019;142:60–8.

[10] Chatterjee T, Basu D, Das A, Wiessner S, Naskar K, Heinrich G. Super thermoplastic vulcanizates based on carboxylated acrylonitrile butadiene rubber (XNBR) and polyamide (PA12). Eur Polym J 2016;78:235–252.

[11] Shahbikian S, Carreau PJ, Heuzey M-C, Ellul MD, Cheng J, Shirodkar P, et al. Morphology development of EPDM/PP uncross-linked/dynamically cross-linked blends. Polym Eng Sci 2012;52:309–22. https://doi.org/10.1002/pen.22084.

[12] Wu H, Tian M, Zhang L, Tian H, Wu Y, Ning N, et al. New Understanding of Morphology Evolution of Thermoplastic Vulcanizate (TPV) during Dynamic Vulcanization. ACS Sustain Chem Eng 2015;3:26–32. https://doi.org/10.1021/sc500391g.

[13] Wang C, Zhang Y, Zhang L, Liu Q, Wang Z. Carbon black reinforced thermoplastic vulcanisates based on ethylene–vinyl acetate copolymer/styrene–butadiene rubber blends. Plast Rubber Compos 2016;45:415–22. https://doi.org/10.1080/14658011.2016.1235831.

[14] Shafieizadegan-Esfahani AR, Abdollahi MM, Katbab AA. Effects of compounding procedure on morphology development, melt rheology, and mechanical properties of nanoclay reinforced dynamically vulcanized EPDM/polypropylene thermoplastic vulcanizates. Polym Eng Sci 2016;56:914–21. https://doi.org/10.1002/pen.24320.

[15] Joseph A, George S, Joseph K, Thomas S. Melting and crystallization behaviors of isotactic polypropylene/acrylonitrile–butadiene rubber blends in the presence and absence of compatibilizers and fillers. J Appl Polym Sci 2006;102:2067–80. https://doi.org/10.1002/app.23986.

[16] Mirzadeh A, Lafleur PG, Kamal MR, Dubois C. Morphology evolution and thermomechanical characteristics of tpv nanocomposites based on pp/epdm prepared by reactive extrusion. Rubber Chem Technol 2013;86:521–37. https://doi.org/10.5254/RCT.13.87996.

[17] Cao L, Liu C, Zou D, Zhang S, Chen Y. Using cellulose nanocrystals as sustainable additive to enhance mechanical and shape memory properties of PLA/ENR thermoplastic vulcanizates. Carbohydr Polym 2019:115618. https://doi.org/10.1016/j.carbpol.2019.115618.

[18] Wu H, Yao P, Ning N, Zhang L, Tian H, Wu Y, et al. A novel dielectric elastomer by constructing dual-network structure of carbon nanotubes and rubber nanoparticles in dynamically vulcanized thermoplastic elastomer. RSC Adv 2016;6:32932–9. https://doi.org/10.1039/C6RA01463A.

[19] Wang L, Hua J, Wang Z. Facile design of heat-triggered shape memory ethylene-vinyl acetate copolymer/nitrile-butadiene thermoplastic vulcanizates via zinc dimethacrylate induced interfacial compatibilization. Polym Test 2019;76:481–9. https://doi.org/10.1016/j.polymertesting.2019.04.011.

[20] Chen Y, Xu C, Liang X, Cao L. In Situ Reactive Compatibilization of Polypropylene/Ethylene–Propylene–Diene Monomer Thermoplastic Vulcanizate by Zinc Dimethacrylate via Peroxide-Induced Dynamic Vulcanization. J Phys Chem B 2013;117:10619–28. https://doi.org/10.1021/jp404427w.

[21] Cao X, Lu K, Li Y. Isolated Protective Char Layers by Nanoclay Network: Significantly Improved Flame Retardancy and Mechanical Performance of TPV/MH Composites by Small Amount of Nanoclay. Ind Eng Chem Res 2015;54:6912–21. https://doi.org/10.1021/acs.iecr.5b01478.

[22] Wei D, Zhao J, Liu T, Wang Z. Mechanical and morphological properties of acrylonitrile–butadiene–styrene terpolymer/nitrile butadiene rubber thermoplastic vulcanizates plasticized by dioctyl phthalate. J Thermoplast Compos Mater 2016;29:366–80. https://doi.org/10.1177/0892705713518796.

[23] Babu RR, Singha NK, Naskar K. Interrelationships of morphology, thermal and mechanical properties in uncrosslinked and dynamically crosslinked PP/EOC and PP/EPDM blends. Express Polym Lett 2010;4:197–209.

[24] Le HH, Lüpke T, Pham T, Radusch H-J. Time dependent deformation behavior of thermoplastic elastomers. Polymer 2003;44:4589–97. https://doi.org/10.1016/S0032-3861(03)00409-9.

[25] Bartolomé L, Aurrekoetxea J, Urchegui MA, Tato W. The influences of deformation state and experimental conditions on inelastic behaviour of an extruded thermoplastic polyurethane elastomer. Mater Des 2013;49:974–80. https://doi.org/10.1016/j.matdes.2013.02.055.

[26] Boyce MC, Kear K, Socrate S, Shaw K. Deformation of thermoplastic vulcanizates. J Mech Phys Solids 2001;49:1073–98. https://doi.org/10.1016/S0022-5096(00)00066-1.

[27] Mars WV, Ellul MD. Fatigue characterization of a thermoplastic elastomer. Rubber Chem Technol 2017;90:367–80. https://doi.org/10.5254/rct.17.83780.

[28] Tobajas R, Elduque D, Ibarz E, Javierre C, Canteli AF, Gracia L. Visco-Hyperelastic Model with Damage for Simulating Cyclic Thermoplastic Elastomers Behavior Applied to an Industrial Component. Polymers 2018;10:668. https://doi.org/10.3390/polym10060668.

[29] Mullins L, Tobin NR. Theoretical Model for the Elastic Behavior of Filler-Reinforced Vulcanized Rubbers. Rubber Chem Technol 1957;30:555–71. https://doi.org/10.5254/1.3542705.

[30] Mullins L, Tobin NR. Stress softening in rubber vulcanizates. Part I. Use of a strain amplification factor to describe the elastic behavior of filler-reinforced vulcanized rubber. J Appl Polym Sci 1965;9:2993–3009. https://doi.org/10.1002/app.1965.070090906.

[31] Mullins L. Softening of Rubber by Deformation. Rubber Chem Technol 1969;42:339–62. https://doi.org/10.5254/1.3539210.

[32] Li Z, Wen F, Hussain M, Song Y, Zheng Q. Scaling laws of Mullins effect in nitrile butadiene rubber nanocomposites. Polymer 2020;193:122350. https://doi.org/10.1016/j.polymer.2020.122350.

[33] Plagge J, Klüppel M. Mullins effect revisited: Relaxation, recovery and high-strain damage. Mater Today Commun 2019;20:100588. https://doi.org/10.1016/j.mtcomm.2019.100588.

[34] Zhong D, Xiang Y, Yin T, Yu H, Qu S, Yang W. A physically-based damage model for soft elastomeric materials with anisotropic Mullins effect. Int J Solids Struct 2019;176–177:121–34. https://doi.org/10.1016/j.ijsolstr.2019.05.018.

[35] Wu H, Yao P, Ning N, Zhang L, Tian H, Wu Y, et al. A novel dielectric elastomer by constructing dual-network structure of carbon nanotubes and rubber nanoparticles in dynamically vulcanized thermoplastic elastomer. RSC Adv 2016;6:32932–9. https://doi.org/10.1039/C6RA01463A.

[36] Wu H, Tian M, Zhang L, Tian H, Wu Y, Ning N, et al. Effect of Rubber Nanoparticle Agglomeration on Properties of Thermoplastic Vulcanizates during Dynamic Vulcanization. Polymers 2016;8:127. https://doi.org/10.3390/polym8040127.

[37] Zhao Y, Liu Z, Su B, Chen F, Fu Q, Ning N, et al. Property enhancement of PP-EPDM thermoplastic vulcanizates via shear-induced break-up of nano-rubber aggregates and molecular orientation of the matrix. Polymer 2015;63:170–8. https://doi.org/10.1016/j.polymer.2015.03.011.

[38] Harwood J a. C, Payne AR. Hysteresis and strength of rubbers. J Appl Polym Sci 1968;12:889–901. https://doi.org/10.1002/app.1968.070120423.

[39] Mullins L. Permanent Set in Vulcanized Rubber. Rubber Chem Technol 1949;22:1036–44. https://doi.org/10.5254/1.3543010.

[40] Payne AR. The dynamic properties of carbon black loaded natural rubber vulcanizates. Part II. J Appl Polym Sci 1962;6:368–72. https://doi.org/10.1002/app.1962.070062115.

[41] Burgoa A, Hernandez R, Vilas JL. New ways to improve the damping properties in high-performance thermoplastic vulcanizates. Polym Int 2020:pi.5977. https://doi.org/10.1002/pi.5977.

[42] Liu J, Lu Y-L, Tian M, Li F, Shen J, Gao Y, et al. The Interesting Influence of Nanosprings on the Viscoelasticity of Elastomeric Polymer Materials: Simulation and Experiment. Adv Funct Mater 2013;23:1156–63. https://doi.org/10.1002/adfm.201201438.

[43] Tang Z, Chen F, Chen Q, Zhu L, Yan X, Chen H, et al. The energy dissipation and Mullins effect of tough polymer/graphene oxide hybrid nanocomposite hydrogels. Polym Chem 2017;8:4659–72. https://doi.org/10.1039/C7PY01068K.

[44] Starý Z, Pemsel T, Baldrian J, Münstedt H. Influence of a compatibilizer on the morphology development in polymer blends under elongation. Polymer 2012;53:1881–9. https://doi.org/10.1016/j.polymer.2012.02.056.

[45] Ning N, Li S, Wu H, Tian H, Yao P, Hu G-H, et al. Preparation, microstructure, and microstructure-properties relationship of thermoplastic vulcanizates (TPVs): A review. Prog Polym Sci 2018;79:61–97. https://doi.org/10.1016/j.progpolymsci.2017.11.003.

[46] Bieliński DM, Stępkowska A. Mechanical properties and friction of rubber vulcanizates: Aspects of crosslink structure. Arch Civ Mech Eng 2013;13:192–8. https://doi.org/10.1016/j.acme.2012.12.004.

[47] Ibarra L, Alzorriz M. Ionic elastomers based on carboxylated nitrile rubber and magnesium oxide. J Appl Polym Sci 2007;103:1894–9. https://doi.org/10.1002/app.25411.

[48] Hirschl Ch, Biebl–Rydlo M, DeBiasio M, Mühleisen W, Neumaier L, Scherf W, et al. Determining the degree of crosslinking of ethylene vinyl acetate photovoltaic module encapsulants—A comparative study. Sol Energy Mater Sol Cells 2013;116:203–18. https://doi.org/10.1016/j.solmat.2013.04.022.

[49] Parenteau T, Bertevas E, Ausias G, Stocek R, Grohens Y, Pilvin P. Characterisation and micromechanical modelling of the elasto-viscoplastic behavior of thermoplastic elastomers. Mech Mater 2014;71:114–25. https://doi.org/10.1016/j.mechmat.2013.06.010.

[50] Rozanski A, Safandowska M, Krajenta A. DSC/SAXS analysis of the thickness of lamellae of semicrystalline polymers-restrictions in the case of materials with swollen amorphous phase. Polym Test 2018;65:189–96. https://doi.org/10.1016/j.polymertesting.2017.11.028.

[51] Vicard C, De Almeida O, Cantarel A, Bernhart G. Experimental study of polymerization and crystallization kinetics of polyamide 6 obtained by anionic ring

opening polymerization of ε-caprolactam. Polymer 2017;132:88–97.
https://doi.org/10.1016/j.polymer.2017.10.039.

[52] Chen Y, Wang Y, Xu C, Wang Y, Jiang C. New Approach to Fabricate Novel Fluorosilicone Thermoplastic Vulcanizate with Bicrosslinked Silicone Rubber-Core/Fluororubber-Shell Particles Dispersed in Poly(vinylidene Fluoride): Structure and Property. Ind Eng Chem Res 2016;55:1701–9.
https://doi.org/10.1021/acs.iecr.5b04676.

[53] Chakraborty SK, Bhowmick AK, De SK. Mixed cross-link systems in elastomers. J Macromol Sci Part C Polym Rev 1981;21:313–332.

[54] Ibarra L, Rodríguez A, Mora-Barrantes I. Crosslinking of unfilled carboxylated nitrile rubber with different systems: Influence on properties. J Appl Polym Sci 2008;108:2197–205. https://doi.org/10.1002/app.27893.

[55] Bartolomé L, Aurrekoetxea J, Urchegui MA, Tato W. The influences of deformation state and experimental conditions on inelastic behaviour of an extruded thermoplastic polyurethane elastomer. Mater Des 2013;49:974–80.
https://doi.org/10.1016/j.matdes.2013.02.055.

[56] Cantournet S, Desmorat R, Besson J. Mullins effect and cyclic stress softening of filled elastomers by internal sliding and friction thermodynamics model. Int J Solids Struct 2009;46:2255–64. https://doi.org/10.1016/j.ijsolstr.2008.12.025.

[57] Kikuchi Y, Fukui T, Okada T, Inoue T. Elastic-plastic analysis of the deformation mechanism of PP-EPDM thermoplastic elastomer: Origin of rubber elasticity. Polym Eng Sci 1991;31:1029–32. https://doi.org/10.1002/pen.760311406.

[58] Boyce MC, Yeh O, Socrate S, Kear K, Shaw K. Micromechanics of cyclic softening in thermoplastic vulcanizates. J Mech Phys Solids 2001;49:1343–60.
https://doi.org/10.1016/S0022-5096(00)00077-6.

[59] C. Boyce M, Socrate S, Kear K, Yeh O, Shaw K. Micromechanisms of deformation and recovery in thermoplastic vulcanizates. J Mech Phys Solids 2001;49:1323–42.
https://doi.org/10.1016/S0022-5096(00)00075-2.

[60] l'Abee RMA, Duin M van, Spoelstra AB, Goossens JGP. The rubber particle size to control the properties-processing balance of thermoplastic/cross-linked elastomer blends. Soft Matter 2010;6:1758–68. https://doi.org/10.1039/B913458A.

[61] Soliman M, Van Dijk M, Van Es M. Deformation mechanism of thermoplastic vulcanizates investigated by combined FTIR- and stress-strain measurements. Polym Mater Sci Eng 1998;79:108.

[62] Oderkerk J, Groeninckx G, Soliman M. Investigation of the Deformation and Recovery Behavior of Nylon-6/Rubber Thermoplastic Vulcanizates on the Molecular Level by Infrared-Strain Recovery Measurements. Macromolecules 2002;35:3946–54.
https://doi.org/10.1021/ma010651v.

[63] Oderkerk J, de Schaetzen G, Goderis B, Hellemans L, Groeninckx G. Micromechanical Deformation and Recovery Processes of Nylon-6/Rubber Thermoplastic Vulcanizates As Studied by Atomic Force Microscopy and Transmission Electron Microscopy. Macromolecules 2002;35:6623–9. https://doi.org/10.1021/ma0113475.

[64] Sankarasubramanian M, Torabizadeh M, Putnam ZA, Moosbrugger JC, Huang MY, Krishnan S. Enhanced elastomer toughness and fracture properties imparted by chemically reactive flat nanoparticles. Polym Test 2019;78:105932. https://doi.org/10.1016/j.polymertesting.2019.105932.

[65] Sasikumar K, Manoj NR, Mukundan T, Khastgir D. Hysteretic damping in XNBR – MWNT nanocomposites at low and high compressive strains. Compos Part B Eng 2016;92:74–83. https://doi.org/10.1016/j.compositesb.2015.04.005.

[66] Drozdov AD, Christiansen J deClaville. Multi-cycle deformation of supramolecular elastomers: Constitutive modeling and structure-property relations. Int J Eng Sci 2018;133:311–35. https://doi.org/10.1016/j.ijengsci.2018.10.002.

[67] Dompas D, Groeninckx G, Isogawa M, Hasegawa T, Kadokura M. Toughening behaviour of rubber-modified thermoplastic polymers involving very small rubber particles: 2. Rubber cavitation behaviour in poly(vinyl chloride)/methyl methacrylate-butadiene-styrene graft copolymer blends. Polymer 1994;35:4750–9. https://doi.org/10.1016/0032-3861(94)90728-5.

[68] Dijkstra K, ter Laak J, Gaymans RJ. Nylon-6/rubber blends: 6. Notched tensile impact testing of nylon-6/(ethylene-propylene rubber) blends. Polymer 1994;35:315–22. https://doi.org/10.1016/0032-3861(94)90696-3.

[69] Kraus G, Childers CW, Rollmann KW. Stress softening in carbon black-reinforced vulcanizates. Strain rate and temperature effects. J Appl Polym Sci 1966;10:229–44. https://doi.org/10.1002/app.1966.070100205.

[70] Bergström JS, Boyce MC. Constitutive modeling of the large strain time-dependent behavior of elastomers. J Mech Phys Solids 1998;46:931–54. https://doi.org/10.1016/S0022-5096(97)00075-6.

[71] Fang Q, Song B, Tee T-T, Sin LT, Hui D, Bee S-T. Investigation of dynamic characteristics of nano-size calcium carbonate added in natural rubber vulcanizate. Compos Part B Eng 2014;60:561–7. https://doi.org/10.1016/j.compositesb.2014.01.010.

[72] Busfield JJC, Deeprasertkul C, Thomas AG. The effect of liquids on the dynamic properties of carbon black filled natural rubber as a function of pre-strain. Polymer 2000;41:9219–25. https://doi.org/10.1016/S0032-3861(00)00306-2.

[73] Azoug A, Constantinescu A, Pradeilles-Duval RM, Vallat MF, Nevière R, Haidar B. Effect of the sol fraction and hydrostatic deformation on the viscoelastic behavior of prestrained highly filled elastomers. J Appl Polym Sci 2013;127:1772–80. https://doi.org/10.1002/app.37800.

[74] Thorin A, Azoug A, Constantinescu A. Influence of prestrain on mechanical properties of highly-filled elastomers: Measurements and modeling. Polym Test 2012;31:978–86. https://doi.org/10.1016/j.polymertesting.2012.07.014.